UNIVERSITÀ DEGLI STUDI DI CATANIA

DIPARTIMENTO DI GESTIONE DEI SISTEMI AGROALIMENTARI E AMBIENTALI

DOTTORATO DI RICERCA INTERNAZIONALE IN INGEGNERIA AGRARIA

XXV CICLO

Dott.ssa Rita Papa

Micrometeorological approaches to measure and model surface energy fluxes of irrigated citrus orchards in a semi-arid environment.

TESI DI DOTTORATO

Tutor
Chiar.ma Prof.ssa Simona Consoli

Coordinatore:
Chiar.ma Prof.ssa Claudia Arcidiacono

PhD attended during 2009-2012

Acknowledgements

With grateful thanks to Professor Simona Consoli for her guidance and support during my PhD course; Professor Francesc Castellví Sentis for the precious collaboration at the research project and for his hospitality in Lleida; Azienda Tribulato for its hospitality; Agrometeorological Service of the Sicilian Region (SIAS) for climatic data provided.

Table of contents

1 Introduction

1.1 Foreword

The general decreasing trends for water supply in Mediterranean regions and the need for a sustainable use of water resources make essential to understand the water relations in the primary sector; in these regions, tree crops like olive, orange and vine, represent one of the most relevant components in the agricultural economy, as well as in the exploitation of water resources. Recent studies have shown that, in arid and semi-arid regions of Mediterranean countries, irrigation consumes more than 70% of the available water. Modern irrigation management is increasingly being based on a better knowledge of actual crop water use. Therefore, the first step toward sound management of scarce water resources in these regions requires accurate estimations of the spatio-temporal variability of crop water exchanges with the atmosphere through evapotranspiration (ET).

The scientific efforts in measuring evapotranspiration of tree crops are all quite recent. Yet, measuring and modelling the evapotranspiration of tree crops either at the plant or at the plot scale over a cropping season is still an issue of debate. A major reason is the sparse canopy condition which determines an important but variable source of evaporation from the soil surface, e.g. measurements by Lascano *et al*. (1992) and Heilman *et al*. (1994) in vineyards showed that soil evaporation can account as much as 60-70% of evapotranspiration. This brings some difficulties in evaluating and modelling the evapotranspiration fluxes. Soil evaporation must be represented separately from tree transpiration as they are regulated differently. In turn, available energy must be partitioned between plant and

bare soil. Another reason is the lack of knowledge about the interaction between transpiration and soil water availability throughout the cropping season. Previous studies about soil-water relations in tree crops mainly have shown that differences in soil water regimes induce differences in leaf water potential and stomatal conductance or transpiration (Fernandez *et al*., 2001).

These studies have greatly contributed to the development and refinement of measurements techniques of evapotranspiration in tree crops, which can be distinguished in four main groups: (i) sap flow techniques; (ii) micrometeorological techniques; (iii) soil water models; (iv) remote sensing methods.

Sap flow techniques have been advanced over the last few years, although the first experiments date back to the 1950's. These techniques determine water flow through the plants and, thus, may be used to assess directly plant responses to irrigation. In some cases, sap flow measurements have been coupled with soil water balance calculations to determine ET at plot scale (Trambouze and Voltz, 2001). One major issue in using this technique is indeed the up-scaling of measurement from the branch to the canopy level.

Micrometeorological techniques have been tested in tree crops and tall canopies, namely the sonic Eddy Covariance method (Simmons *et al*., 2007), large aperture scintillometry (Meijninger and de Bruin, 2000), etc. However, due to the geometrical complexity of tree crops and the conditions of heterogeneity often encountered in the interested surfaces, micro-meteorological methods are inherently affected by uncertainties which are difficult to quantify. Sonic eddy covariance (SEC) is considered as the reference micrometeorological technique to directly measure the

latent heat and CO_2 fluxes. It is based on the use of high frequency (10 Hz) measurements of the three components of wind speed by means of sonic anemometers and concentrations of water vapour and CO_2 by means of fast optical gas analysers. These measurements are interpreted by considering the equations of turbulence in the atmospheric boundary layer (Foken, 2008). SEC has been intensively used in several locations around the world to monitor mass and energy exchanges in the soil-plant-atmosphere *continuum*, even in remote locations and for long time intervals. However, SEC systems are quite complex to operate and several alternative simpler methods have been developed in the context of water management (Paw U *et al*., 1995; Snyder *et al*., 1996, 1997).

Modern unsaturated soil water flow models can simulate the performance of various irrigation designs and can evaluate specific objectives such as stress management. Technical advances include more rigorous treatment of multidimensional soil water flow models and temporal patterns of root water uptake. The complexity of parameters needed to describe multidimensional root water uptake in heterogeneous media represents a severe constraint for the application of the modelling approaches. Experimental evaluations are still needed to assess the suitability of one-dimensional modelling approach based on the solution of Richards' equation for water flow in the soil-plant-atmosphere *continuum* to heterogeneous canopies and complex root geometry systems under irrigated conditions.

Remote sensing from satellite observations has been used for about three decades to monitor land surface patterns. Some reviews can be found in Norman *et al*. (1995) and Bastiaanssen *et al*. (1998). All these methods are based on the measurement of radiometric temperature of the surface to

evaluate crop evapotranspiration. The fundamental problem with using radiometric temperature in the energy balance of tree crops is that its value depends on the fraction of the radiometer view (pixel) that is occupied by scene elements with different temperatures (leaves, soil, stems, etc.); furthermore, this apparent scene composition depends on radiometer view angle. It is therefore important to evaluate separately the contribution of soil and canopy to the surface energy balance by means of the so-called "two-sources" approach of Norman *et al*. (1995). The use of remote sensing in the assessment of crop water requirements through the estimation of crop coefficients, K_c, from remotely sensed vegetation indices (VI_s) has a long development history. Heilman *et al*. (1982) exposed the possibility of reflectance derived VI_s to describe crop evolution. Choundhury *et al*. (1994) established a relation between normalized difference vegetation index (NDVI) derived from a radiative transfer model and a transpiration coefficient calculated for wheat. Johnson *et al*. (2003) have shown a significant correlation between NDVI and LAI (leaf area index) values in vines. Consoli *et al*. (2006a) also showed a linear relationship between NDVI and basal crop coefficient for orange orchard in semi-arid environments. Other relationships were reported for herbaceous crops, but using the soil adjusted vegetation index (SAVI) as the reference VI to relate with K_c (Duchemin *et al*. 2006; Er-Raki *et al*. 2007).

Therefore, accurate evapotranspiration data are crucial for irrigation management projects, especially in drought prone regions. As mentioned in the previous section of this paragraph, evapotranspiration rates can be estimated by micrometeorological methods, including the energy balance equation, mass exchange methods, etc. The most recognized methods used

for ET estimation are usually expensive, difficult to operate and some of them present problems for measurements in heterogeneous vegetation. Therefore, the search for accurate methods to estimate ET fluxes using low-cost, transportable and robust instrumentations is a subject of interest.

For example, the Eddy Covariance (EC) method is the commonly used micrometeorological technique providing direct measurements of latent heat flux (or evapotranspiration). It adopts a sonic anemometer to measure high-frequency vertical wind speed fluctuations around the mean and an infrared gas analyzer to measure high frequency water concentration fluctuations. These fluctuations are paired to determine the mean covariance of the wind speed and humidity fluctuations around the mean to directly estimate latent heat flux (LE). In the EC method, the sensible heat flux is also estimated using the covariance of the fluctuation in vertical wind speed and variations in temperature around their means. While the preferred method for measuring turbulent fluxes is the eddy covariance one, the lack of closure is unresolved and a full guidance on experimental set up and raw data processing is still unavailable.

Other energy balance approaches, such as the Bowen ratio and aerodynamic methods, have a sound theoretical basis and can be highly accurate for some surfaces under acceptable conditions.

Biometeorological measurements and theories identified large organized eddies embedded in turbulent flow, called “coherent structures”, as the entities which exchange water vapour, heat and other scalars between the atmosphere and plant communities.

Based on these studies, a new method for estimating scalar fluxes called Surface Renewal (SR) was proposed by Paw U and Brunet (1991). SR theory, in conjunction with the analysis of the observed ramp-like

patterns in the scalar traces, provides an advantageous method for estimating the surface flux density of a scalar. The method was tested with air temperature data recorded over various crop canopies. Results of the studies (Snyder *et al*., 1996; Spano *et al*., 1997; Consoli *et al*., 2006a; Castellví *et al*., 2008) have demonstrated good SR performance in terms of flux density estimations, well correlated to EC measurements. The approach has the advantages to (i) require as input only the measurement of scalar trace; (ii) involve lower costs for the experiment set-up, in respect to the EC method; (iii) operate in either the roughness or inertial sub-layers; (iv) avoid levelling, shadowing and high fetch requirements. Snyder *et al*. (1996) and Spano *et al*. (1997), however, have indicated that SR method currently requires an appropriate calibration factor, depending on the surface being measured.

Within this context of research, the aim of my PhD work was to investigate, develop and validate integrated approaches to better understand and quantify mass (water) and energy (solar radiation) exchange processes for one of the main tree crop species of the Mediterranean environment.

Different techniques for measuring evapotranspiration fluxes in orange orchard were developed and tested, starting from *in-situ* observations applied at different spatial scale (micrometeorology measurements, energy balance, sap flow method).

Furthermore, different easy to operate, low cost and affordable methods were implemented and tested for sensible heat flux (energy exchanges between the plant-atmosphere system) estimation, starting from SR theory.

The results of this study could allow the comprehension of the complex mass and energy exchange processes within the heterogeneous agricultural

context of Sicily. This could further facilitate the definition of suitable techniques and methodologies for the rational management of water resources under water scarcity conditions.

1.2 Objectives

The focus of my PhD study was to propose and develop innovative theoretical methods for evaluating the exchange of mass and energy within the soil-plant-atmosphere *continuum* of heterogeneous citrus stands in Sicily.

Different micrometeorological methods, mainly based on Surface Renewal theory, were studied and tested, in order to provide reliable and low cost estimates of sensible heat fluxes within the plant-atmosphere system.

Micrometeorological techniques were integrated with *in situ* measurements of transpiration by up-scaled sap flow techniques, physiological plant features (leaf area index, crop surface resistance, etc.), and microclimatic characteristics of the study area to define the evapotranspiration processes and address irrigation water scheduling towards water saving measures.

2 General concepts

2.1 Micrometeorology

Meteorology is a science that investigates an open system with a great number of atmospheric influences time-operating with changing intensity, and it is subdivided into branches. The main branches are theoretical meteorology, observational meteorology and applied meteorology; the latter includes weather prediction and climatology. Over the last 50 years, the applications of time and space scales became popular and subdivisions into macro-, meso- and micrometeorology were developed (Foken, 2008a).

Micrometeorology gives the theoretical, experimental and climatological basis for most of the applied parts of meteorology, which are related to the surface layer and the atmospheric boundary layer (Foken, 2008a). It is the branch of meteorology which deals with small-scale or micro-scale atmospheric phenomena and processes occurring in the lowest layer of the atmosphere, commonly called the atmospheric or planetary boundary layer (PBL) (Arya, 2005). So, it's not restricted to particular processes, but to the time and space scales of these processes, and the living environment of mankind is the main object of micrometeorological research (Foken, 2008a). Due to the coupling of time and space scales in the atmosphere, the relevant time scale of micrometeorology is less than the diurnal cycle (Foken, 2008a). Micrometeorology deals with all these earth-atmospheric exchange processes and the resulting vertical distributions (profiles) of mean wind, temperature, humidity and carbon dioxide. Micrometeorological measurements aim to capture the whole wide range of eddy motions, ranging from very rapid, random fluctuations to more organized, large eddy structures. They also include the various

components of the energy and the moisture budgets at or near the surface, including the active soil layer and the vegetation canopy layer (Arya, 2005).

The planetary boundary layer can be defined as the lowest part of the troposphere near the ground that is directly influenced by the presence of the Earth's surface and responds to surface forcings with a timescale of about an hour or less. These forcings include frictional drag, evaporation and transpiration, heat transfer, pollutant emission and terrain induced flow modification (Stull, 1988). Its thickness varies over a wide range (several tens of meters to several kilometres) and depends on the rate of heating or cooling of the surface, strength of winds, the roughness and topographical characteristics of the surface, large-scale vertical motion, horizontal advection of heat and moisture, the presence of low-level clouds in the PBL and other factors. In response to the strong diurnal cycle of heating and cooling of land surfaces during fair-weather conditions, the PBL height increases and decreases between its lowest typical value of the order of 100 m (range ~ 20÷500 m) in the morning to the highest value of the order of 1 km (range ~ 0.2÷5 km) during late afternoon. Mean winds, temperatures and other properties, as well as turbulent fluxes, also exhibit strong diurnal variations. Diurnal variations of the PBL height and other properties are found to be considerably smaller or almost absent over large lakes, seas and oceans, as well as over high latitude land areas during winter (Arya, 2005). Over oceans, the boundary layer depth varies relatively slowly in space and time. Over both land and oceans, the general nature of boundary layer is to be thinner in high-pressure regions than in low-pressure regions. Over land surfaces in high-pressure regions the boundary layer has a well defined structure that evolves with the diurnal

cycle (Fig. 2.1). The three major components of this structure are the mixed layer, the residual layer, and the stable boundary layer. When clouds are present in the mixed layer, it is further subdivided into a cloud layer and a sub-cloud layer. The surface layer is the region at the bottom of the boundary layer where turbulent fluxes vary by less than 10% of their magnitude. Thus, the lowest 10% of the boundary layer is called the surface layer, regardless of whether it is part of a mixed layer or stable boundary layer (Stull, 1988). It is one of the main energy-exchange layers of the atmosphere and, accordingly, the transformations of solar energy into other forms of energy are an important subject of micrometeorology. Furthermore, the surface layer is a source of friction, which causes a drastic modification of the wind field and the exchange processes between the Earth's surface and the free atmosphere (Foken, 2008a).

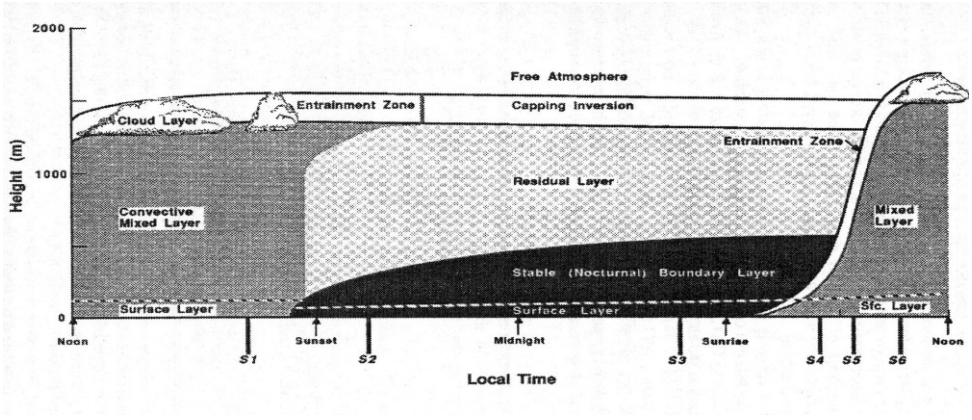

Fig. 2.1. The boundary layer in high pressure regions consists of three major parts: a very turbulent mixed layer; a less-turbulent residual layer containing former mixed-layer air; a nocturnal stable boundary layer of sporadic turbulence. The mixed layer can be subdivided into a cloud layer and a sub-cloud layer (Stull, 1988).

The surface layer is also called the constant flux layer because of the assumption of constant fluxes with height within the layer. This offers the

possibility to estimate, for example, the fluxes of sensible and latent heat in this layer while in the upper layers flux divergences dominate (Foken, 2008a).

The atmospheric boundary layer has a large degree of turbulence; only within a few millimetres above the surface the molecular exchange processes dominate (Foken, 2008a). Indeed, a thin layer called a microlayer or interfacial layer has been identified in the lowest few centimetres of air, where molecular transport dominates over turbulent transport (Stull, 1988). Since the turbulent processes are about 10^5 fold more effective than molecular processes and because of the assumption of a constant flux, the linear vertical gradients of properties, very close to the surface, must be very large. Between this molecular boundary layer (term used for scalars) or laminar boundary layer (term used for fluids) and the turbulent layer, a viscous sublayer (buffer layer) exists with mixed exchange conditions and a thickness of about 1 cm. According to similarity theory of Monin and Obukhov (1954), a layer with a thickness of approximately 1 m (dynamical sublayer) is not influenced by the atmospheric stability – this layer is nearly neutral in time (Foken, 2008a).

Although the PBL comprises only a tiny fraction of the atmosphere, the small-scale processes occurring within the PBL, especially in the surface layer, provide most of the energy and moisture exchanges between the surface and the atmosphere which are vital to the evolutions of mesoscale and large-scale weather. Almost one-half of the dissipation of the atmospheric kinetic energy on an annual basis occurs within the PBL. Thus, an accurate parameterization of land-surface and PBL exchange processes is considered an important part of the current weather forecasting and climate models (Arya, 2005).

Above the boundary layer lays a mostly statically-stable layer (inversion) with intermittent turbulence. The exchange processes between the atmospheric boundary layer and the troposphere take place in the entrainment zone; the thickness of this layer is approximately 10% of the atmospheric boundary layer (Foken, 2008a).

The daily cycle in the PBL is highly variable. After sunrise, the atmosphere is warmed by the turbulent heat flux from the ground surface, and the inversion layer formed during the night brakes up. The new layer is very turbulent, well mixed (mixed layer) and bounded above by an entrainment zone (Foken, 2008a). The turbulence in the mixed layer is usually convectively driven; convective sources include heat transfer from a warm ground surface, and radiative cooling from the top of the cloud layer. The mixed layer reaches its maximum depth in late afternoon. About a half hour before sunset the thermals cease to form (in the absence of cold air advection), allowing turbulence to decay in the formerly well-mixed layer. The resulting layer of air is sometimes called the residual layer because its initial mean state variables and concentration variables are the same as those of the recently decayed mixed layer (Stull, 1988). The residual layer is capped by a free (capping) inversion (the upper border of the boundary layer) (Foken, 2008a). As the night progresses, the bottom portion of the residual layer is transformed by its contact with the ground into a stable boundary layer. This is characterized by statically stable air with weaker, sporadic turbulence. Although the wind at ground level frequently becomes lighter or calm at night, the winds aloft may accelerate to supergeostrophic speeds in a phenomenon that is called the low-level jet or nocturnal jet. The stable air tends to suppress turbulence, while the developing nocturnal jet enhances wind shears that tend to generate

turbulence. As a result, turbulence sometimes occurs in relatively short bursts that can cause mixing throughout the stable boundary layer. During the non-turbulent periods, the flow becomes essentially decoupled from the surface. As opposed to the daytime mixed layer which has a clearly defined top, the stable boundary layer has a poorly defined top that smoothly blends into the residual layer above. The top of the mixed layer is defined as the base of the stable layer, while the stable boundary layer top is defined as the top of the stable layer or the height where turbulence intensity is a small fraction of its surface value. Stable boundary layers can also form during the day, as long as the underlying surface is colder than the air. These situations often occur during warm-air advection over a cold surface, such as after a warm frontal passage or near shorelines (Stull, 1988). After sunrise, the developing mixed layer quickly destroys the stable boundary layer and the residual layer. On cloudy days and in winter, when the solar radiation and the energy transport to the surface are weak, the mixed layer will not disturb the residual layer and the boundary layer is generally stratified. On days with strong solar radiation, the boundary layer structure will be destroyed by convective cells, which develop some 10 m above the ground. These cells have relatively small upwind cells, relatively high vertical wind speeds, and typically develop over large areas with uniform surface heating. This is according to model studies over areas which are larger than 200-500 m^2 (Foken, 2008a).

The vertical distribution of air temperature in the PBL depends on the surface temperature, air temperature at the top of the PBL, the surface heat flux, divergence or vertical gradient of sensible heat flux, divergence of net radiation, horizontal and vertical advections of heat by mean motions, entrainment of free-atmospheric air into the PBL, and local heating or

cooling associated with phase changes of H_2O during cloud condensation or evaporation processes. An 'ideal' surface may be expected to have a well defined surface temperature, which is determined by the surface energy budget, thermal properties of the surface and the subsurface medium, and the air mass characteristics affecting the PBL (Arya, 2005).

The vertical distribution of specific humidity in the PBL depends on the type of surface and its moisture content, the rate of evapotranspiration from the surface, specific humidity of air mass above the PBL, advection of moisture by mean motions, and local evaporation and cloud condensation processes within the PBL (Arya, 2005).

Atmospheric motions in the PBL are found to be generally turbulent, although in very stable conditions turbulence is often weak, highly intermittent, and sometimes mixed with internal gravity waves. Turbulence is manifested in the form of very irregular, almost random, three-dimensional fluctuations around some mean motion. The PBL turbulence is also characterized by its efficient mixing, diffusive and dissipative properties, as well as by a wide range of scales and eddies (e.g., length scales from 10^{-3} to 10^{4} m) (Arya, 2005).

Using Reynolds' decomposition, any variable in a turbulent flow can be expressed as the sum of its mean and turbulent fluctuation. A statistical description is used to describe the properties of individual fluctuating variables (with zero means) and their correlations with other variables, either at the same time and location in space, or with separations in time and space. All the sophisticated statistical measures, such as probability, correlation and spectrum functions of space and time series of randomly fluctuating variables, are often utilized in the analysis and description of turbulence (Arya, 2005).

Measurements of turbulence in the PBL indicate that turbulence intensities are typically less than 10% in the stable boundary layer, 10-20% in the near-neutral planetary boundary layer, and greater than 20% in the convective boundary layer. Turbulence intensities are generally largest near the surface and decrease with height as mean wind speed increases and fluctuation levels decrease (Arya, 2005).

Each of the three broad categories into which air flow, or wind, can be divided (mean wind, turbulence, waves) can exist in the planetary boundary layer; each can exist separately, or in the presence of any of the others. Transport of quantities such as moisture, heat, momentum and pollutants is dominated in the horizontal by the mean wind, and in the vertical by turbulence. Mean wind is responsible for very rapid horizontal transport, or advection. Friction causes the mean wind speed to be slower near the ground. Vertical mean winds are much smaller than horizontal winds. Waves, which are frequently observed in the night-time boundary layer, transport little heat, humidity and other scalars such as pollutants. They are, however, effective at transporting momentum and energy. These waves can be generated locally by mean-wind shears and by mean flow over obstacles. Waves can also propagate from some distant source, such as a thunderstorm or an explosion. The relatively high frequency of occurrence of turbulence near the ground is one of the characteristics that makes the boundary layer different from the rest of atmosphere. Turbulence, the gustiness superimposed on the mean wind, can be visualized as consisting of irregular swirls of motion called eddies. Usually turbulence consists of many different size eddies superimposed on each other. The relative strengths of these different scale eddies define the turbulence spectrum. Much of the boundary layer turbulence is generated

by forcings from the ground (i.e., solar heating, frictional drag, obstacles) (Stull, 1988).

2.2 Energy Balance at the Earth's surface

The Earth's surface is the main energy transfer area for atmospheric processes. It is heated by the shortwave down-welling radiation from the sun and only a part of this radiation is reflected back. Furthermore, the surface absorbs longwave down-welling radiation due to longwave emission by clouds, particles and gases. The absorbed energy is emitted only partly into the atmosphere as longwave up-welling radiation. In the total balance, the Earth's surface receives more radiation energy than that lost (i.e., the net radiation at the ground surface is positive). The surplus of supplied energy will be transported back to the atmosphere due to two turbulent energy fluxes: the sensible heat flux and the latent heat flux. Furthermore, energy is transported into the soil due to the ground heat flux and will be stored by plants, buildings, etc. The sensible heat flux is responsible for heating the atmosphere from the surface up to some 100 m during the day, except for days with strong convection (Foken, 2008a).

Using the principles of the energy conservation at an 'ideal' surface, which is assumed to be flat, bare, extensive and opaque to radiation, the surface energy budget can be expressed as

$$R_N = H + \lambda E + G \tag{2.1}$$

in which R_N is the net radiation, H is the sensible heat flux density, λE is the latent heat flux density to or from the atmosphere and G is the soil heat flux density to or from the subsurface medium (Kidston *et al*., 2010). All the fluxes are normal to the surface and can be expressed in the SI units of W m^{-2} or J $s^{-1}m^{-2}$ (Arya, 2005). It is a convention that radiation and energy

fluxes are positive if they transport energy away from the Earth's surface (into the atmosphere or into the ground), otherwise they are negative (Foken, 2008a).

The net radiation is the sum of the shortwave down-welling radiation mainly from the sun (global radiation) and transmitted through the air, the longwave down-welling diffusive infrared (heat) radiation emitted by clouds, aerosols and gases, the shortwave up-welling reflected (solar) radiation, and the longwave up-welling infrared (heat) emitted radiation (Foken, 2008a; Stull, 1988). In general, the up-welling longwave radiation is greater than the down-welling longwave radiation, since Earth's surface is warmer than clouds and aerosols. It is only in the case of fog that up-welling and down-welling radiations are equal. The down-welling radiation may be greater if clouds appear in a previously clear sky and the ground surface has cooled (Foken, 2008a).

The soil heat flux at the surface can be estimated as

$$G = G_T + \Delta S \tag{2.2}$$

where G_T is the conductive heat flux measured by soil heat flux plates placed in the first 10 cm below the soil surface and ΔS is the rate of heat storage change in the layer between the heat flux plates and the surface (Foken, 2008a; Kidston *et al.*, 2010).

All the components of the surface energy budget show strong diurnal variations, in response to the diurnal variation of net radiation and the diurnal cycle of heating and cooling of the surface. They also show large seasonal variations. Both the diurnal and seasonal variations are dependent on the latitude, the surface characteristics including thermal properties such as albedo and emissivity, and prevailing weather conditions. The ratios H/R_N, $\lambda E/R_N$ and G/R_N, which represent relative partitioning of net

radiation, are expected to show much less variability than the individual fluxes. Empirical estimates of these ratios for different types of surfaces can be used to parameterize other energy fluxes in terms of R_N.

In many aspects the Earth's surface may not be considered 'ideal,' because it is very rough and may be covered by vegetation, buildings and water, which are not opaque to radiation. For such vegetation and urban canopies, as well as water layers, which may store or release energy, the following energy budget equation for a near-surface layer is more appropriate:

$$R_N = H + \lambda E + G + Q \tag{2.3}$$

where Q is the sum of storage fluxes from any other energy sinks or sources, e.g. photosynthesis and change in the above-ground biomass heat storage; it represents the change in the energy storage in the layer per unit time, per unit horizontal area, which can be expressed in terms of the average rate of warming or cooling of the layer and its thickness (Arya, 2005; Kidston *et al*., 2010).

Net radiation (R_N) at the Earth's surface is either absorbed into the ground in the form of ground heat flux (G), or transferred to the atmosphere in the form of sensible (H) and latent heat (λE) flux (Twine *et al*., 2000).

The surface energy balance is closed when the energy flux into a system is equal to the energy flux leaving the system, i.e. $R_N - G = H + \lambda E$ (Kidston *et al*., 2010). Closure is one tool used to quantify the reliability and accuracy with which these components of the surface energy budget are measured. Unfortunately, most field measurements have failed to show closure of the surface energy budget (Twine *et al*., 2000).

Analyses of numerous datasets obtained over various surface types have shown that the total surface-layer heat flux ($H + \lambda E$) is often about 70–90% of the available energy flux ($R_N - G$) (Kidston *et al*., 2010). In most cases, the sum of the net radiation and the ground heat flux was found to be larger than the sum of the turbulent fluxes of sensible and latent heat. The problem cannot be described only as an effect of statistically distributed measuring errors because of the clear underestimation of turbulent fluxes or overestimation of the available energy (Foken, 2008b).

Several explanations for this systematic imbalance have been hypothesized including different source locations for ($H + \lambda E$) versus ($R_N - G$), measurement errors, neglected energy sinks, loss of low- or high-frequency contributions to the turbulent fluxes contained within ($H + \lambda E$), and neglected transport processes of the surface-layer fluxes (Kidston *et al.*, 2010).

In 1998, several reasons for lack of closure of the surface energy budget have been discussed by Mahrt and may include the following: (1) lack of coincidence of the source areas among various flux components measured very close to a surface such as evaporation from leaves and sensible heat from a hot, dry soil surface; (2) flux divergence arising from transport that is not one-dimensional such as insufficient fetch; (3) non-stationarity of measured time series over the typical 30 min averaging periods so that covariance arising from very low frequency fluctuations is missed; (4) turbulent dispersive fluxes arising from organized planetary-boundary-layer circulations that may have preferred locations so that the mean vertical velocities at an instrument location may be systematically different from zero rising the vertical advective flux; and (5) measurement errors related to sensor separation, frequency response, alignment

problems, and interference from tower or instrument-mounting structures. The accuracy of the surface energy fluxes measurements can be assessed, to increase confidence in the evaluation, by: (1) evaluating the closure of the surface energy balance using independent measurements of all the components of the energy budget and (2) comparing measurements at the same time and same site using Eddy Covariance (EC) and Bowen Ratio (BR) instrumentation. Closure can be quantified using $D = [H + \lambda E] / [R_N - G - Q]$ or specified as a residual flux density, ε. Agreement between two independent methods for measuring surface fluxes increases confidence in both approaches; therefore, comparisons between the EC and BR methods are valuable. The BR method, which is based on measurements of temperature and vapour pressure gradients, provides estimates of H and λE that are independent of the EC method even though R_N, G and Q would not be independent. Because the BR method assumes closure of the energy budget to solve for H and λE, differences between BR and EC methods include the lack of closure issue with the EC method along with differences of measured Bowen-ratios (Twine *et al*., 2000).

Currently, there is still no common opinion on the causes of the heat imbalance in the atmospheric boundary layer, and the various hypotheses mainly reduce to instrumental or methodological errors (Panin and Bernhofer, 2008). Thus, reasons for the imbalance are partly the relatively large errors of the single components of the energy balance equation and the use of different measuring methods. The single terms of the energy balance equation are not measured directly at the surface, but either in the air above or in the soil. Furthermore, the information of the measured fluxes comes from different source areas. This is very critical for the turbulent fluxes where the measurement is connected with large areas

according to the footprint (that is the effective area of influence; the underlying surface upwind of the sensor). The energy balance equation is the basis for most atmospheric models. Therefore, the energy balance closure problem is still an ongoing issue of research to validate models with experimental data (Foken, 2008a).

Anyway, it has been shown that the heat imbalance is caused not by experimental (instrumental) errors, but has a conceptual origin. The main reason is that the modern methods of measuring and calculating the surface fluxes between the natural land surface and the atmosphere rely upon the theories based on the stationarity and horizontal homogeneity (SHH) hypothesis. In recent years, however, measurements of surface fluxes are often conducted over inhomogeneous surfaces. The SHH conditions break down in such measurements, and the air flow moving over surface inhomogeneities (aerodynamic roughness, albedo, LAI, soil moisture, temperature, etc.) develops new internal boundary layers (coherent structures), which generate an additional contribution of energy to the spectra and cospectra of surface fluxes (Panin and Bernhofer, 2008).

As hypothesis, the energy balance closure problem can be assumed as a scale problem and a closure is only possible on a landscape scale, including the turbulent exchange of the smaller eddies with the classical eddy covariance method and exchange of larger eddies, which can be up to now only measured with area-averaging measuring systems like scintillometers or airborne sensors (Foken, 2008b).

Furthermore, in literature it was found that time-averaged fluxes (Finnigan *et al*., 2003) or spatially averaged fluxes including turbulent organized structures (Kanda *et al*., 2004) can close the energy balance.

Since instrument error, changes in surface heterogeneity and fetch can affect measurements of closure of the surface energy balance, one way to identify systematic problems associated with closure is to evaluate the performance of collocated, independent measurement systems. Eddy Covariance (EC) and Bowen Ratio (BR) methods are two such independent systems for measuring surface fluxes (Brotzge and Crawford, 2003).

If field measurements of surface fluxes are not consistent with energy balance equation, then modellers will have to make adjustments to the measured fluxes or accept uncertainties in their models that are of the same magnitude as the measured energy conservation discrepancy (Twine *et al*., 2000).

2.3 The Soil-Plant-Atmosphere Continuum

Facing atmosphere constitutes an extraordinary challenge for each plant. On the one hand atmosphere is the source of carbon dioxide (CO_2) that is necessary for the photosynthetic process, on the other hand it is quite dry compared to plant tissues and can easily dehydrate and wither plants. In order to minimize water losses even maximizing CO_2 absorption, plants have developed adaptations processes. In particular, they can control water loss from their leaves and at the same time they can substitute that one lost into the atmosphere. However, the problem gets worse because of the leaf area, since a bigger one maximize solar radiation interception and provides a continuous CO_2 absorption. So, water conservation need contrasts with CO_2 assimilation need. To solve this vital contrast, terrestrial plants have been structured with: a very branched and extended root system to extract water from the soil; a way between root system and

leaves inside a low resistance conductive tissue, the xylem; a hydrophobic cuticle around leaves to minimize evaporation; microscopic openings in each leaf (the stomata) allowing gaseous exchange with the outside (especially CO_2, O_2, H_2O); highly specialized cells (guard cells) regulating stomata diameter. This morpho-physiological adaptation makes the plant an organism transporting water from the soil towards the atmosphere just in response to physical forces. Plants don't directly use any type of energy to transport water, even if developing and maintaining the above mentioned structures need a certain energetic consumption (Mugnai, 2004).

For all these features, plant can be considered as a continuous hydraulic system that links water in the soil to water vapour in the atmosphere. At each point of this system, water content can be described by the 'water potential' (Ψ_w) thermodynamic measurement that expresses the water energy state. It is a convention that pure water at 25 °C temperature and 0,1 MPa atmospheric pressure has Ψ_w equal to zero. In plant tissues, Ψ_w may be separated in two components: turgor potential (Ψ_P) and osmotic potential (Ψ_O); their relationship can be expressed by the equation $\Psi_W = \Psi_P + \Psi_O$. On the one hand, Ψ_P represents the pressure component of cellular water potential and results from hydrostatic pressure into the cells. It usually assumes positive values, Ψ_P intensity depending on cell wall elasticity (ε). On the other hand, Ψ_O is based on solute concentration in water. Intracellular water contains high solute quantities that are able to move osmotic potential until the extreme value of -5 MPa (about twice the sea water one). Even the soil water state can be described through the matrix potential (Ψ_S) concept (Mugnai, 2004).

Similarly to an electric circuit, water flow in a plant can be described through a potential, resistance and capacitance network (Fig. 2.2).

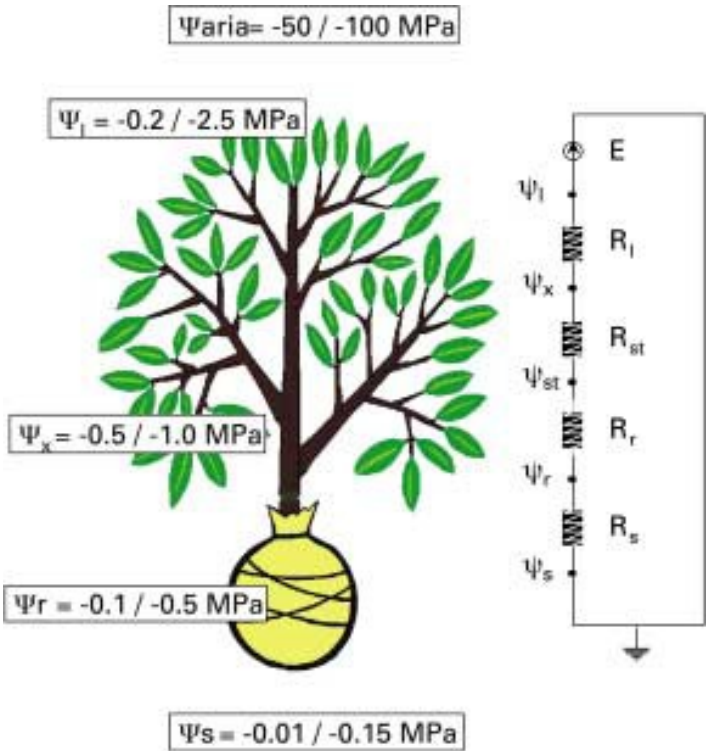

Fig. 2.2. Scheme of potential, resistance and capacitance network for a plant water flow. Ψ_s is the soil water potential, Ψ_r the root water potential, Ψ_x the xylematic water potential, Ψ_l the leaf water potential, Ψ_{aria} the atmosphere water potential, R_s the soil resistance, R_r the root resistance, R_{st} the trunk resistance, R_l the leaf resistance, E the outside environment (Mugnai, 2004).

The potential gradient in the soil-plant-atmosphere *continuum* (SPAC) is the force leading water transport through the plant: water flow will move from a high (less negative) water potential point to a lower (more negative) water potential point. So, water flow will normally follow the direction from the soil ($\Psi_S = -0.01 \div -0.15 MPa$) towards the atmosphere ($\Psi_{atm} = -50 \div -100 MPa$) going through the plant (Mugnai, 2004).

Although not exactly analogous, comparisons between the soil–plant–atmosphere *continuum* and the flow of electricity through a resistance network has enhanced our understanding of the system (Coelho *et al*., 2003). Therefore, water movement through the SPAC is treated as a continuous process analogous to the flow of electricity in a conducting system and it is described by an analog of Ohm's Law, where Flow = Difference in water potential/Resistance. This is a logical extension of the cohesion theory of the ascent of sap (Kramer, 1974).

Soil water flow to plant roots has been studied by a great number of researchers. The microscopic approach considered the radial flow of water to a single root, and the macroscopic or whole root system approach assumed the soil-root system to be a continuum in which water flow is essentially one-dimensional flow. One of the greatest difficulties is to estimate the resistances along the pathway. In general, the resistance to water flow in the rhizosphere and within the roots is calculated using empirical equations (Coelho *et al*., 2003).

The SPAC approach provides a useful, unifying theory in which water movement through soil, roots, stems and leaves, and its evaporation into the air can be treated in terms of the driving forces and resistances operating at each stage. It also provides a model useful to investigators in analyzing the importance of various factors affecting water movement. Actually it is an oversimplification, because it assumes steady state conditions which seldom exist, and constant resistances, whereas root resistance appears to vary with rate of water flow. Furthermore, complications occur because movement in the liquid phase is proportional to difference in water potential ($\Delta\psi$) and movement in the vapour phase is proportional to the gradient in vapour pressure or water vapour

concentration. However, these are minor problems compared to the overall usefulness of the concept (Kramer, 1974).

3 Micrometeorological approaches for actual evapotranspiration measurement and estimation

From an energetic point of view, evapotranspiration can be considered as equivalent to the energy employed for transporting water from the inner cells of leaves and plant organs and from the soil to the atmosphere. In this case, it is called latent heat (λE, with λ latent heat of vaporization equal to 2.45×10^6 J kg^{-1} at 20 °C) and is expressed as energy flux density (W m^{-2}). Under this form, evapotranspiration (ET) can be measured with the so called micrometeorological methods. These techniques are physically-based and depend on the laws of thermodynamics and of the transport of scalars into the atmosphere above the canopy. For applying the micrometeorological methods, it is usually necessary to accurately measure meteorological variables on a short temporal scale with sensors and suitable equipment placed above the canopy (Katerji and Rana, 2008).

There are a great variety of methods for measuring ET; some methods are more suitable than others because of their accuracy or cost or because they are particularly suitable for given space and time scales (Katerji and Rana, 2008).

Due to the conservative hypothesis of all the flux densities above the crop, the micrometeorological methods can be applied only on large flat surfaces with uniform vegetation. As a consequence, three conditions should be accurately analysed before using these techniques in the Mediterranean semi-arid region: i) advection, i.e. the contribution of supplementary energy (under the form of heat) from the dryer surrounding surfaces to the cropped surface by means of horizontal fluxes. This contribution increases the energy available for evapotranspiration; ii) since

the energy fluxes must be conservative, they can only be measured up to the height of the so-called internal boundary layer, i.e. the layer of air downwind of the leading edge affected by canopy. It interferes in particular through two parameters: the height of the canopy and its roughness length; iii) the position of the sensors above the canopy. They should be placed close enough to the canopy so to be inside the internal boundary layer, and far enough from the canopy allowing to appreciate larger gradients (Katerji and Rana, 2008).

Micrometeorological methods for measuring or estimating actual crop evapotranspiration are generally referred to a plot scale.

3.1 Eddy Covariance method

The transport of scalar (vapour, heat, CO_2) and vectorial quantities (momentum) is mostly governed by air turbulence in the low atmosphere in contact with the canopies (Katerji and Rana, 2008). The Eddy Covariance (EC) method is a direct measure of a turbulent flux density of a scalar across horizontal wind streamlines (Paw U *et al*., 2000). It is very accurate with a large time resolution. However, it needs also the most comprehensive knowledge and great experimental effort (Foken, 2008a); some disadvantages include sensitivity to fetch and high cost and maintenance requirements (Brotzge and Crawford, 2003).

The calculation of turbulent fluxes is based on the Navier-Stokes equation and similar equations for temperature or gases by the use of the Reynolds' postulates. The equations for determination of surface fluxes are obtained by further simplifications. These are:

– stationarity of the measuring process, i.e. $\delta X / \delta t = 0$ (X represents the horizontal wind velocity u, the vertical wind velocity w, the temperature T and so on; t is the time);

– horizontal homogeneity of the measuring field, i.e. $\delta X / \delta x = 0$ and $\delta X / \delta y = 0$ (x is the component into the direction of the mean wind, and y is the component perpendicular to x);

– validity of the mass conservation equation, i.e. $\delta w / \delta z = 0$ and $\overline{w} = 0$ (z the height);

– negligible density flux, i.e. $\rho' / \rho << 1$ (with ρ the air density);

– statistical assumptions, for example statistical independence and the definition of the averaging procedure;

– the Reynolds' postulates $\overline{a'} = 0$, $\overline{ab'} = 0$, $\overline{ab} = \overline{a} \cdot \overline{b}$ and the postulate which is used for the calculation of the eddy covariance method $\overline{ab} = \overline{a} \cdot \overline{b} + \overline{a'b'}$ should be valid;

– the momentum flux in the surface layer as well as the temperature flux (analogue equations for water vapour and gaseous fluxes) doesn't change with the height within about 10% to 20% of the flux (Foken and Wichura, 1996).

The vertical component of the fluctuating wind is responsible for the flux across a plane above a horizontal surface. Since there is a net transport of energy across the plane, there will be a correlation between the vertical wind component and temperature or water vapour. For example, if water vapour is released into the atmosphere from the surface, updrafts will contain more vapour than downdrafts, and vertical velocity (positive upwards) will be positively correlated with vapour content (Drexler *et al*., 2004).

The EC method is based on direct measurements of the product of vertical velocity fluctuations (*w'*) and scalar concentration fluctuations (*c'*) yielding a direct estimate of H and λE assuming that the mean vertical velocity is negligible. It provides estimates of H and λE separately, so that, when combined with measurements of R_N and G, all the major components of the energy balance are independently measured (Twine *et al*., 2000).

So, a direct method for measuring the latent heat flux above a vegetative surface over a homogeneous canopy is to measure simultaneously vertical turbulent velocity and specific humidity fluctuations and to determine their covariance over a suitable sampling time. With these measurements, theory predicts that fluxes from the surface can be measured by correlating the vertical wind fluctuations from the mean (*w'* in m s^{-1}) with the fluctuations from the mean in concentration of the transported water vapour (*q'* in kg m^{-3}). So that, for latent heat we can write the following covariance of vertical wind speed and vapour density:

$$\lambda E = \lambda \overline{w'q'} \tag{3.1}$$

If we take measurements of the instantaneous fluctuations of vertical wind speed *w'* and humidity *q'* at a frequency sufficient for obtaining the contribution from all the significant sizes of eddy, by summing their product over a hourly time scale, the above equation calculates the actual crop evapotranspiration. A representative fetch (distance from the canopy edge) is required; fetch to height ratios of 100 are usually considered adequate, but longer fetches are desirable. To measure ET with this method, vertical wind fluctuations must be measured and acquired at the same time as the vapour density. The first one can be measured by a sonic

anemometer; the second one by a fast response hygrometer (Katerji and Rana, 2008).

The sensible heat, H, using the EC technique by analogy with the expression above (Eq. 3.1), can be written as

$$H = \rho c_p \overline{w'T'} \tag{3.2}$$

with ρ the air density and c_p the specific heat of air at a constant pressure. The wind speed and temperature fluctuations are measured by means of sonic anemometer and fast response thermometer, respectively (Katerji and Rana, 2008), so that the EC method requires sensitive, expensive instruments to measure high-frequency wind speeds and scalar quantities (Foken, 2008a).

Sensor must measure vertical velocity, temperature and humidity with sufficient frequency response to record the most rapid fluctuations important to the diffusion process. Typically, a frequency of the order of 5-10 Hz is used, but the response-time requirement depends on wind speed, atmospheric stability and the height of the instrumentation above the surface. Outputs are sampled at a sufficient rate to obtain a statistically stable value for the covariance (Drexler *et al*., 2004). If a 30-minute sampling time is used over the whole day, then remarkable errors will be reduced (Foken, 2008a).

Wind speed and humidity sensors should be installed close to each other but sufficiently separated to avoid interference. When the separation is too large, underestimation of the flux may result. High-frequency wind vector data are usually obtained with a triaxial sonic anemometer. The triaxial instruments provide the velocity vector in all three directions and, therefore, corrections can be applied for any tilt in the sensor and mean streamline flow. A wide range of humidity sensors have been used in EC

systems including thermocouple psychrometers, Lyman-alpha and krypton hygrometers, laser-based systems and other infrared gas analysers (Drexler *et al*., 2004). Since the size of the turbulence eddies increases with distance above the ground surface, both the measuring path length and the separation between a sonic anemometer and an additional device (e.g. hygrometer) depend on the height of measurement. These additional instruments should be mounted downwind of the sonic anemometers, 5-10 cm below the measuring path. Therefore, to reduce the corrections of the whole system the measurement height must be estimated on the basis of both the path length of the sonic anemometer and the separation of the measuring devices. Also, the measuring height should be twice the canopy height in order to exclude effects of the roughness sublayer (Foken, 2008a).

The Eddy Covariance technique is the most direct method for quantifying the turbulent exchange of energy and trace gases between the Earth's surface and the atmosphere (Mauder *et al*., 2010). However, the derivation of the mathematical algorithm is based on a number of simplifications so that the method can be applied only if these assumptions are exactly fulfilled. The quality of the measurements depends more on the application conditions and the exact use of the corrections than on the available highly sophisticated measuring systems. Therefore, experimental experience and knowledge of the special atmospheric turbulence characteristics have a high relevance. The most limiting conditions are: horizontally homogeneous surfaces and steady-state conditions (Foken, 2008a). These requirements are often violated in complex terrain, and their non-fulfilment reduces the quality of the measurement results. Foken and Wichura (1996) address this problem by assigning quality flags to the

fluxes in accordance with the deviations found between parameterisations under ideal conditions and those actually measured. Secondly, in a heterogeneous environment the land use types contributing to the measurements change with the source area of the fluxes. This source area, which can be calculated by footprint models, defines the region upwind of the measurement point which influences the sensor's measurements and is dependent on measurement height, terrain roughness, and boundary layer characteristics, such as the atmospheric stability. As most sites in monitoring networks are set up to measure fluxes over a specific type of vegetation, the changing contribution of this type of land use, under different meteorological conditions, has to be considered in order to assess how representative the measurements are (Göckede *et al*., 2004).

The latter can lead to a bias of the flux estimate that becomes apparent in a lack of energy balance closure, usually ranging between 10 and 30% of the available energy at the surface. Several large-eddy simulations (LESs) support the thesis that single-tower eddy-covariance measurements, using temporal averaging, cannot completely represent the actual surface flux. According to these studies, the resulting flux bias depends on several factors, such as wind speed, measurement height, averaging time, degree of horizontal heterogeneity and atmospheric stability. Large-eddy simulation results show that the entire flux can be captured if spatial instead of, or in addition to, temporal averaging is applied when calculating the covariance (Mauder *et al*., 2010).

It is possible to minimize the deviation between actual and measured EC fluxes through an optimal equipment configuration and through application of adequate correction methods. The typical steps are: tilt correction, buoyancy correction (also Schotanus correction), density

correction (also WPL correction, see Webb *et al*. 1980) and damping (attenuation) correction (Spank and Bernhofer, 2008).

The application of correction methods is closely connected with the data control; it starts with the exclusion of missing values and outliers. A basic condition for applying the EC method is the assumption of a negligible mean vertical wind component; otherwise advective fluxes must be corrected. This correction is called tilt correction and includes the rotation of a horizontal axis into the mean wind direction. The first correction is the rotation of the coordinate system around the *z*-axis into the mean wind. The second rotation is around the new *y*-axis until the mean vertical wind disappears. With these rotations, the coordinate system of the sonic anemometer is moved into the streamlines (Foken, 2008a).

The most commonly applied technique for determining the angles necessary to place the sonic anemometer into a streamwise coordinate system involves a series of two rotations, applied at the end of each turbulent averaging period. The first rotation sets $\bar{v} = 0$ by swinging the *x* and *y*-axes about the *z*-axis so that the new velocities are given by

$$u_1 = u_m \cos\theta + v_m \sin\theta \tag{3.3}$$

$$v_1 = -u_m \sin\theta + v_m \cos\theta \tag{3.4}$$

$$w_1 = w_m \tag{3.5}$$

where

$$\theta = \tan^{-1}\left(\frac{\bar{v}_m}{\bar{u}_m}\right) \tag{3.6}$$

and where subscript *m* is for ‘measured’ and subscript *1* denotes the velocities after the first rotation. The second rotation sets $\bar{w} = 0$ by

swinging the new *x* and *z*-axes about *y* so that the *x*-axis points in the mean streamline direction. The final velocities are then given by

$$u_2 = u_1 \cos\phi + w_1 \sin\phi \tag{3.7}$$

$$v_2 = v_1 \tag{3.8}$$

$$w_2 = -u_1 \sin\phi + w_1 \cos\phi \tag{3.9}$$

where

$$\phi = \tan^{-1}\left(\frac{\overline{w}_1}{\overline{u}_1}\right) \tag{3.10}$$

The above double rotation aligns the *x*-axis with the mean wind vector, but allows the *y* and *z*-axes to freely rotate about *x*. That is, there are an infinite number of anemometer rotations that simultaneously satisfy $\overline{v} = \overline{w} = 0$. The anemometer's final orientation in the *y*-*z* plane after the double rotation depends on its initial orientation (Wilczak *et al*., 2001).

This very commonly used method, involving a double rotation of the anemometers' axes, is shown to result in significant run-to-run stress errors due to the sampling uncertainty of the mean vertical velocity (Wilczak *et al*., 2001).

The previous analysis shows that if the error in the *y*-*z* plane is only 1 degree then the error in $\overline{vw}$ can be of the same order as the true stress. Over land, a third sonic rotation can be applied to remove this ambiguity by requiring that $\overline{vw} = 0$. In this step the new *y* and *z*-axes are rotated around *x* until the cross-stream stress becomes zero, and the third set of rotation equations then become

$$u_3 = u_2 \tag{3.11}$$

$$v_3 = v_2 \cos\psi + w_2 \sin\psi \tag{3.12}$$

$$w_3 = -v_2 \sin\psi + w_3 \cos\psi \tag{3.13}$$

where

$$\psi = \tan^{-1}\left[\frac{2\overline{v_2 w_2}}{\left(\overline{v_2^2} - \overline{w_2^2}\right)}\right] \tag{3.14}$$

This alternative method, requiring a triple rotation of the anemometer axes, is shown to result in even greater run-to-run stress errors due to the combined sampling errors of the mean vertical velocity and the cross-wind stress (Wilczak *et al*., 2001).

Another kind of rotation is the so called planar-fit method, that is a rotation into the mean stream lines. With this method, the differences between the measuring device and the mean stream field for an unchanged mounting of the anemometer is estimated over a long time period (days to weeks) for a given measuring place; this means that the measuring device must be orientated over this period without any changes. The planar-fit coordinate system fitted to the mean-flow streamlines is characterized by $\overline{w_p} = 0$. After the rotation into the mean streamline level, each single measurement must be rotated into the mean wind direction (Foken, 2008a). It is shown to reduce the run-to-run stress errors due to sampling effects, and provides an unbiased estimate of the lateral stress (Wilczak *et al*., 2001).

An important correction to the actual available turbulence spectra is the adjustment of the spectral resolution of the measuring system. Hence, the resolution in time (time constant), the measuring path length, and the separation between different measuring paths must be corrected. The spectral correction is made using transfer functions (Foken, 2008a).

The so called WPL-correction is a density correction, caused by ignoring density fluctuations, a finite humidity flux at the surface, and the measurement of gas concentration per volume unit instead of per mass

unit. The WPL-correction is large if the turbulent fluctuations are small relative to the mean concentration. The conversion from volume into mass-related values using the WPL-correction is not applicable if the water vapour concentrations or the concentrations of other gases are transferred into mol per mol dry air before the calculation of the eddy-covariance. However, the calculation is possible depending on the sensor type and if it is offered by the manufacturers (Foken, 2008a).

Hence, the quality assurance of turbulence measurements with the EC method is a combination of the complete application of all corrections and the exclusion of meteorological influences such as internal boundary layers, gravity waves, and intermitted turbulence. Quality tests are used to validate the theoretical assumptions of the method such as steady-state conditions, homogeneous surfaces, and developed turbulence (Foken, 2008a).

3.2 Surface Renewal technique

It is difficult to achieve a good closure of the surface energy balance equation when all the energy fluxes are independently measured. This problem involves different shortcomings which are a matter of research. The footprint effect, which is the lack of coincidence of the source area among the terms of the surface energy balance measured using different instruments and techniques, is recognized as one of the problems in achieving a good closure. For determining the flux of a scalar, fetch requirements may depend on the method applied and while Eulerian analytical models and Lagrangian stochastic dispersion models are available, the well known rule of thumb 100:1 (fetch to height) is often applied for practical purposes. The Surface Renewal (SR) method to

estimate scalar surface fluxes is based on the scalar conservation equation and requires the measurement of the scalar (at high frequency) taken at one height as input. The distance downwind from the leading edge needed to deploy instrumentation depends on the measurements required as input in the method used for scalar flux estimation (Castellví, 2012).

Traces of high-frequency temperature data show ramp-like structures resulting from turbulent coherent structures. The coherent structure theory assumes that an air parcel sweeps from above to the surface. The transfer between the air and the canopy elements lead to heating or cooling of the air while is at the surface. Because these fluctuations are coherent, ramps are observed when high-frequency temperature measurements are taken at a point at or above the canopy top. Two parameters characterize these mean temperature ramps for stable and unstable atmospheric conditions: the amplitude (a) and the inverse ramp frequency ($l+s$, with l the period with gradually increasing or decreasing temperature and s the quiescent period). The mean values of these two parameters during a time interval can be used to estimate H over several crop canopies using SR analysis (Snyder *et al*., 1996; Zapata and Martínez-Cob, 2001, 2002).

In SR analysis, a parcel of air is assumed to originate above the canopy with a characteristic scalar value (Chen *et al*., 1997b).

Consider an air parcel, with some scalar concentration, travelling at a given height above the surface. SR analysis assumes that at some instant the parcel suddenly moves down to the surface and remains connected with the sources (sinks) for a period of time during which it is horizontally travelling along the sources. By continuity, the parcel ejects upwards and is replaced by another parcel sweeping in from aloft. During the connect time with the surface, scalar transfers to or from the sources to the air parcel.

Thus, the parcel has been enriched (depleted) with the scalar. Scalar turbulent exchange at the surface (vegetation) – atmosphere interface is therefore driven by the regular replacement of air parcels in contact with the sources (sinks). This continuous renewal process is responsible for the majority of vertical transport. The renewal process is associated to an organized low frequency flow (canopy-scale coherent structures). The signature of a coherent eddy motion, at a fixed measurement point, can be abstracted when the high-frequency measurement of the scalar is plotted versus time. Even measuring well above the canopy, the signature is visualized in the trace as a regular and low-frequency ramp-like (asymmetric triangle shape) pattern. Paw U *et al*. (1995) presented a diagram of the surface renewal process (Fig. 3.1) and abstracted an ideal scheme for a ramp-like event in the trace (Scheme 1 in Fig. 3.1). Chen *et al*. (1997a) presented a slightly different version (Scheme 2 in Fig. 3.1) that neglects the quiescent period but includes a micro-front period instead of an instantaneous ejection.

Whatever the model, a ramp is characterized by an amplitude, a, and period, τ (that equals to $l+s$, such as to L_r+L_q). According to the diagram in Fig. 3.1, the variation in scalar concentration versus time is Lagrangian during the time that the air parcel remains connected to the surface (i.e. (L_q+L_r) and L_r for Schemes 1 and 2, respectively) (Castellví *et al*., 2008).

For unstable conditions, when the leaves and canopy elements are warmer than the air, the parcel instantaneously penetrates and sweeps into the canopy and begins to be heated by the canopy. The expected temperature pattern observed by a sensor at the canopy height would therefore be a sudden temperature drop when the parcel penetrated the

canopy, and then a gradual temperature rise as the canopy heated the air (Paw U *et al*., 1995).

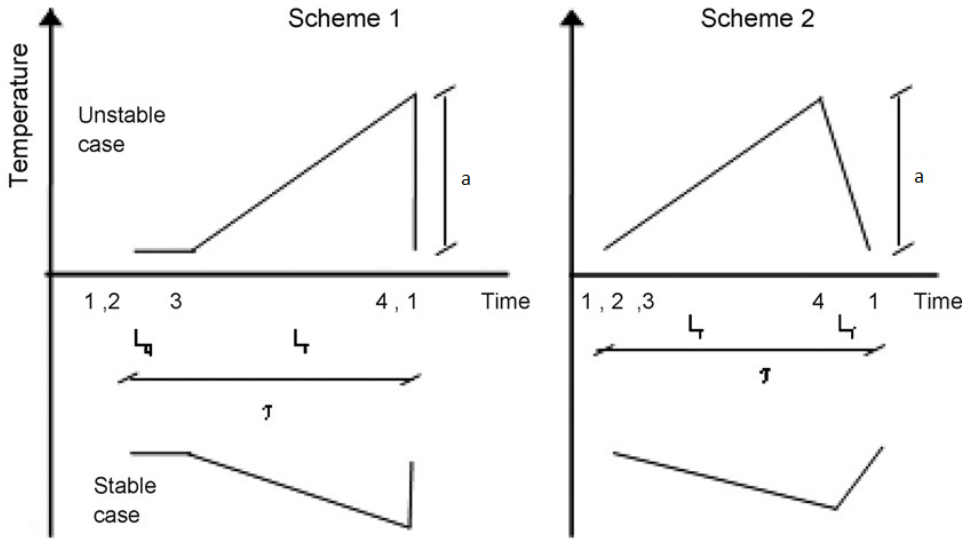

Fig. 3.1. Air parcel diagram of the renewal process. The time course of the scalar concentration for the positions shown in the diagram are idealized in two air temperature ramp models. Scheme 1 assumes a quiescent period and a sharp instantaneous drop in temperature. Scheme 2 neglects the quiescent period and assumes a finite micro-front. L_r, L_q and L_f denote the warming, quiescent and micro-front periods, respectively; a is the ramp amplitude and τ is the total ramp duration (Castellví, 2008).

The increase is associated with the quiescent period during which the air is warmed by small-scale transport (both laminar and turbulent) from canopy elements and the underlying surface. The sharp drop in temperature indicates the occurrence of a large turbulent eddy that replaces the warmed air with cooler air from above (Chen *et al*., 1997b). The repeated saw-tooth patterns are called 'ramp events'. Conversely, if the canopy elements are cooler than the air (stable conditions), then the initial sweep of air would be seen as a sudden rise in the temperature trace, with a slow cooling following this rise (Paw U *et al*., 1995); the air cools during the quiescent

period and is replaced by warmer air from above. It is assumed that for each ramp event most of the heat exchange is associated with the large-scale turbulent eddy, with very little occurring during the quiescent period. For a typical measurement period, e.g., a half hour, the average H at any z is the net heat exchange associated with all ramps in this period (Chen *et al.*, 1997b).

If the parcel of air is defined to have a volume V, then the temperature change rate with time (dT/dt) can be shown to be directly related to the sensible heat flux H:

$$H = \rho c_p \frac{dT}{dt}\left(\frac{V}{A}\right) \tag{3.15}$$

where ρ is the air density, c_p is the specific heat per unit mass at constant pressure, T is the air temperature, t the time and the ratio (V/A) represents the volume of the parcel over the horizontal area at the parcel base. This ratio converts the heating rate per unit volume (W m^{-3}) of the parcel into a sensible heat flux density (W m^{-2}). It can be seen that if the vertical dimension of the parcel is considered to be the height of the canopy, that the ratio (V/A) is equal to the canopy height z. The general validity of Eq. 3.15 holds for both small control volumes and for larger volumes, so long as the heat flux density H is properly interpreted (Paw U *et al.*, 1995). The temperature change in time dT/dt can be substituted by a/l and the result is multiplied by the relative duration of the heating or cooling $l/(l+s)$ (Foken, 2008a; Snyder *et al.*, 1996). This way, the average H for a given time interval is obtained from the following expression:

$$H = \alpha \rho c_p \frac{a}{l+s} z \tag{3.16}$$

The weighting factor α accounts for the spatially averaged (vertical) air temperature derivative from the bottom to the top of the air parcel (Snyder *et al*., 1996; Zapata and Martínez-Cob, 2001), i.e. for the non-uniform heating of the mean air parcel under the measurement level (Duce *et al*., 1997; Spano *et al*., 1997a).

Mean values for a and $l+s$ during a half hour interval are used to estimate H. Structure functions (Eq. 3.17) and the analysis technique (Eqs. 3.18÷3.21) from Van Atta (1977) are used to determine a and $l+s$:

$$S^n(r) = \frac{1}{m-j}\sum_{i=1+j}^{m}\left(T_i - T_{i-j}\right)^n \tag{3.17}$$

where m is the number of data points in the 30-minute interval measured at frequency (f) in Hz, n is the power of the function, j is a sample lag between data points corresponding to a time lag ($r=j/f$) and T_i is the i^{th} temperature sample. According to Van Atta, the time lag r must be much less than $l+s$ (Snyder *et al*., 1996, 1997).

An estimate of the mean value for amplitude a during the time interval is determined by solving the following equation for the real roots:

$$a^3 + pa + q = 0 \tag{3.18}$$

where

$$p = 10S^2(r) - \frac{S^5(r)}{S^3(r)} \tag{3.19}$$

and

$$q = 10S^3(r) \tag{3.20}$$

The inverse ramp frequency ($l+s$) is calculated using

$$l + s = -\frac{a^3 r}{S^3(r)} \tag{3.21}$$

Then Eq. 3.16, assuming $\alpha = 1$, is used to calculate non-calibrated SR sensible heat flux density (H'_{SR}). The need for α and its value are tested by computing a regression of H from a sonic anemometer (H_{EC}) versus H'_{SR} (Snyder *et al*., 1996, 1997).

The resulting H values are then used with net radiation and soil heat flux density measurements to calculate latent heat flux density, λE, (Snyder *et al*., 1997) through the closure of the energy balance.

The Surface Renewal method needs careful analysis of the turbulence structure and promises possibilities for the application of fluxes above high vegetation, especially for predominant stable stratification with significant ramp structures (Foken, 2008a).

3.3 The Bowen Ratio method

The Bowen ratio-energy balance (BREB) is an indirect micrometeorological method often used to estimate latent heat flux because of its simplicity, robustness and cost. This method estimates latent heat flux from a surface using measurements of air temperature and humidity gradients, net radiation, and soil heat flux. Its advantages include straight-forward, simple measurements; it requires no information about the aerodynamic characteristics of the surface of interest; it can integrate latent heat fluxes over large areas (hundreds to thousands of square meters); it can estimate fluxes on fine time scales (less than an hour); and it can provide continuous, unattended measurements. Disadvantages include sensitivity to the biases of instruments which measure gradients and energy balance terms; the possibility of discontinuous data when the Bowen ratio approaches value −1, and the requirement, common to

micrometeorological methods, of adequate fetch to ensure adherence to the assumptions of the method (Todd *et al*., 2000).

The BREB method relies on several assumptions: transport is assumed to be one-dimensional, with no horizontal gradients; sensors which measure gradients are assumed to be located within the equilibrium sublayer where fluxes are assumed to be constant with height; the surface is assumed to be homogeneous with respect to sources and sinks of heat, water vapour and momentum; the ratio of turbulent exchange coefficients for heat and water vapour is assumed to be 1. The first two assumptions are usually met if adequate upwind fetch is available. A fetch to height-above-surface ratio of 100:1 is often considered a rule of thumb, although a ratio as low as 20:1 is considered adequate when Bowen ratios are small and positive. Sensors at different heights respond to different upwind source areas, so that all sensors must have adequate fetch (Todd *et al*., 2000).

The Bowen-ratio method is a profile measurement and is based on the Bowen ratio similarity, that is a special case of flux-gradient similarity (a relation that considers the flux determinable by the vertical gradient of the state variable and a diffusion coefficient) and on the energy balance equation (Foken, 2008a).

The BR technique determines the flux of a species C by reference to the flux of a species C_r that is more amenable to direct measurement, following the relation:

$$F_{BR} = \beta F_r = \frac{C(z_2) - C(z_1)}{C_r(z_2) - C_r(z_1)} F_r = \frac{\Delta C}{\Delta C_r} F_r \tag{3.22}$$

Here F_r is the flux of the reference species and the Bowen ratio $\beta \equiv F/F_r$ is commonly estimated by measuring vertical concentration

differences of the two species over a common height interval, z_2-z_1 (Horst, 1999).

So, for determining sensible and latent heat fluxes, the BR method adopts vertical gradients of temperature and water vapour pressure, and surface energy budget measured by the surface energy and radiation balance system, but it does not use information provided by the similarity law and measurements of wind speed in the surface layer (Zhang *et al*., 2004). The BREB method must be consistent with conservation of energy because it forces energy-balance closure (Twine *et al*., 2000).

It is defined as the ratio of the sensible to the latent heat flux:

$$\beta = \frac{H}{\lambda E} \tag{3.23}$$

So, the energy balance can be rearranged to give

$$\lambda E = \frac{R_N - G}{1 + \beta} \tag{3.24}$$

β can be measured by the ratio of the air temperature difference between two levels (ΔT) and the vapour pressure difference (Δe), with e (kPa) air vapour pressure, measured at the same two levels, so that

$$\beta = \gamma \frac{\Delta T}{\Delta e} \tag{3.25}$$

where γ (kPa °C^{-1}) is the psychrometric constant (Katerji and Rana, 2008).

The partitioning between latent λE and sensible H heat flux, that is, the Bowen ratio β, is critical in determining the hydrological cycle, boundary layer development, weather and climate. The surface resistance (r_c) for a vegetated surface plays an important role in determining how the available energy $R_N - G$ is partitioned between H and λE, as β can be interpreted as an indicator of water stress. The process of accommodation of plants to

water demand is coupled with that of thermal accommodation in the lower atmosphere. The behaviour of stomata in response to the environment is interpreted as a physiological response. The response to radiation is linked to the process of photosynthesis and this is the basis for optimizing models of stomatal resistance. It seems that the dependence between the energy partitioning β and r_c shows that attention should be focused on estimating and quantifying the energy partitioning. At the surface, energy partitioning is a complex function of interactions between plant physiology and the development of the atmospheric boundary layer. So, the Bowen ratio can be expressed as

$$\beta = \frac{1+(r_c / \ r_a)-(r_i / \ r_a)}{(\Delta / \ \gamma)+(r_i / \ r_a)} \tag{3.26}$$

with r_a the aerodynamic resistance and where the climatological resistance r_i is

$$r_i = \frac{\rho c_p (e^* - e)}{\gamma (R_N - G)} = \frac{\rho c_p D}{\gamma (R_N - G)} \tag{3.27}$$

with ρ the mean air density at constant pressure (kg m^{-3}), c_p the specific heat of moist air at constant pressure (1004 J kg^{-1} $°C^{-1}$); e^* and e, respectively, the saturation and actual vapour pressure of the air (Pa), and $D = e^* - e$ (Pa) the atmospheric vapour pressure deficit; γ is the psychrometric constant (Pa $°C^{-1}$) and Δ the slope of the saturation vapour pressure curve with respect to temperature (Pa $°C^{-1}$); R_N and G are, respectively, the net radiation and soil heat flux and $R_N - G$ (W m^{-2}) the available energy (Perez *et al*., 2008).

Once all the necessary precautions have been adopted for measuring the air temperature and humidity gradients, the Bowen ratio method can be considered a valid reference method for measuring evapotranspiration. The

suitability of the Bowen ratio technique as a reference method is valid for both short and tall crops, cropped in well-watered and under water-stress conditions (Katerji and Rana, 2008).

The crucial disadvantage of the Bowen ratio method is that because of the apparent unclosed energy balance the residual is either added to the net radiation or distributed according to the Bowen ratio to the sensible and latent heat flux. In general, the fluxes determined with the Bowen ratio method are larger than those determined with the Eddy Covariance method. But they fulfil the energy balance equation, which is part of the method. The quantitative correctness of the fluxes may be limited. Furthermore, the heat storage in the soil should be calculated very accurately to reduce the influence of the residual of the energy balance closure (Foken, 2008a).

The BR system requires less maintenance than Eddy Covariance and is generally cheaper; however, closure is forced, and the eddy diffusivities of heat and moisture must be assumed equal (Brotzge and Crawford, 2003).

For periods in which atmospheric stability is near neutral or slightly stable (transition periods and night-time hours), measurements of heat fluxes and temperature gradients become much more demanding. Measurements of other scalar fluxes and gradients, in theory, provide the same information about atmospheric mixing as sensible heat flux, but are not so constrained to available solar energy to drive the surface flux. Along with assuming equality among the scalar transfer coefficients, application of the Bowen-ratio technique assumes that the vertical gradients are consistent with the turbulent fluxes. That is, over uniform vegetated surfaces, if the gradient is negative the flux of material is away from the surface, and vice versa (Meyers *et al*., 1996).

The Bowen ratio method can be considered as a reference to calibrate the other measurement methods (Katerji and Rana, 2008).

3.4 Aerodynamic method

The aerodynamic method is another micrometeorological method often used during experimental campaigns where it is necessary to characterize the soil-plant-atmosphere *continuum*. If we assume that a flux density can be related to the gradient of the concentration in the atmospheric surface layer, the latent heat flux by the aerodynamic technique can be determined directly by means of the scaling factors u^* and q^*, with q being the specific air humidity (kg kg^{-1}):

$$\lambda E = -\lambda \rho u^* q^* \tag{3.28}$$

with ρ the density of air (kg m^{-3}) and the friction velocity u^* (m s^{-1}) derived from the wind profile measurement:

$$u^* = \frac{ku}{\ln\left(\frac{z-d}{z_0}\right) - \Psi_m} \tag{3.29}$$

where k = 0.41 is the von Karman constant, d (m) is the zero plane displacement height, z_0 (m) is the roughness length of the surface and Ψ_m is the stability correction function for momentum transport. q^* is determined similarly from the humidity profile measurement:

$$q^* = \frac{k(q-q_0)}{\ln\left(\frac{z-d}{z_0}\right) - \Psi_v} \tag{3.30}$$

where q_0 is the air humidity extrapolated at $z = d + z_0$ and Ψ_v is the correction function for latent heat transport (Katerji and Rana, 2008; Rana and Katerji, 2000).

The major difficulty with this method is the correct measurement of vapour pressure at different heights above the crop. For this reason, λE can be derived indirectly by the energy balance equation if the sensible heat flux is determined by the flux-gradient relationship:

$$H = -\rho c_p u^* T^* \tag{3.31}$$

where T^* is deduced by the air temperature profile:

$$T^* = \frac{k(T - T_0)}{\ln\left(\frac{z-d}{z_0}\right) - \Psi_h} \tag{3.32}$$

where T_0 is the temperature extrapolated at $z = d + z_0$ and Ψ_h is the correction function for the heat transport. In this form, from the applicative point of view, the main advantage of the aerodynamic method consists in avoiding humidity measurements. Nevertheless, its accuracy depends on the number of measurement levels of wind speed and temperature profiles, at least three or four levels are suggested (Katerji and Rana, 2008).
For stable atmospheric conditions $\Psi_m = \Psi_v = \Psi_h$ (Figuerola and Berliner, 2005).

With a flux–gradient approach, surface roughness and heterogeneity are typically characterized by two aerodynamic parameters, aerodynamic roughness length, z_0, and zero-plane displacement height, d. Aerodynamic roughness length relates to the efficiency of momentum exchange at the surface and d represents the effective height of momentum absorption within the roughness elements. Both z_0 and d are important in aerodynamic formulations for modeling energy exchange processes across the soil–plant–atmosphere *continuum*. The traditional logarithmic wind profile approach uses multiple levels of wind speed measurements to

mathematically solve for z_0 and d by minimizing the sum of square errors for wind speed and measurement height (Prueger *et al*., 2004).

4 Approaches for transpiration measurements

These methods measure water loss at the plant scale, either from a whole single plant or from a small group of plants, so that they cannot directly supply the ET on the plot scale. To achieve this purpose, it is necessary to adopt a specific methodology for each situation, in order to achieve the up-scaling from the measurement at the plant level to the ET at the plot scale (Katerji and Rana, 2008).

4.1 Sap Flow methods

Sap flow is closely linked to plant transpiration by means of simple accurate models (Katerji and Rana, 2008). Sap flow methods are easily automated, so continuous records of plant water use with high time resolution can be obtained. Moreover, these methods can be used anywhere with very little disturbance to the site. However, when sap flow measurements are adopted to estimate transpiration for stands of vegetation, appropriate methods of scaling from plant to unit area of land must be used (Smith and Allen, 1996).

Different methods are used to measure sap flow in plant stems or trunks; the most common are: heat pulse methods; heat balance method; thermal dissipation probe method or Granier method.

In the heat pulse methods, sap flow is estimated by measuring heat velocity, stem area and xylem conductive area (Katerji and Rana, 2008), using a linear heater and temperature probes inserted radially into the plant stem or trunk (Green *et al*., 2003) and parallel to each other (Cohen *et al*., 1981). Thermocouples or thermistors are positioned along the length of the temperature probe to monitor temperature rise at various radial positions

within the stem. At each position, the heat pulse velocity is determined by measuring the time between the introduction of the heat pulse and the occurrence of the maximum temperature rise. Heat pulse velocities are converted into the sap flux densities and then integrated over the cross-sectional area of the stem or trunk to yield the volumetric sap flow rate (Kluitenberg and Ham, 2004). These methods include the Heat Pulse Velocity (HPV) method and the T-max method.

HPV method is based on the compensation heat pulse method. Swanson (1962) was one of the first to utilize Marshall's analytical solutions to the heat flow equation (Marshall, 1958), by applying them to the analysis of the 'compensation' heat pulse method in which two temperature probes are placed asymmetrically in either side of a line heater source that is inserted radially into the tree stem (Fig. 4.1). The heater introduces a brief 1-2 s pulse of heat into the stem and a data logger measures the time delay (t_z) for an equal temperature rise at both sensors (Green, 2009).

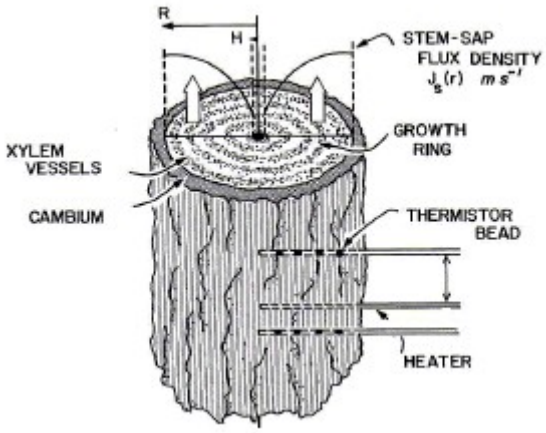

Fig. 4.1. Configuration of the compensation method for sap flow measurement (Green, 2009).

Swanson showed that if the temperature rise following the release of a pulse of heat is measured at distances X_u (m) upstream and X_d (m) downstream from the heater, then the heat-pulse velocity can be calculated from

$$V_z = \left(\frac{X_d + X_u}{2t_z} \right) \tag{4.1}$$

where t_z (s) is the time delay for the temperatures at points X_d and X_u to become equal. In effect, Equation 4.1 implies that, following the application of an instantaneous heat-pulse, the centre of the heat-pulse is convected downstream, from the heater, to reach the midway point between the two temperature sensor after t_z. Equation 4.1 is particularly suited to data logging since it only requires electronics to detect a null temperature difference and an accurate timer to measure t_z. The t_z's are the only data to be recorded, since the distances X_u and X_d remain constant. This estimate of V (m s^{-1}) is the 'raw' heat -pulse velocity.

Marshall (1958) also derived an alternative T-max method that uses a single temperature sensor located downstream from a line heater probe (Fig. 4.2).

In this case data logger records the time, t_M, for a maximum temperature rise at a distance x_D from the heater. The heat-pulse velocity, V_M (m s^{-1}) is then calculated from

$$V_M = \sqrt{x_D^2 - 4\kappa t_M} \, / \, t_M \tag{4.2}$$

where κ (m^2 s^{-1}) is the thermal diffusivity that can be determined at zero flow, using the equation

$$\kappa = x_D^2 / 4t_M \tag{4.3}$$

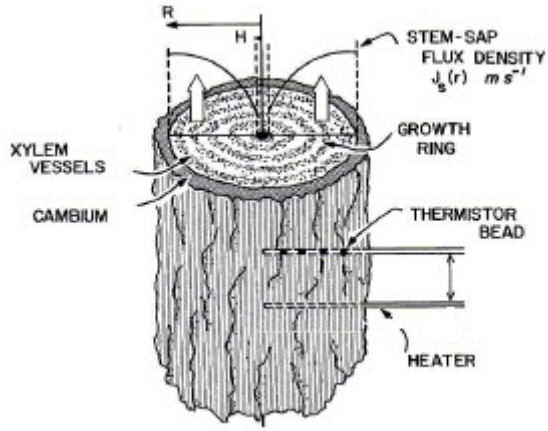

Fig. 4.2. Configuration of the T-max method for sap flow measurement (Green, 2009).

The calculation of V from Eqs. 4.1 and 4.2 are based on Marshall's (1958) idealized theory and assumes that heat-pulse probes have no effect on the measured heat flow. Actually, convection of the heat pulse is disturbed by the presence of the heater and temperature probes, and by the disruption of xylem tissue associated with their placement. These disturbances produce a systematic underestimation of the measured heat-pulse velocity (Cohen *et al*., 1981). Consequently, the heat-pulse velocity must be corrected for the probe-induced effects of wounding. This correction can be applied empirically, or it can be based on sound physical principals, using an equation of the form:

$$V_c = a + bV + cV^2 \tag{4.4}$$

where V_c (m s^{-1}) is the corrected heat-pulse velocity and V is the raw heat-pulse velocity given by Eq. 4.1 or 4.2. The correction coefficients a, b, and c have been derived by Swanson and Whitfield (1981) from numerical solutions of Marshall's (1958) equations, for various wound sizes. Once the corrected heat-pulse velocity, V_c, has been determined, the next step is to relate it to the actual sap flow. Marshall's (1958) analysis showed that if

the sap and woody matrix are considered to form a homogeneous medium, then the sap flux density, J (m s^{-1}), can be calculated from

$$J = \left(kF_M + F_L\right)V_c \tag{4.5}$$

where F_M and F_L are the volume fractions of wood and water, respectively; k is a coefficient related to the thermal properties of the woody matrix (Becker and Edwards, 1999), and it is assumed to be constant within and between species (Green *et al*., 2003; Green, 2009). Volume fractions F_{M} and F_{L} implicit in Eq. 4.5 are determined from the Archimede's principle, as in the following: firstly, a core sample is taken and its fresh weight, M_{F} (kg), is determined. This weight is equal to the mass of water and the mass of dry wood, since the mass of air is negligible. The core sample is then immediately submerged in a beaker of water where a mass balance is determined. The balance reading will indicate an immediate increase in mass, which equals the displacement of water, D_T (kg). The total volume, V_T (m^3), of the sample is then equal to ρ_L times D_T, where the density of water, ρ_L, is assumed to be 1000 kg m^{-3}. The core sample is then oven-dried to determine the mass of dry wood, M_D (kg). The difference between the fresh weight and the dry weight, (M_F-M_D) is equal to the mass of water, M_L (kg), in the fresh core sample. Thus, the volume fraction of water is $F_L = M_L/\left(\rho_L V_T\right)$. Similarly, the volume fraction of wood $F_M = M_D/\left(\rho_M V_T\right)$ where the density of dry wood, ρ_M equals 1530 kg m^{-3}.

Equation 4.5 provides an estimate of J at any point in the conducting sapwood. It is widely recognized that sap flux density is not uniform throughout the sapwood, but rather peaks at a depth of 10-20 mm from the cambium. Consequently, sampling at several depths in the sapwood is necessary to characterize the sap flow velocity profile. A volumetric

measure of total sap flux can be obtained by integrating these point estimates over the sapwood conducting area (Green, 2009).

In the heat balance method, plant transpiration can be estimated by determining the sap mass flow; this is done using gauges that are attached to, or inserted in, the plant stem. A heater element is placed around the plant stem to provide energy to the system. Thermocouples are used to determine how much heat is lost by conduction up, down and radially in the stem from the heater element (Fig. 4.3). The difference between the heat input and these losses is assumed to be dissipated by convection with the sap flow up the stem and may be directly related to water flow.

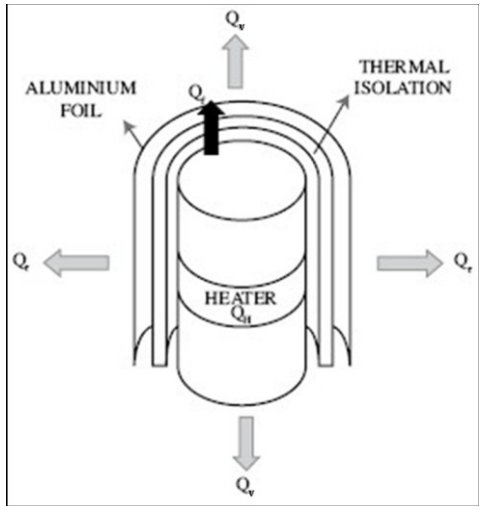

Fig. 4.3. Heat balance method for sap flow measurement. Q_H is the flow of heat supplied by the heater, Q_f represents the convective flow of heat transported by the sap, Q_v represents the flow of heat lost by conduction in vertical direction and Q_r represents the radial heat loss transferred by conduction to the environment (from Reyes et al., 2007 - modified).

The energy balance of a heated portion of plant stem can be expressed by

$$Q_H = Q_v + Q_r + Q_f + S \tag{4.6}$$

where Q_H represents the heat supplied, Q_v is the heat transferred by conduction in the vertical direction, Q_r is the radial heat transferred by conduction, Q_f the heat energy transported by mass flow of sap and S the rate of change of heat storage in the stem segment. All variables are measured in units of Watts. Convective energy transferred by the sap can be defined as:

$$Q_f = c_w F \delta T \tag{4.7}$$

where c_w is the specific heat of water (J kg^{-1} K^{-1}), F the rate of sap flow in the stem (kg s^{-1}) and δT is the temperature difference between the upstream and downstream thermocouples. The heat storage term, S, is usually ignored, assuming steady state conditions within the system. From Eqs. 4.6 and 4.7, the mass flow rate F is expressed by the relationship:

$$F = \frac{\left(Q_H - Q_v - Q_r\right)}{c_w \delta T} \tag{4.8}$$

(Katerji and Rana, 2008; Rana and Katerji, 2000; Rana *et al*., 2005).

Xylem sap flow measurement with the Thermal Dissipation Probe (TDP) method was first developed by Granier (Granier, 1987; Lu *et al*., 2004). The idea behind the method is that heat dissipation in woody tissue is caused by sap flow (Liu *et al*., 2008). Two cylindrical probes of 2 mm diameter are inserted radially into the stem, with one probe placed approximately 100 mm above the other (Smith and Allen, 1996). The upper sensor (2 cm long) is coupled with a heater powered constantly (i.e. the heated sensor), and the lower sensor measures the temperature in an unaffected region, i.e. the reference temperature (Fig. 4.4).

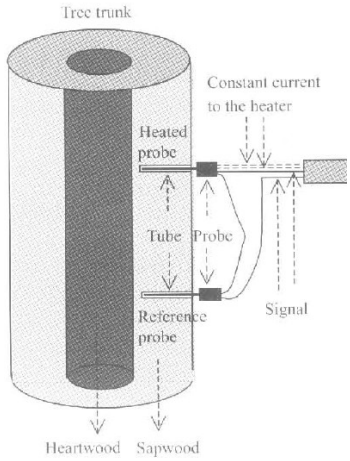

Fig. 4.4. Configuration of the Granier system for sap flow measurement. Each probe contains a thermocouple (Lu et al., 2004).

The temperature difference between the two sensors (ΔT) is used to compute sap flux density (SFD) with an equation proposed by Granier (1987). As SFD in the proximity of the heated probe increases, more heat is removed from this sensor and ΔT decreases. The maximum temperature difference (ΔT_M) is obtained when SFD is zero. The equation used to compute SFD is (Granier, 1987):

$$U = 119 * 10^{-6} \left(\frac{\Delta T_M - \Delta T}{\Delta T} \right)^{1.231} \tag{4.9}$$

where U (m^3 m^{-2} s^{-1}) is the mean SFD along a radius (m s^{-1}) and ΔT_M (K) and ΔT (K) are maximum temperature difference and temperature difference when SFD is 0 and when it is >0, respectively. The ΔT_M between the two sensors represents the steady state temperature difference due to the heat transfer by conduction (no convection by water flow). It generally occurs during long-lasting rain events or after several night-time hours with high relative humidity. The TDP temperature sensors are thermocouples whose signal is read as a voltage. For the T-type (copper-

constantan) thermocouple, when temperature ranges between 0°C and 100°C, the coefficient relating temperature and voltage is about 38 μV°C^{-1}. Since the coefficient is constant and applied to both the numerator and denominator, Eq. 4.9 can be converted in:

$$U = 119 * 10^{-6} \left(\frac{\Delta V_M - \Delta V}{\Delta V} \right)^{1.231} \tag{4.10}$$

where ΔV_M and ΔV are maximum voltage difference and voltage difference when SFD is zero and when it is >0, respectively. If the cross-sectional area of the active sapwood is A (m^2), the total SF (m^3 s^{-1}) can be computed as:

$$SF = U \times A \tag{4.11}$$

(Liu *et al*., 2008). The mass flow rate of sap, F (kg s^{-1}), is then calculated by multiplying the total SF by the density of sap, ρ_s (kg m^{-3}) (Smith and Allen, 1996):

$$F = \rho_s SF \tag{4.12}$$

For the sap flow method, to be correctly applied for determining transpiration (T) at the stand level, it is necessary to scale up the transpiration measurement from the plant to the field scale. This is only possible if the canopy structure and the spatial variability of the plant's characteristics (density, height, LAI) are accurately known. In fact, the scaling up of sap flow from the single plant to the field stand requires an analysis of the variability of plant size in order to correctly determine the "mean" plant dimensions. This can be carried out with two different methods: the first one is a direct method which links transpiration to the evaporative green surface and is based on the analysis of the spatial variability of the plant leaf area; the second method is indirect and supposes the existence of a relationship between the stem diameter and the

transpiration leaf area of the plant, so that the determination of the mean plant at plot scale can be carried out simply through a spatial variability analysis of the plant diameter (Katerji and Rana, 2008; Rana and Katerji, 2000).

The sap flow method is only able to measure transpiration and neglects soil evaporation, which for well-watered crops can represent about 15% of ET (Katerji and Rana, 2008).

5 The estimation of evapotranspiration (ET_0)

Methods that do not directly estimate the water consumption of a crop can evaluate it as a fraction of the reference evapotranspiration (ET_0):

$$ET_c = K_c ET_0 \tag{5.1}$$

where K_c is the experimentally derived single crop coefficient. This coefficient, specific for each vegetative surface, evolves in function of the development stage of the crop considered (Katerji and Rana, 2008) and covers the effect of both crop transpiration and soil evaporation. Otherwise, according to the dual crop coefficient approach, K_c can be separated into a basal crop K_{cb} and a soil water evaporation K_e coefficients (Er-Raki *et al*., 2010).

The reference evapotranspiration ET_0 can be either directly measured on a reference surface (well-watered grass meadow, free water in a standard pan) or estimated from indirect semi-empirical formulations based on an analytical approach (Katerji and Rana, 2008).

5.1 Direct measurement of reference crop

5.1.1 From an irrigated grass meadow

Reference evapotranspiration can be directly measured by means of a lysimeter; the reference grass to measure ET_0 must be 8 to 16 cm in height, actively growing, and in well-watered conditions, subject to the same weather as the crop for which the water consumption has to be estimated (Katerji and Rana, 2008).

The term lysimeter means differential measuring instrument and may be taken, in general, to apply to all instruments which measure weight changes, especially weight reduction due to evapotranspiration in a

particular volume of soil (Johnson and Odin, 1978). More specifically, lysimeters can be defined as tanks filled with soil in which crops are grown under natural conditions to measure the amount of water lost by evaporation and transpiration (Jia *et al*., 2006).

There are two main types of lysimeter in use: the drainage and the weighing one. In the first case, potential evaporation is obtained as the difference between added and drained water quantity. In the second case, changes in the total weight of the soil sample are measured, whereby the real evapotranspiration can be estimated during a short time as a ten-minute one. Furthermore, there are two types of weighing lysimeter, the mechanical and the hydraulic one. In the mechanical weighing lysimeter (Fig. 5.1) the soil sample is placed directly on the balance.

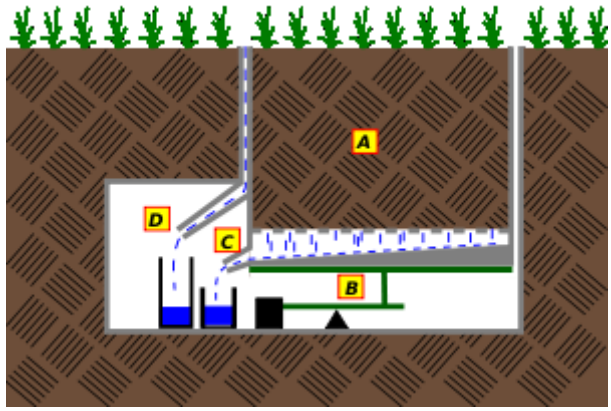

Fig. 5.1. Scheme of a mechanical weighing lysimeter. A represents the soil volume investigated; B is the platform scales; C is the drainage water collecting; D is the run-off water collecting.

The sensitivity will be high, if friction can be reduced using an advanced support construction. In the hydraulic weighing lysimeter the soil sample is placed in a tank floating on a fluid. Changes in level reflect weight changes in the sample. Extremely small weight changes can be

detected using this method, that is the most commonly lysimeter method adopted for directly measuring ET_0 (Johnson and Odin, 1978).

Lysimeters demand large soil volumes in order to have heat and water transport within the soil sample comparable with undisturbed soil. It is possible to compare the results of the direct measurements using the lysimeter with the meteorologically estimated evapotranspiration. Differences can arise owing to a number of factors, the most important is the advection. The effects of advection must be ignored when using meteorological methods (Johnson and Odin, 1978). Hence, the application of this method requires horizontal advection to be negligible when compared to the magnitude of the vertical fluxes (Figuerola and Berliner, 2005).

In precision weighing lysimeters, where the water loss is directly measured by the change of mass, evapotranspiration can be obtained with an accuracy of a few hundredths of a millimetre, and small time periods such as an hour can be considered. In non-weighing lysimeters the evapotranspiration for a given time period is determined by deducting the drainage water, collected at the bottom of the lysimeters, from the total water input. A requirement of lysimeters is that the vegetation both inside and immediately outside of the lysimeter be perfectly matched (same height and leaf area index) (Allen *et al*., 1998).

When the lysimeter does not contain the reference grass, but the plant of interest, by monitoring the change in water storage in the lysimeters, along with other components in the water balance (e.g., precipitation, irrigation, and drainage), the actual evapotranspiration rate can be obtained over the measurement interval. Evapotranspiration accuracy is influenced

by the measurement duration, lysimeter shape, weighing mechanisms, and construction materials as well as site maintenance (Jia *et al*., 2006).

However, lysimeters are expensive to build and maintain and therefore usually not available. Moreover, the variability of ET with lysimeters located in the same field reached 15% in some cases (Todd *et al*. 2000).

5.1.2 From an evaporation pan

The evaporation rate from pans filled with water is easily obtainable. In the absence of rain, the amount of water evaporated during a period (mm d^{-1}) corresponds with the decrease in water depth in the same period. Pans provide a measurement of the integrated effect of radiation, wind, temperature and humidity on the evaporation from an open water surface. Although the pan responds in a similar fashion to the same climatic factors affecting crop transpiration, several factors produce significant differences in loss of water from a water surface and from a cropped surface. Reflection of solar radiation from water in the shallow pan might be different from the assumed 23% for the grass reference surface (Allen *et al*., 1998); the underground pans are very sensitive to the surrounding environment; the need to maintain a sufficient edge can cause a wind break effect, which can disturb the evaporation in a way that is difficult to estimate (Katerji and Rana, 2008). One big difference is that much of the energy stored within the pan during daylight hours will contribute to night-time evaporation, whereas energy stored in the soil, under short crop canopy with a high canopy resistance to water vapour transfer, will exhibit little night-time evaporation (Snyder *et al*., 2005). So there are differences in turbulence, temperature and humidity of the air immediately above the respective surfaces (Allen *et al*., 1998).

Notwithstanding the difference between pan-evaporation and the evapotranspiration of cropped surfaces, the use of pans to predict ET_0 for periods of 10 days or longer may be warranted. The pan evaporation is related to the reference evapotranspiration by an empirically derived pan coefficient (Allen *et al*., 1998):

$$ET_0 = K_p E_{pan} \tag{5.2}$$

where K_p is dependent on the type of pan involved and the pan environment in relationship to nearby surfaces and the climate; its values are highly dependent on the upwind fetch, the saturation vapour deficit of the air and the local advection (Katerji and Rana, 2008).

Different types of pans exist. As the colour, size, and position of the pan have a significant influence on the measured results, the pan coefficients are pan specific. It is recommended that the pan should be installed inside a short green cropped area with a size of a square of at least 15 by 15 m. The pan should not be installed in the centre but at a distance of at least 10 m from the green crop edge in the general upwind direction (Allen *et al*., 1998).

The Class A evaporation pan (Fig. 5.2) is circular, 120.7 cm in diameter and 25 cm deep. It is made of galvanized iron (22 gauge) or Monel metal (0.8 mm).

The pan is mounted on a wooden open frame platform which is 15 cm above ground level. The soil is built up to within 5 cm of the bottom of the pan. The pan must be levelled. It is filled with water to 5 cm below the rim, and the water level should not be allowed to drop to more than 7.5 cm below the rim. The water should be regularly renewed, at least weekly, to eliminate extreme turbidity.

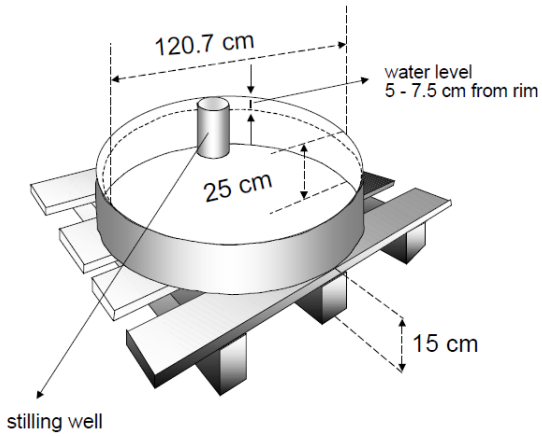

Fig. 5.2. Scheme of the class A evaporation pan (Allen et al., 1998).

The pan, if galvanized, is painted annually with aluminium paint. Screens over the pan are not a standard requirement and should preferably not be used. Pans should be protected by fences to keep animals from drinking. The site should preferably be under grass, 20 by 20 m, open on all sides to permit free circulation of the air. It is preferable that stations are located in the centre or on the leeward side of large cropped fields. Pan readings are taken daily in the early morning at the same time that precipitation is measured. Measurements are made in a stilling well that is situated in the pan near one edge. The stilling well is a metal cylinder of about 10 cm in diameter and some 20 cm deep with a small hole at the bottom.

The Colorado sunken pan (Fig. 5.3) is 92 cm square and 46 cm deep, made of 3 mm thick iron, placed in the ground with the rim 5 cm above the soil level. Also, the dimensions 1 m square and 0.5 m deep are frequently used. The pan is painted with black tar paint. The water level is maintained at or slightly below ground level, i.e. 5÷7.5 cm below the rim. Measurements are taken similarly to those for the Class A pan. Siting and

environment requirements are also similar to those for the Class A pan. Sunken Colorado pans are sometimes preferred in crop water requirements studies, as these pans give a better direct estimation of the reference evapotranspiration than does the Class A pan. The disadvantage is that maintenance is more difficult and leaks are not visible (Allen *et al*., 1998).

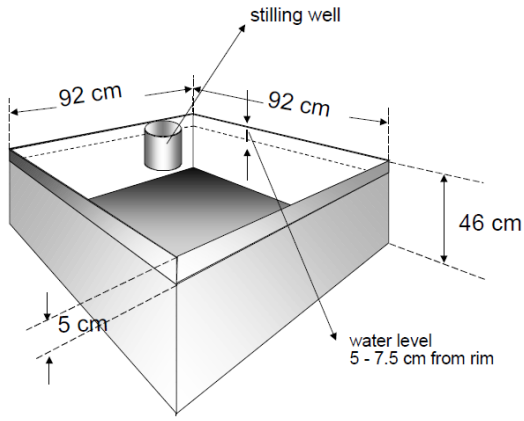

Fig. 5.3. Scheme of the Colorado sunken pan (Allen et al., 1998).

5.2 Indirect formulations for reference crop

These formulations are generally based on the physical laws concerning the energy balance and the convective exchanges on a well-irrigated grass surface. Starting from data collected in standard agro-meteorological stations, an empirical element is introduced in these formulations to facilitate the calculation. These stations are usually situated to be representative of the catchment, i.e. an area of several square kilometres in extension. The main formulas in this class are: the Penman's formula and its by products; the Penman-Monteith formula proposed by Allen *et al*. (1998), i.e. the approach by FAO paper no. 56 (Katerji and Rana, 2008).

5.2.1 The Penman's formula and its by-products

A semi-empirical approach to estimate ET_0 was proposed by Penman (1956):

$$ET_0 = \frac{\Delta R_N + \gamma E_a}{\Delta + \gamma} \tag{5.3}$$

where R_N is the net radiation (W m^{-2}), Δ is the slope of the saturation vapour pressure curve (kPa $°C^{-1}$), γ is the psychrometric constant (kPa $°C^{-1}$) and $E_a = f(u)(e^* - e)$; in turn, e^* is the saturation vapour pressure at air temperature (kPa), e is the measured vapour pressure (kPa) and the wind function f(u) = 1+0.54u_2 (mm kPa^{-1} h^{-1}), with u_2 being wind speed measured 2 meters above the soil surface. In the next years, Penman himself and other authors proposed other formulas, called "corrected Penman", in order to solve the problem of the inaccuracy of Penman's original formula. These new formulas are different from the original one only with respect to the correction of the mathematical expression of the function f(u). There are two main reasons for the empiricism of Penman's formula: a) this formula is only valid under permanent regime, i.e. for a time scale going from a few minute to one hour. Its use on the daily scale leads to the introduction of daily averages of the variables R_N, e^*-e, and u_2 in Eq. 5.3, which can be unrepresentative of the actual meteorological conditions during the period when evapotranspiration is effectively measured; b) the wind function f(u) is just a linear regression adjustment to take into account the differences between estimated and observed ET_0 for grass grown in England. Therefore, it is a pseudo-exchange coefficient, which is supposed to take into account the ET grass regulation. This explains why it is necessary to adapt the function f(u) to each site, in order to apply the Penman formula in the Mediterranean region. Furthermore, it

is quite clear that the wind function decreases going from North toward South and these results point out the dependence of canopy resistance on the vapour pressure deficit, which increases going from northern to southern Europe (Katerji and Rana, 2008).

The most commonly used corrected Penman formula is the one proposed by Doorenbos and Pruitt (1977). It was considered in FAO (Food and Agriculture Organization) paper no. 24 and tested with respect to ET_0, measured on the grass in a few sites in the Mediterranean region (Katerji and Rana, 2008). These scientists calibrated the wind function of the Penman equation using micrometeorological and lysimeter data to have an hourly estimate of ET_0, obtaining $f(u) = 0.030 + 0.576u_2$ if $R_N > 0$ and $f(u) = 0.125 + 0.0439u_2$ if $R_N \leq 0$ (Ventura *et al*., 1999).

However, the FAO Penman method was found to frequently overestimate ET_0 (Allen *et al*., 1998); the results were often contradictory, underlining a general lack of adaptation by Penman's formula, despite the correction, to correctly estimate ET_0 measured on grass, especially in the Mediterranean region. Following the recommendations of a group of experts supported by FAO, Penman's formula has been replaced by a new formula proposed by Allen *et al*. (1998), which is based on a Penman-Monteith approach. This formula was adopted in FAO paper no. 56 as a replacement of Penman's formula (Katerji and Rana, 2008).

5.2.2 The approach by FAO56

The FAO Penman-Monteith method was developed by defining the reference crop as a hypothetical grass crop with an assumed height of 0.12 m, with a surface resistance of 70 s m^{-1} and an albedo of 0.23, closely resembling the evaporation from an extensive surface of green grass of

uniform height, actively growing, completely shading the ground and adequately watered. The method overcomes the shortcomings of the previous FAO Penman method and provides values that are more consistent with actual crop water use data worldwide (Allen *et al*., 1998).

As a result of an Expert Consultation held in May 1990, the FAO Penman-Monteith method is now recommended as the sole standard method for the definition and computation of the reference evapotranspiration. The FAO Penman-Monteith method requires radiation, air temperature, air humidity and wind speed data (Allen *et al*., 1998).

The FAO Penman-Monteith method (FAO56) (Allen *et al*., 1998) has received favorable acceptance and application over much of the world, including the United States, for establishing a reference evapotranspiration index as a function of weather parameters. The majority of applications of the FAO56 method have been made with weather data summarized and reported for 24-h periods, so that the calculation time steps have typically been on a 24-h basis. With the increased development and installation of networks of electronic weather stations around the world, weather data are becoming increasingly available for calculation of ET_0 on an hourly basis. There has been question and debate as well as studies on the appropriate expression and parameterization for the surface resistance (r_s) parameter of the PM equation and the associated coefficient for the reduced form FAO56 equation when applied hourly (Allen *et al*., 2006).

In 1948, Penman combined the energy balance with the mass transfer method and derived an equation to compute the evaporation from an open water surface from standard climatological records of sunshine, temperature, humidity and wind speed. This so-called combination method was further developed by many researchers and extended to cropped

surfaces by introducing resistance factors. The resistance nomenclature distinguishes between aerodynamic resistance and surface resistance factors. The surface resistance parameters are often combined into one parameter, the 'bulk' surface resistance parameter which operates in series with the aerodynamic resistance. The surface resistance, r_s, describes the resistance of vapour flow through stomata openings, total leaf area and soil surface. The aerodynamic resistance, r_a, describes the resistance from the vegetation upward and involves friction from air flowing over vegetative surfaces. The Penman-Monteith form of the combination equation is:

$$ET_0 = \frac{\Delta(R_N - G) + \rho_a c_p \dfrac{(e_s - e_a)}{r_a}}{\left[\Delta + \gamma\left(1 + \dfrac{r_s}{r_a}\right)\right]\lambda} \tag{5.4}$$

where R_N is the net radiation, G is the soil heat flux, (e_s-e_a) represents the vapour pressure deficit of the air, ρ_a is the mean air density at constant pressure, c_p is the specific heat of the air, Δ represents the slope of the saturation vapour pressure temperature relationship, γ is the psychrometric constant, r_s and r_a are the (bulk) surface and aerodynamic resistances and λ is the latent heat of vaporization. The Penman-Monteith approach as formulated above includes all parameters governing energy exchange and corresponding latent heat flux (evapotranspiration) from uniform expanses of vegetation. Most of the parameters are measured or can be readily calculated from weather data. The equation can be utilized for the direct calculation of any crop evapotranspiration as the surface and aerodynamic resistances are crop specific (Allen *et al*., 1998).

The aerodynamic resistance (r_a in s m^{-1}) determines the transfer of heat and water vapour from the evaporating surface into the air above the canopy:

$$r_a = \frac{\ln\left[\frac{z_m - d}{z_{om}}\right] \ln\left[\frac{z_h - d}{z_{oh}}\right]}{k^2 u_z} \tag{5.5}$$

where z_m is the height of wind measurements (m), z_h is the height of humidity measurements (m), d is the zero plane displacement height (m), z_{om} is the roughness length governing momentum transfer (m), z_{oh} is the roughness length governing transfer of heat and vapour (m), k is the von Karman constant (0.41) and u_z is the wind speed at height z (m s^{-1}).

The equation is restricted for neutral stability conditions, i.e., where temperature, atmospheric pressure and wind velocity distributions follow nearly adiabatic conditions (no heat exchange). The application of the equation for short time periods (hourly or less) may require the inclusion of corrections for stability. However, when predicting ET_0 in the well watered reference surface, heat exchanged is small, and therefore stability correction is normally not required (Allen *et al*., 1998).

The 'bulk' surface resistance (r_s in s m^{-1}) describes the resistance of vapour flow through the transpiring crop and evaporating soil surface. Where the vegetation does not completely cover the soil, the resistance factor should indeed include the effects of the evaporation from the soil surface. If the crop is not transpiring at a potential rate, the resistance depends also on the water status of the vegetation. An acceptable approximation to a much more complex relation of the surface resistance of dense full cover vegetation is:

$$r_s = \frac{r_l}{LAI_{active}} \tag{5.6}$$

where r_l (s m^{-1}) is the bulk stomatal resistance of the well-illuminated leaf and LAI_{active} is the active (sunlit) leaf area index (m^2 m^{-2}).

The Leaf Area Index (LAI), a dimensionless quantity, is the leaf area (upper side only) per unit area of soil below it. It is expressed as m^2 leaf area per m^2 ground area. The active LAI is the index of the leaf area actively contributing to surface heat and vapour transfer. It is generally the upper, sunlit portion of a dense canopy. The LAI values for various crops differ widely but values of 3÷5 are common for many mature crops. For a given crop, green LAI changes throughout the season and normally reaches its maximum before or at flowering. LAI further depends on the plant density and the crop variety. The bulk stomatal resistance, r_l, is the average resistance of an individual leaf. This resistance is crop specific and differs among crop varieties and crop management. It usually increases as the crop ages and begins to ripen. There is, however, a lack of consolidated information on changes in r_l over time for the different crops. The information available in the literature on stomatal conductance or resistance is often oriented toward physiological or ecophysiological studies. The stomatal resistance, r_l, is influenced by climate and by water availability. However, influences vary from one crop to another and different varieties can be affected differently. The resistance increases when the crop is water stressed and the soil water availability limits crop evapotranspiration. Some studies indicate that stomatal resistance is influenced to some extent by radiation intensity, temperature, and vapour pressure deficit. To obviate the need to define unique evaporation parameters for each crop and stage of growth, the concept of a reference

surface (as described at the beginning of this paragraph) was introduced. Evapotranspiration rates of the various crops are related to the evapotranspiration rate from the reference surface (ET_0) by means of crop coefficients. In the past, an open water surface has been proposed as a reference surface. However, the differences in aerodynamic, vegetation control and radiation characteristics present a strong challenge in relating ET to measurements of free water evaporation. Relating ET_0 to a specific crop has the advantage of incorporating the biological and physical processes involved in ET from cropped surfaces. The requirements that the grass surface should be extensive and uniform result from the assumption that all fluxes are one-dimensional upwards. The FAO Penman-Monteith method is selected as the method by which the evapotranspiration of this reference surface (ET_0) can be unambiguously determined, and as the method which provides consistent ET_0 values in all regions and climates. From the original Penman-Monteith equation (Eq. 5.4) and the equations of the aerodynamic (Eq. 5.5) and surface resistance (Eq. 5.6), the FAO Penman-Monteith method to estimate ET_0 (mm d^{-1}) can be derived:

$$ET_0 = \frac{0.408\Delta(R_N - G) + \gamma \frac{900}{T+273} u_2 (e_s - e_a)}{\Delta + \gamma(1 + 0.34u_2)} \tag{5.7}$$

where T is the mean daily air temperature at 2 m height (°C), u_2 is the wind speed at 2 m height (m s^{-1}), e_s is the saturation vapour pressure (kPa), e_a is the actual vapour pressure (kPa), Δ is the slope of vapour pressure curve (kPa $°C^{-1}$) and γ is the psychrometric constant (kPa $°C^{-1}$).

The reference evapotranspiration provides a standard to which: evapotranspiration at different periods of the year or in other regions can be compared; evapotranspiration of other crops can be related.

The equation uses standard climatological records of solar radiation (sunshine), air temperature, humidity and wind speed. To ensure the integrity of computations, the weather measurements should be made at 2 m (or converted to that height) above an extensive surface of green grass, shading the ground and not short of water (Allen *et al*., 1998).

However, the above equation is applicable only on the daily time scale. The empiricism of this approach consists in: a) the chosen daily time scale; thus, as for Penman's formula, the permanent regime conditions are not respected; b) the determination of the biological regulation in this formula is well-distinguished by the exchange coefficient, contrary to Penman's formula. However, the biological resistance in this formula is supposed to be constant during the day and is set independently on climatic conditions, in particular on the vapour pressure deficit of the air. This last hypothesis has been criticized by the ecophysiologists, who demonstrated that a well-established linear relationship exists between the decrease in stomatal conductance and the increase in the saturation pressure deficit of the air. It is also in contrast with experimental trials demonstrating that the daily averaged stomatal resistance in well-irrigated grass is not constant (Katerji and Rana, 2008). A new version of this formula, suitable for the hourly scale, has been proposed by Allen *et al*. (2006).

So, the FAO56 equation can be more generically written as:

$$ET_0 = \frac{0.408\Delta\left(R_N - G\right) + \gamma \dfrac{C_n}{T + 273} u_2 \left(e_s - e_a\right)}{\Delta + \gamma\left(1 + C_d u_2\right)} \tag{5.8}$$

where C_n and C_d are coefficients that differ with calculation time step, reference crop type and, in some cases, with time of day. Units for C_n is K mm s^3 mg^{-1} day^{-1} or K mm s^3 mg^{-1} h^{-1} and units for C_d is s m^{-1}. C_n = 900

for 24-h and C_n = 37 for hourly time steps; parameter C_d = 0.34 in Allen *et al*. (1998) for all time steps for FAO56, representing rs = 70 s m^{-1}. C_d = 0.24 for hourly time steps during daytime (defined as when $R_N > 0$) and C_d = 0.96 for hourly time steps during nighttime. The 0.24 and 0.96 values for C_d for hourly applications stem from the use of r_s = 50 s m^{-1} during daytime and r_s = 200 s m^{-1} during nighttime, rather than assuming r_s = 70 s m^{-1} for hourly time periods (Allen *et al*., 2006).

6 The experimental site

6.1 Field site description

The experimental activities have been carried out within a citrus orchard located in Lentini (Eastern Sicily, Lat. 37° 16' N, Long. 14° 53' E) (Fig. 6.1). This area has a Mediterranean semi-arid climate (annual mean air temperature 17°C and rainfall less than 600 mm), with warm summer and moderate rainfall distributed during autumn and winter.

The experimental field (of about 25 ha) is planted with 15÷25-year-old orange trees (*Citrus sinensis* (L.) *Osbeck*, cv. Tarocco Ippolito), grown in an orchard of about 120 ha.

Fig. 6.1. Location of the experimental site and a satellite view of the orchard by Google Earth.

The site is flat and the orchard spacing is of 4 m between trunks within rows and 5.5 m between rows. The soil surface is partially covered (10–15%) by natural grass for most of the year. The mean canopy height was 3.75 m. Leaf Area Index (LAI) was estimated using a Licor LAI-2000 (LI-COR, Biosciences) digital analyser and ranged from 3.7 to 4.6 m^2 m^{-2}; the mean LAI was 4.25 m^2 m^{-2}. The foliage is dense from 0.2 m above the ground to the canopy top, and the canopy is nearly continuous along the

rows, thus the PAR light interception was 100% in a row and about 50% between rows.

For the dominant wind direction (mainly W and NW), the fetch was larger than 550 m. For the other sectors, the minimum fetch was 400 m (SE). The crop was well-watered by irrigation supplied every day during the hot months (May÷October). Water was supplied by drip irrigation, with 4 online labyrinth drippers per plant, spaced at 0.80 m, with a discharge rate of 4 l/h at a pressure of 100 kPa. Soil texture is loam, with 46.85% of sand, 36.25% of silt and 16.90% of clay.

The experimental site has ideal conditions for canopy homogeneity, flat slope, size and dominant wind direction; all these characteristics make the field suitable for micrometeorological techniques application. In summer periods, regional advection for sensible heat fluxes has been reported, i.e. in daily hours H values were lower than zero (negative) and so opposite in sign to net radiation, R_N (positive).

6.2 Instrumentation

Numerous instruments were installed at the experimental site in order to derive continuous measurements of energy and mass exchanges in the soil-plant-atmosphere continuum (SPAC); measurements include: weather features, soil water content and sap fluxes. The majority of the equipment is set up on a 10 meter high mast (Fig. 6.2). Low (30 min) and high (10 Hz) frequency data are recorded by four data loggers: a CR3000 Campbell Sci. and three CR1000 Campbell Sci..

Fig. 6.2. Micrometeorological tower.

Net radiation (R_N) is measured with two net radiometers: one four components (CNR1, Kippen&Zonen) and one integrated (NR-Lite, Kippen&Zonen), deployed above the canopy on a 6 meter mast and facing South (Fig. 6.3).

Fig. 6.3. Net radiometers.

Soil heat flux density (G) is measured with three soil heat flux plates (HFP01, Campbell Sci.) placed horizontally 0.05 m below the soil surface. Three different measurements of G have been selected: in the trunk row (shaded area), at 1/3 of the distance to the adjacent row, and at 2/3 of the distance to the adjacent row (Fig. 6.4).

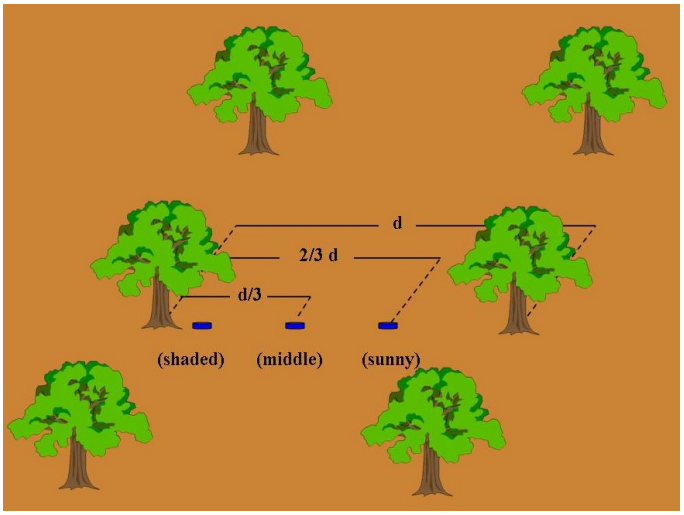

Fig. 6.4. Probes positioning in the orchard for G measurement.

The soil heat flux is measured as the mean output of the three soil heat flux plates. Data from the soil heat flux plates are corrected for heat storage in the soil above the plates. The heat storage (ΔS) is quantified in the upper layer by measuring the rate of temperature change. The net storage of energy (ΔS) in the soil column is determined from the temperature profile taken above each soil heat flux plate. Three probes (TCAV, Campbell Sci.) are placed in the soil to sample soil temperature; these sensors are placed 0.01÷0.04 m (z) below the surface (Fig. 6.5).

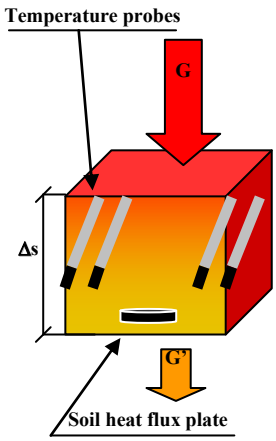

Fig. 6.5. Temperature probes and heat flux plates positioning into the soil.

The volumetric heat capacity of the soil C_v ($J \cdot m^{-3} \cdot K^{-1}$) is estimated from the volumetric fractions of minerals (V_m), organic matter (V_o) and volumetric water content (θ). Therefore, G at the surface is assessed by measuring G_0 at a depth of 0.05 m and the change in temperature over time of the soil layer above the heat flux plates to determine ΔS:

$$G = G' + \Delta S = G' + C_v \left(\frac{T_f - T_i}{t_f - t_i} \right) d_g \qquad (6.1)$$

where G' is the heat flux density measured by the plate, ΔS is the heat storage, T_f is the final temperature at time t_f, T_i is the initial temperature at time t_i (the measurement time interval is of 30 min), d_g is the depth (m) of the heat flux plates.

At two heights, 4 and 8 meters, the equipment for Surface Renewal and Eddy Covariance measurements is deployed, so that air temperature, three wind speed components and water vapour are measured. At both levels there is one fine wire thermocouple (FW3, Campbell Sci., 76.2 μm diameter), one 3-D sonic anemometer (Windmaster Pro, Gill Instruments,

at 4 m and CSAT3, Campbell Sci., at 8 m) and one open-path gas analyzer (LI-7500, LI-COR Biosciences) (Fig. 6.6). Wind components were rotated to force the mean vertical wind speed to zero and to align the horizontal wind speed to the mean streamwise direction; the freely distributed TK2 package (Mauder and Foken, 2004) was used to determine the first and second order statistical moments and fluxes in half-hourly basis following the protocol taken as a reference for comparison described in Mauder *et al*. (2007).

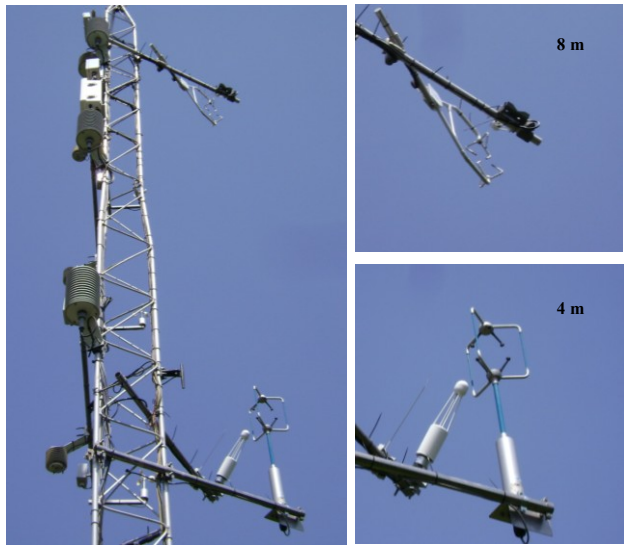

Fig. 6.6. The two levels for SR and EC measurements.

Air temperature and humidity, wind speed and direction profiles are realized within the orchard with sensors (HMP45C, Vaisala, and A100, Vector Instruments, respectively) installed at 4.5, 6.5, 8.0 and 10.0 meter above the soil surface (Fig. 6.7).

Fig. 6.7. Temperature, humidity and wind profile.

Atmospheric pressure (CS106, Campbell Sci.), rainfall (ARG 100, Waterra) and PAR, Photosynthetically Active Radiation (SKP215, Skye Instruments), are measured too. Moreover, to monitor canopy temperature and detect stress conditions onset, four infrared thermometers (IR120, Campbell Sci.) are installed within the orchard, each one pointing at a tree from a cardinal point.

Volumetric water content is measured by using the time domain reflectometry theory (TDR) with four probes (CS 616, Campbell Sci.) set up at two different depths below the soil surface (Fig. 6.8).

Heat Pulse Velocity probes (2 in each of the monitored tree, in the North and South faces of the trunk, respectively) 50 mm long, with sensing parts at 5, 15, 25, 45 mm (HP4TC, TranzFlo, NZ) and heaters (HTR5, TranzFlo, NZ) are installed on three orange trees to measure transpiration by the Sap Flow method (Fig. 6.9).

Fig. 6.8. TDR probes into the soil.

Fig. 6.9. HPV probes installed for Sap Flow measurements.

7 Sensible heat flux estimates using two different methods based on surface renewal analysis

Acquisition and maintenance of the instrumentation required to directly measure scalar surface fluxes (i.e., the eddy covariance, EC, system) are expensive. Therefore, alternative methods are of interest and, if proven reliable, they may also be implemented to overcome routinely problems in direct measurements, such as gap filling (Dias *et al*., 2009; Guo *et al*., 2009b). Alternative methods are especially useful when they are affordable, and when operating simultaneously with direct methods they do not share shortcomings. The surface renewal, SR, analysis method to estimate the flux of a scalar (pioneered by Paw U *et al*., 1995) is appropriate because the theoretical grounds invoked are different from the EC method. As a consequence, to apply the SR method the three dimensional sonic anemometer is not required and it can operate either in the roughness or inertial sublayers. SR studies mostly centred on sensible heat flux, H, estimation, and the earlier SR method, SR1, has been recommended for more than a decade (Anandakumar, 1999; Anderson *et al*., 2003; Consoli *et al*., 2006b; Drexler *et al*., 2004, 2008; Katul *et al*., 1996; Mengistu and Savage, 2010; Paw U *et al*., 2005; Snyder *et al*., 1996, 1997; Spano *et al*., 1997; Zapata and Martínez-Cob, 2001, 2002).

Method SR1 requires calibration of one parameter, the so-called parameter α (see Eq. 7.1). However, the assumption to take α as a constant appeared stringent because earlier studies shown dependency on stability cases, canopy architecture and measurement height (Castellví, 2004). The parameter α has been a matter of research which may be summarized as follows. An expression to estimate α (half-hourly) was derived that was

capable to explain the performance observed in previous experiments (Castellví, 2004). Therefore, the SR method using half-hourly α estimates, method SR2, became exempt of calibration, provided the input required is available.

When measurements are taken in the inertial sublayer over a rather homogeneous surface, there is evidence that the method SR2 is superior to SR1 (Castellví, 2004) and that SR2 may be considered as an independent method for estimating scalar fluxes (Castellví, 2004, 2010; Castellví and Snyder, 2009a, 2010a; Castellví *et al*., 2008). When measurements are taken in the roughness sublayer, the performance of method SR2 only has been analyzed for H (according to our knowledge). Earlier studies consisting on short datasets mainly gathered under unstable cases (Castellví, 2004; Castellví *et al*., 2006) and at a windy site regardless of the stability case (Castellví and Martinez-Cob, 2005) shown that method SR2 performed close to the EC method using estimations of the roughness sublayer depth (from the ground), z^*, and the zero-plane displacement, d, as a portion of the canopy height, h_c. Over grapevines it was shown that portions of multiple pairs (z^*/h_c, d/h_c), can provide reliable H estimates (Castellví and Snyder, 2010b) and an objective method was derived to determine a reliable pair for near neutral cases over homogeneous and moderately heterogeneous canopies. For these experiments, relationships to account for the variability of z^* were not required because the H estimates were close to the determined using the EC method. However, over rice (Castellví and Snyder, 2009b) and peach orchard (Castellví and Snyder, 2009c), methods SR2 and EC were close when it was coupled with semi-empirical relationships to estimate z^* half-hourly. It was recommended to check these relationships and a set of equations were

derived to facilitate this task (Castellví and Snyder, 2009b). Therefore, in the roughness sublayer there is a need to establish a general procedure for estimating α in SR2, valid for different surfaces and weather conditions. For field applications, the latter will state which is the input required to apply SR2.

For sensible heat flux, two earlier studies (133 and 43 half-hourly samples gathered under unstable cases over grapevines and wheat, respectively) shown that using reasonable scaling for (z^*/h_c, d/h_c) SR2 performed superior to SR1 (Castellví, 2004). Likely, because there is not a unique α-procedure to apply SR2 and methods SR1 and EC are highly correlated for unstable cases recent studies have recommended SR1 without analyzing the performance of SR2 (Drexler *et al*., 2008; Mengistu and Savage, 2010). This study was motivated in light to compare SR1 and SR2 using a procedure to estimate α that accounts for variability of z^* depending on weather conditions and canopy characteristics (Castellví and Snyder, 2009c). Therefore, differences in input requirements and performance between the SR methods can be compared. An experiment (from February to October 2010) was carried out to estimate H over a mature orange orchard. The experiment offers the optimal conditions for our purpose because the morphology of a mature orange tree is fairly constant through the year. Thus, calibration and validation depend on weather conditions.

7.1 Theory

SR analysis for estimating scalar surface fluxes uses SR theory (pioneered by Higbie, 1935) in conjunction with the analysis of the scalar trace to extract the mean ramp dimensions (amplitude and period) of the

ramp like (or asymmetric triangle shape) pattern observed in the trace (typically, half-hourly). Ramp dimensions identify a coherent structure which can be defined as an eddy capable to provide organization within the turbulent motion and responsible for the main vertical turbulent mixing (Hongyan *et al*., 2004; Paw U *et al*., 1995). The SR method is based on a solution of the scalar conservation equation for an incompressible steady and planar homogeneous turbulent flow. For sensible heat flux, assuming that the air parcel renewed (i.e., the associated with the coherent structure) is uniformly heated (cooled) with no heat lost through the parcel top while it remains in contact with the sources (sinks), it can be estimated as (Paw U *et al*., 1995; Castellví, 2004):

$$H_{SR} = \rho C_p (\alpha z)\frac{A}{\tau}\begin{cases} \text{method SR1}: \alpha = \text{constant} & \text{for } h_c < z \\ \text{method SR2}: \alpha = \left[\dfrac{\kappa}{\pi}\dfrac{(z^* - d)}{z^2}\pi u_* \phi_h^{-1}(\zeta)\right]^{1/2} & \text{for } h_c < z \le z^* \end{cases} \quad (7.1)$$

where ρ and C_p are, respectively, the density and specific heat at constant pressure of air, z, is the measurement height of the air temperature trace which represents the volume, V, per unit area, S, of the parcel (i.e., $z = V/S$), the parameter α is included to correct the volume for the unequal heating within the air parcel, and A and τ are, respectively, the mean amplitude and period of the ramp pattern observed in the temperature trace. Since method SR1 assumed parameter α as a constant to be calibrated against the EC method, the implication was sound because the only input required is the measurement of the air temperature trace at one height above the source. Method SR2 estimates α half-hourly and in Eq. 7.1 $\kappa = 0.4$ is the Von Kármán constant, u_* is the friction velocity which can be estimated as $u_* = 0.5\sigma_u$, where σ_u is the turbulent standard deviation of the horizontal wind speed measured at the canopy top (Kaimal

and Finnigan, 1994), $\phi_h(\zeta)$ is the flux-gradient stability function and ζ is a stability parameter, $\zeta = (z-d)/L_O$, where L_o is the Obukhov length, $L_O = -\left(u_*^3 / \kappa g\left(\overline{w'T_v'}\right)\right)T_v$ [T_v and g are the air virtual temperature and acceleration due to gravity, respectively, and $\overline{w'T_v'}$ is the kinematic buoyant sensible heat flux]. In practice, when T_v is not available it is replaced by the air temperature. Regardless, a widely accepted formulation for $\phi_h(\zeta)$ is (Foken, 2006; Högström, 1988):

$$\phi_h(\zeta) = \begin{cases} (0.95 + 7.8\zeta) & 0 \le \zeta \le 1 \\ 0.95(1 - 11.6\zeta)^{-1/2} & -2 \le \zeta \le 0 \end{cases} \tag{7.2}$$

Castellví and Snyder (2009c) combined a model based on a mixing-length theory for momentum (Harman and Finnigan, 2007), mixing-layer analogy (Raupach *et al*., 1996), semi-empirical canopy-relationships (Graefe, 2004) and the relationship $u_* \approx 0.5\sigma_u$ to estimate z^* half-hourly:

$$z^* = h_c + \frac{(h_c - h_*)^2}{(h_c - d)} \frac{I_u^2}{(c_d LAI)} \tag{7.3}$$

where h_* is the height from the ground to the bottom of the canopy, c_d is the leaf drag coefficient, *LAI* is the leaf area index, and $I_u = (\sigma_u / u)$ is the turbulent intensity, with u the horizontal mean wind speed at the canopy top.

The zero-plane displacement can be estimated as a portion of the canopy height where an intermediate scaling is $d = 0.75h_c$ (Brutsaert, 1988). Estimation of the mean drag coefficient at the leaf scale is a compromise. It depends on the shape and orientation of the leaves and, in principle, it may depend on the velocity field within the canopy through the Reynolds number, *Re*, though such relationship is not still clear

(Brutsaert, 1988; Pingtong and Takahashi, 2000). Models of transfer of momentum of different order support that c_d can be taken as a constant, that is not depending on *Re* (Pingtong and Takahashi, 2000).

Ramp dimensions. They were determined as described in Van Atta (1977) using structure functions, $S^n_{(r)}$ (*r* denotes time lag) of order *n* = 2, 3 and 5. For solving the ramp period, several time lags were used to linearize the following relationship that holds for r much smaller than the warming (cooling) period, L_r, while the air parcel to be renewed remains in contact with the surface; $A^3 = -\left(S^3_{(r)}/r\right)\tau$. According to Chen *et al*. (1997a), the shortest time lag to be used for linearization, r_{1G}, is that which produces the first global maximum of $S^3_{(r)}/r$. To estimate the maximum time lag, r_{end}, to be used for linearization so that $r << L_r$, the second global maximum of $S^3_{(r)}/r$ was determined. The second global maximum occurs at a time lag, r_{2G}, giving $r_{2G} \approx ¾\tau$. Based on Qiu *et al*. (1995) that showed $\left(\tau - L_r\right) \approx 0.25\tau$, it follows that $r_{2G} \approx L_r$. Accordingly, the last time lag used for linearization was determined as 1% of r_{2G} to insure $r_{end} << L_r$.

The H estimates. For method SR1, once α is known, determination of *H* is immediate from measurements taken with a fine-wire thermocouple. For method SR2, provided c_d, d, h_* and *LAI* are known (or estimated), z^* is determined half-hourly and *H* can be iterated. Starting at neutral case, $\phi_h(\zeta) = 0.95$, α is determined which provides the initial H_{SR2}, H_{SR2_i}. Therefore, $\left(\overline{w'T'}\right)_i = H_{SR2\_i}/\left(\rho C_p\right)$ gives the first iterated L_0 and ζ which allows for the next $\phi_h(\zeta)$ value. The process is iterated until convergence for ζ is achieved.

7.2 Calibration and validation: datasets and procedure for performance evaluation

The measurements taken at z=4m were used to estimate H using methods SR1 and SR2, H_{SR1_4m} and H_{SR2_4m}, respectively. However, for completeness the H estimated using method SR1 operating at z=8m, H_{SR1_8m}, was also determined.

The reference. Since the SR method requires calibration against the EC method, the H_{EC} estimates were compared at 4 m and at 8 m. The following analysis was carried out for the second and third week of each month. Series of one hour were used to determine the sensible heat flux cospectra, wT, at 4 m and 8 m using Multiresolution Flux Decomposition, MFD (Howell and Mahrt, 1997; Vickers and Mahrt, 2003). MFD is applied to study the cospectral gap scale which is the timescale that separates turbulent and mesoscale fluxes. We note that SR analysis only accounts for turbulent mixing. The cospectral gap was obtained determining the zero-crossing or stabilization of the cospectra versus the averaging time scale (Vickers and Mahrt, 2003). Cospectral gaps were mostly observed for averaging time scales not longer than 13.653 min (i.e., a decomposition of 13 bins). For each period of two weeks, the averaged cospectra was determined for stable and unstable cases. Figure 7.1 shows the averaged cospectra at both levels for June (days 159÷172). The patterns shown in Fig. 7.1 were rather similar for the other months. For stable cases, regardless of the measurement height, Fig. 7.1 shows that the averaged cospectra peaked at an averaging time scale slightly shorter than 10 s. For the shortest and largest time scales the cospectra were similar.

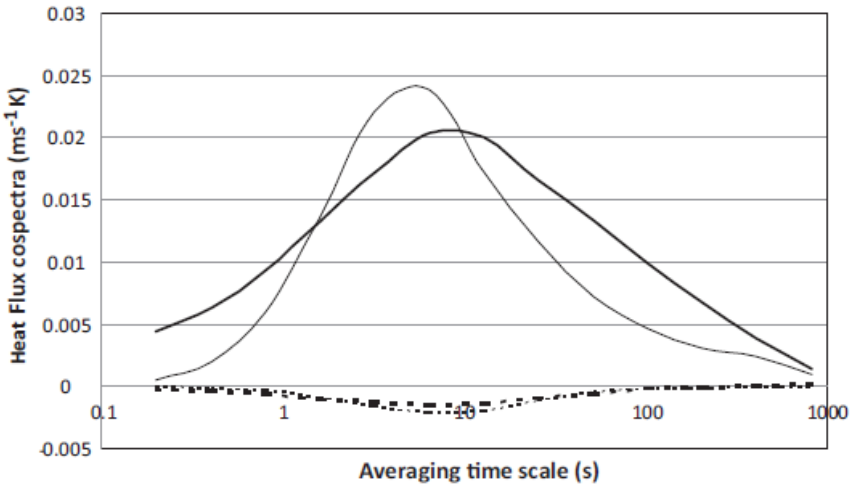

Figure 7.1. Averaged sensible heat flux cospectra, wT, for days 159÷172. The cospectra are shown for stable (dashed line) and unstable (solid line) cases at 8 m (thick) and 4 m (thin). The x-axis is in log scale.

While the latter was observed in summer, the averaged cospectra at 4 m, *cos_4*, was slightly higher than at 8 m, *cos_8*, in winter, spring and fall. For unstable cases, for the whole period it was found that, except for a short interval of averaging time scales centred close to the peak of *cos_4m*, *cos_8* was larger than *cos_4m*. Consistently, *cos_8* peaked at time scales higher than *cos_4*. Thus, main mixing was carried out by larger eddies at *z*=8m than at *z*=4m. The difference between the cospectra (the higher level minus the lower level), $df = \cos\_8 - \cos\_4$, was determined for stable and unstable cases. Table 7.2 shows the integrated *df* value to show the vertical differences (in W m^{-2}) for each month in the two-weeks averaged half-hourly *H*. For stable cases, *df* was small, but not for unstable cases. Mean flux divergence was not observed being the *H* measured at *z*=8m consistently higher than at z=4m. The main differences corresponded to months (from May to August) where clear skies predominate with high incoming solar radiation (Table 7.1). For each two-weeks period, the half-

hourly covariances, $\overline{w'T'}$, determined using package TK2 that passed the Foken's quality control test up to level 7 [this level includes high and moderate quality measurements that may be considered useful for routinely applications and gap filling (Mauder and Foken, 2004)] and MFD were very close to each other. The slopes, s, of the linear regression analysis (TK2 versus MFD) were all around one, $0.995 \leq s \leq 1.02$, and the determination coefficients, R^2, were $R^2 \geq 0.985$.

Table 7.1. Climate observed at the experimental site. For periods of three months the average and standard deviation (in parenthesis) were determined using half-hourly values for the following measurements taken at z=8m; T is the air temperature, RH is the relative humidity, R_s is the solar radiation, u is the horizontal wind speed, u_* is the friction velocity, H is the sensible heat flux and R_N is the net radiation. Rain is the total precipitation measured nearby.

Period	Rain (mm)	T (°C)	RH (%)	R_s (W m^{-2})	u (m s^{-1})	u_* (m s^{-1})	H (W m^{-2})	R_n (W m^{-2})
February÷April	110	13.8 (4.9)	68 (23)	193 (279)	2.4 (1.6)	0.27 (0.21)	34 (89)	76 (172)
May÷July	31	22.7 (6.4)	46 (22)	299 (341)	2.5 (1.7)	0.30 (0.24)	71 (109)	157 (246)
August÷October	18	23.4 (5.9)	57 (24)	229 (304)	1.9 (1.4)	0.22 (0.19)	34 (77)	113 (212)

Table 7.2. Differences (higher level minus lower level) for the averaged half-hourly sensible heat flux (W m^{-2}) determined using Multiresolution Flux Decomposition for stable and unstable cases. The average corresponds to the second and third week of each month.

Case \ Month	February	March	April	May	June	July	August	September	October
Stable	-1.0	-1.5	-1.0	-2.0	2.0	3.0	4.0	4.0	1.0
Unstable	9.5	13.5	15.0	19.0	33.5	25.0	26.0	7.0	8.5

Therefore, since for unstable cases the larger motions were best captured at the higher level and deployment of the EC system at a height of at least twice the canopy top is recommended (Foken, 2008a), H_{EC_8m} was taken as a reference for calibration and validation. For completeness, H_{EC_4m} was included in the comparison.

Calibration and validation. It was made for stable and unstable cases. However, stable cases were split to discriminate surface cooling, $(R_N - G) \leq 0$ W m^{-2} (i.e., mostly night hours), from daylight hours with $(R_N - G) > 0$ W m^{-2} (i.e., influenced by regional advection of sensible heat flux). For method SR1, α was calibrated forcing the linear regression to have a zero intercept. For method SR2, the drag coefficient c_d was fit by trial and error to minimize the root mean square error (Rmse) of H. The initial trial was c_d = 0.2; increments of 0.025 were performed covering a wide range (i.e., without taking care of unreasonable c_d values). The c_d that minimized the Rmse was next refined using increments of 0.005.

Datasets and data selection. For calibration, the datasets selected corresponded to the central two weeks within a three-month period. Thus, the datasets used for calibration were from day of year (DOY) 75 to 90, 159 to 172 and 244 to 258, respectively, for the corresponding three-month periods February÷April, May÷July and August÷October. The three-month periods were then used for validation. The samples analyzed passed the following three requirements: (1) rain was not observed; (2) The Foken's quality control test up to level 7; (3) H estimates falling out of range, the boundaries were set as the global maximum (minimum) of H_{EC_8m} ± 50Wm^{-2}, were removed as outliers to not distort calibration and the statistics to evaluate the performance. The samples removed correspond to periods that ramps in traces were not well formed (1.8% for unstable cases and 2.1% for stable cases). The total half-hourly samples available for comparison under unstable and stable cases were 4566 and 5721, respectively. The larger dataset for stable cases resulted from the influence of the regional advection.

Performance evaluation. Linear regression analysis, R^2 and Rmse were used to compare H_{SR1_4m}, H_{SR1_8m}, H_{SR2_4m} and H_{EC_4m} versus H_{EC_8m}. Since regression analysis assumes that H_{EC_8m} (the reference) is free of random sampling errors, the coefficient $D\left(=\sum H / \sum H_{EC\_8m}\right)$ was also determined as an integrated evaluation in daily, weekly, monthly, etc. time scales by averaging out errors in the half-hourly estimates (i.e., the bias is (D−1) times the mean of H_{EC_8m}).

7.3 Results

7.3.1 Calibration

For each calibration period, Table 7.3 shows the number of samples, *N*, available, the calibrated α for H_{SR1_4m} and H_{SR1_8m}, $\alpha_{z=4m}$ and $\alpha_{z=8m}$, respectively, the calibrated c_d for H_{SR2_4m} and the linear regression analysis (slope, *s*, and intercept, *int*), R^2 and Rmse comparing H_{EC_4m} versus H_{EC_8m}. Either $\alpha_{z=4m}$ and $\alpha_{z=8m}$ were smaller and larger than 0.5 for stable and unstable cases, respectively. This corroborates other experiments that show α calibration for stable and unstable cases (Paw U *et al*., 1995; Castellví, 2004) and calibration using datasets with most of the samples gathered under unstable cases (Snyder *et al*., 1996; Paw U *et al*., 2005). For stable cases, regardless of the measurement height, the trend observed to have higher α for positive than for negative (R_N-G) can be explained by the different rate of momentum absorbed by the canopy during the day and the night. In fact, regardless of the advective conditions, larger eddies are responsible of the mixing during the day and α is proven to be a measure of the efficiency of the turbulence to mix the scalar within the air parcel to be renewed (Castellví and Snyder, 2009a). For unstable cases, Table 7.3

shows some significant differences between the α values determined for each period. The variability suggests that method SR1 may require a rather continuous calibration through the year, regardless of the surface. The need to calibrate α monthly for a changing surface (wetlands) was shown in Drexler *et al*. (2008).

Table 7.3. Calibration of parameter α for method SR1 at heights z =4m and z =8m, $\alpha_{z=4m}$ and $\alpha_{z=8m}$, respectively, and c_d for method SR2. In bold, the performance of H_{EC_4m} versus H_{EC_8m}. The Rmse and the int are in Wm^{-2}.

Case	N	$\alpha_{z=4m}$	Rmse	$\alpha_{z=8m}$	*Rmse*	c_d	Rmse	*s*	*int.*	R^2	Rmse
(P: 75÷90)											
Unstable	304	0.66	61	0.64	*56*	0.075	37	**0.85**	**-4**	**0.94**	**35**
Stable$^-$	286	0.32	13	0.17	*10*	0.2	16	**0.67**	**-1**	**0.70**	**12**
(P: 159÷172)											
Unstable	271	0.58	75	0.53	*67*	0.075	62	**0.81**	**2**	**0.86**	**49**
Stable$^-$	108	0.21	17	0.18	*15*	0.2	16	**0.53**	**-8**	**0.55**	**14**
Stable$^+$	29	0.41	14	0.27	*17*	0.2	15	**0.35**	**-9**	**0.23**	**21**
(P: 244÷258)											
Unstable	183	0.76	51	0.61	*45*	0.075	35	**0.89**	**2**	**0.86**	**25**
Stable$^-$	274	0.25	13	0.17	*11*	0.2	13	**0.42**	**-7**	**0.29**	**15**
Stable$^+$	61	0.38	9	0.29	*9*	0.2	11	**0.74**	**-3**	**0.38**	**13**

+ and – denotes *(R_N-G)* positive and negative, respectively.

For method SR2, the fitted c_d value was robust (Table 7.3) and this suggests that after few days of calibration the method is ready to operate. Despite the procedure used to apply SR2 involves different uncertain scales (i.e., among others the scales relating $u*$ with σ_u and d with h_c were set as a rule of thumb), the analytical form of Eq. 7.3 packs all uncertainties on the parameter to be fit, c_d. Though irrelevant for this study, the latter implies that the c_d values obtained may not necessarily be realistic. Therefore, the uncertainty in SR2 due to scaling was corrected in relation to stability cases. The c_d values obtained still were within a range shown in other experiments. For unstable cases (c_d = 0.075) is in the order of the value found for beans (Thom, 1971; Pingtong and Takahashi, 2000)

and in a close agreement with the model for transfer of momentum under neutral conditions within a uniform canopy derived by Mohan and Tiwari (2004). Assuming a constant foliage vertical distribution, for a ratio of about $d/h_c \approx 0.7$, the Mohan and Tiwari's model predicts c_d for LAI ≈ 0.35, which suggests a c_d of about 0.08 for LAI = 4.25. For stable cases, the c_d value obtained is within the range found for pine forest (Amiro, 1990), and the same of that found for corn (Wilson and Shaw, 1977; Pingtong and Takahashi, 2000) and peach orchard (Castellví and Snyder, 2009c).

The method SR1 gave the largest Rmse for unstable cases. In a review of experiments showing the performance of method SR1 operating in the roughness sublayer, such as over forest, walnut and maize canopies (Paw U *et al*., 1995), over grapevines and avocado (Paw U *et al*., 2005), and over wheat (Castellví, 2004), the Rmse obtained were smaller than those shown in Table 7.3. However, all these experiments are not directly comparable because temperature traces were taken at the same (or close) height to the sonic anemometer and H was measured using a one-dimensional sonic anemometer. For H_{SR1_8m}, the Rmse shown in Table 7.3 are slightly smaller than for H_{SR1_4m}. The latter may suggest calibration and application of method SR1 using as input temperature traces measured close to the deployment of the EC system. However, we anticipate caution because other factors play a role. In any case, in general the Rmse obtained for H_{SR2_4m} were comparable to those obtained for H_{EC_4m}, and smaller than those obtained for H_{SR1_4m} and H_{SR1_8m}.

For unstable cases, H_{EC_4m} and H_{EC_8m} were rather well correlated ($R^2 \geq 0.86$, for the three periods). Fig. 7.2 shows H_{EC_4m} versus H_{EC_8m} for all the campaign ($R^2 = 0.94$, Table 7.4). However, when different EC systems measuring H are deployed in the inertial sublayer, $R^2 \geq 0.97$ are

expected (Mauder *et al*., 2007). The EC method is not necessarily accurate when fluxes and friction velocities are small (Vickers and Mahrt, 2003; Terradellas *et al*., 2001, 2005). Under such conditions, in general for stable cases, SR analysis is also limited because few ramps are observed in the trace. Table 7.3 shows, regardless of the method (SR1, SR2 and the EC operating at z=4m), that for stable cases the Rmse fall within the measurement error of the EC method which is about 20÷25 W m^{-2} (Twine *et al*., 2000; Mauder *et al*., 2007; Foken, 2008a).

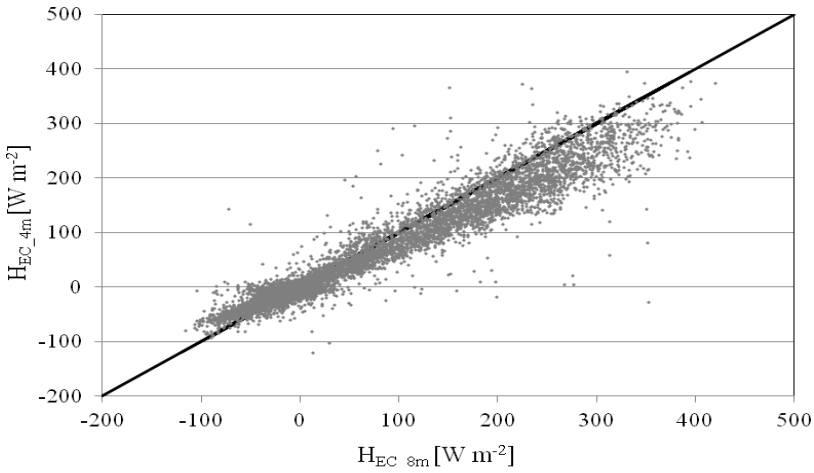

Figure 7.2. Sensible heat flux measurements using the EC method at z = 4 m, H_{EC_4m}, versus at z =8 m, H_{EC_8m}, for all the data.

7.3.2 Validation

Table 7.4 shows the results to compare the performance for H_{EC_4m}, H_{SR1_4m}, H_{SR1_8m} and H_{SR2_4m}. For H_{EC_4m} it is shown that, in general, the D values obtained were smaller than one, regardless of the period and case. Thus, H_{EC_4m} consistently underestimated H_{EC_8m}. For all the data (Fig. 7.2), it was found D = 0.82, so the general underestimation was 18%. For

unstable cases, Table 7.4 shows that the Rmse for H_{EC_4m} were in the range 35 W m^{-2} ≤ Rmse ≤ 51 W m^{-2}. For stable cases, the Rmse was small because H was small for most of the samples (Fig. 7.2).

Table 7.4. Comparison of H_{EC_4m} and validation of H_{SR1_4m} , H_{SR1_8m} and H_{SR2_4m} versus H_{EC_8m} for each three months period, P (Julian days), for unstable, Un., and stable, St., cases. The Rmse and the int. are in W m^{-2}.

Case	N	Method																			
		$H_{EC\ 4m}$					$H_{SR1\ 4m}$					$H_{SR1\ 8m}$					H_{SR2}				
		s	*int.*	R^2	Rmse	D	*s*	*int.*	R^2	Rmse	D	*s*	*int.*	R^2	Rmse	D	*s*	*int.*	R^2	Rmse	D
P: 47÷120																					
Unstable	1570	0.85	-3	0.93	37	0.82	0.92	-11	0.78	56	0.83	1.00	11	0.65	72	1.10	0.93	-4	0.87	39	0.90
Stable$^-$	1545	0.66	-2	0.77	14	0.75	0.42	-8	0.51	19	0.79	0.53	-6	0.47	19	0.81	0.60	-7	0.72	15	0.90
P: 121÷212																					
Unstable	1883	0.81	6	0.81	51	0.84	0.90	-15	0.64	73	0.81	1.00	6	0.59	77	1.04	1.01	-3	0.77	52	1.00
Stable$^-$	2021	0.48	-7	0.46	17	0.97	0.19	-11	0.23	20	0.96	0.44	-13	0.30	20	1.32	0.41	-19	0.29	23	1.60
Stable$^+$	94	0.17	-10	0.02	29	0.62	0.20	-10	0.09	21	0.67	0.28	-5	0.09	23	0.56	0.45	-12	0.13	22	1.05
P: 213÷288																					
Unstable	1113	0.79	7	0.85	35	0.85	1.11	-24	0.70	56	0.92	1.14	-2	0.59	72	1.12	1.04	-3	0.79	41	1.01
Stable$^-$	1827	0.51	-7	0.41	14	1.22	0.27	-12	0.21	16	1.62	0.41	-10	0.29	16	1.36	0.44	-17	0.21	22	2.15
Stable$^+$	234	0.67	-3	0.54	11	0.86	0.58	-5	0.42	12	0.91	0.60	-2	0.33	14	0.76	0.66	-7	0.50	11	1.09
All data	10287	0.83	0	0.94	36	0.82	0.87	-3	0.83	45	0.81	1.10	-4	0.79	71	1.06	1.00	-5	0.91	35	0.92

+ and – denotes (R_N-G) positive and negative, respectively.

For method SR1, H_{SR1_4m} consistently performed closer to H_{EC_8m} than H_{SR1_8m} for unstable cases. In principle, this performance would not be expected because it is not consistent with that found during calibration (i.e., Table 7.3 showed that the Rmse for H_{SR1_8m} was smaller than for H_{SR1_4m}). An explanation may be as follows. For all the data, Fig. 7.3 shows the frequency to have $z^* < 8$ m versus time (i.e., the half-hourly z^* estimates were determined using Eq. 7.3). In general, it is shown that when (R_N-G) < 0 W m^{-2}, the measurement height at z=8m mostly was within the inertial sub-layer. For (R_N-G) > 0 W m^{-2}, z^* was oscillating around z=8m for about the 50% of the samples from sunrise until about two hours after noon. In late afternoon, the height z=8m tended to be within the inertial sublayer. Since above the canopy the friction velocity and the ramp period

remain fairly constant with height (Kaimal and Finnigan, 1994; Paw U *et al.*, 2005), Eq. 7.1 shows that (αz) scales with (z^*-d) when measurements are taken in the roughness sublayer, while in the inertial sublayer the scale is (z-d) (Zapata and Martínez-Cob, 2001; Castellví, 2004). Therefore, best performance for method SR1 may be expected when the following two requirements are met during calibration and validation: (1) SR1 operates close to the EC method [i.e., same traces (turbulence) are processed]. It is of interest to mention that calculations involved in methods SR1 and EC are different, so sharing the trace does not alter the comparisons; (2) the SR1 measurement height remains in a sublayer (roughness or inertial).

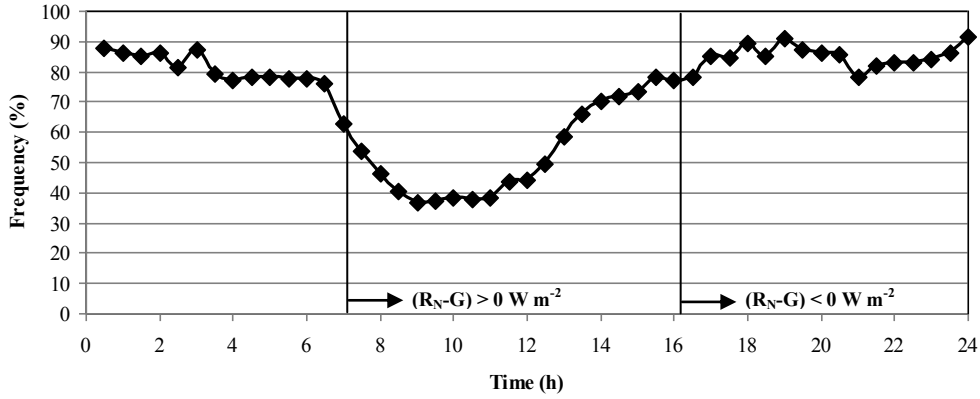

Figure 7.3. Frequency (%) versus time (GMT) to have z < 8 m for each half-hour determined using Eq. (3) for all the data, and time (averaged for the campaign) where (Rn – G) was positive and negative.*

Therefore, during calibration (15 days) the first requirement could prevail, but not during validation (three months). These two requirements were not accomplished. That is, at z=4m the eddies sensed in the air temperature trace are different than at z=8m and Fig. 7.3 suggests that z^* was oscillating around z=8m along the day. Therefore, it may explain the

higher Rmse values found with respect to other experiments, and the changeable performance between levels depending on the period compared. Determining z^* from Eq. 7.3 for unstable cases, the measurement height that would be required to gather the 98% of the samples above z^* is 4 times the canopy height. Therefore, in practice the method SR1 best operates at the canopy top.

The method SR2 was closer than SR1 to H_{EC_8m}. For SR2, the Rmse shown in Table 7.4 were in the range, 39 W m^{-2} ≤ Rmse ≤ 52 W m^{-2}, while for $SR1_{4m}$ and $SR1_{8m}$ the range was 56 W m^{-2} ≤ Rmse ≤ 77 W m^{-2}. The Rmse obtained for H_{EC_4m} was slightly better than for H_{SR2_4m} as a consequence that H_{EC_4m} was best correlated. For all the data, Fig. 7.4 A and B shows H_{SR1_4m} and H_{SR2_4m} versus H_{EC_8m}, respectively. For unstable cases, H_{SR2_4m} was not biased for the full range of H_{EC_8m} while in general H_{SR1_4m} was biased and with a large dispersion around the 1:1 line. Regardless of the validation period, Table 7.4 shows that for unstable cases H_{SR2_4m} provided D coefficients closer to one than H_{EC_4m}. For stable cases, Fig. 7.4 shows that H_{SR1_4m} tended to underestimate H_{EC_8m}. H_{SR2_4m} essentially performed poor around neutral cases in the range, $-40 \text{Wm}^{-2} \leq H_{EC\_8m} \leq 40 \text{Wm}^{-2}$. Regardless of the under or over estimations obtained for methods SR1 and SR2 (D = 0.67 for H_{SR1_4m} and D ≥ 1.60 for H_{SR2_4m}) the Rmse values fall within the EC measurement error. For all the data, H_{SR2_4m} provided the best statistics except for R^2 that H_{EC_4m} was the best.

7.4 Concluding remarks

We examined the reliability of methods SR1 and SR2 over a mature orange orchard to estimate the sensible heat flux. The alpha-procedure

used in SR2 can be considered of general application because it accounts for variability of z^* depending on weather conditions and canopy characteristics. Consequently, differences between SR1 and SR2 with regard to input requirements are stated. It is shown that the assumption required to apply SR1 (i.e., α is fairly constant for a given canopy and measurement height) did not hold. Thus, suitability of α in future experiments, such as year by year, is uncertain due to the inherent inter-annual climate variability. Therefore, in contrast to other studies (based on shorter datasets) that recommend application of SR1, this study proves that SR1 is stringent and questions its reliability. For method SR2 a period of 15 days was enough for calibration, it was superior to SR1, it was less biased than an EC method operating at the canopy top and performed close to the reference.

The instrumentation required to apply SR2 (a 2-D sonic anemometer and a thermocouple) can be deployed at the canopy top using a mast shorter than the canopy height (i.e., the instrumentation is light and can be deployed at the canopy top by a thinner mast) and there is no need to measure the horizontal wind speed and air temperature at same point in the flow.

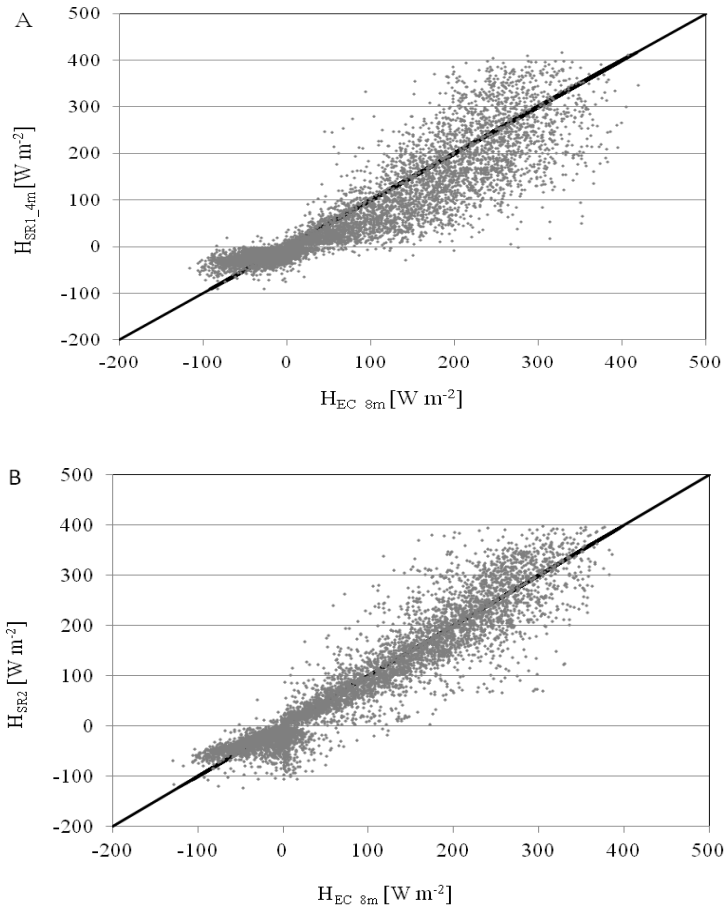

Figure 7.4. Sensible heat flux estimates using the SR methods. (A) Method SR1 operating at z = 4 m, H_{SR1_4m}, and (B) H_{SR2} versus the H measured using the EC method at z = 8 m, H_{EC_8m}, for all the data.

Thus flow distortion and sensor positioning are less relevant for SR2 than for the EC method. Therefore, SR2 could have the potential to provide an alternative H to the EC method for samples affected by flow distortion. Because reliability is mandatory for method selection, it is concluded that over a moderately tall and heterogeneous canopy the use of SR2 is recommended.

8 A method for estimating the flux of a scalar from high-frequency concentration and averaged gradient measurements. A study case for sensible heat flux.

When the vertical gradient of the scalar concentration (C) in the atmospheric surface layer is non-zero, time series of C recorded at high frequency and measured at any height show a ramp-cliff pattern which can be idealised as shown in Fig. 8.1 (Van Atta, 1977; Paw U *et al*., 1995; Chen *et al*., 1997a). This pattern is characterised by a ramp amplitude (A) and a time period (τ) that identifies a low-frequency coherent motion, or coherent structure, capable of imposing some organisation in the turbulence, and it is responsible for most of the vertical turbulent mixing (Kovasznay *et al*., 1970; Sparrow *et al*., 1970; Raupach and Thom, 1981; Gao *et al*., 1989; Raupach *et al*., 1991; Paw U *et al*., 1992, 1995; Braaten *et al*., 1993; Holzer and Siggia, 1994; Raupach *et al*., 1996; Katul *et al*., 1996, 1997; Hongyan *et al*., 2004; Garai and Kleissl, 2011). The latter is the basis of the Surface Renewal (SR) analysis for estimating the flux of a scalar, which was pioneered by Paw U *et al*. (1995). In SR analysis, the kinematic flux of a scalar (F) is estimated as:

$$F_{SR} = \alpha Z \frac{A}{\tau} \tag{8.1}$$

where Z is the measurement height above the ground and α corrects for the volume (V) per unit area (A) (i.e., $V/A=Z$) of the air parcel because in Eq. 8.1 it is assumed that the volume αZ is uniformly heated (Paw U *et al*., 1995; Snyder *et al*., 1996). Several experiments have shown that α depends on the measurement height and stability conditions (Katul *et al*., 1996; Snyder *et al*., 1996; Zapata and Martínez-Cob, 2001; Castellví,

2004). Combining SR analysis, the one-dimensional diffusion equation and the flux-gradient relationship, it was shown that α scales with $\sqrt{\frac{K_c}{\pi}\frac{\tau}{Z^2}}$, where K_c is the turbulent eddy diffusivity associated with the coherent eddy that changes the local gradient (Castellví, 2004). It is of interest to mention that the latter's scaling was derived using the ramp model shown in scheme 2 of Fig. 8.1 and, since K_c is unknown, it was assumed to be constant during the ramp formation, such as during the quiescent, warming and micro-front periods. In relation to the ramp model, however, it is important to note that this scaling is not dependent on the ramp model used. By implementing α as $\alpha = f_c\sqrt{\frac{K_c}{\pi}\frac{\tau}{Z^2}}$, where f_c is a constant, in Eq. 8.1, F can be estimated from measurements taken at one height above the canopy as:

$$F_{SR} = f_c\sqrt{\frac{K_c}{\tau\pi}}A \tag{8.2}$$

In the inertial sublayer, by estimating K_c using the Monin-Obukov similarity theory (MOST) and setting f_c=1, F_{SR} performes close to the F measured using the Eddy Covariance (EC) method (Castellví, 2004; Castellví *et al*., 2008; Castellví and Snyder, 2010a) and it offers advantages over other methods based on MOST (Castellví *et al*., 2006; Castellví and Snyder, 2009a).

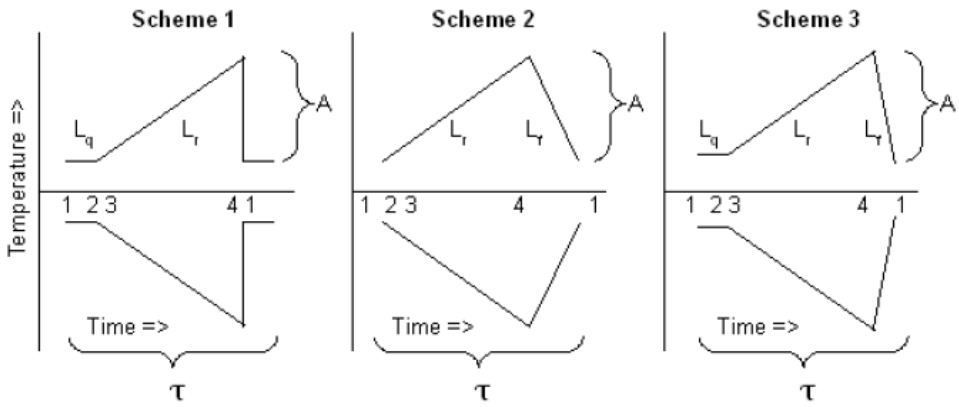

Figure 8.1. Ramp-like models associated with the time course of the scalar concentration observed at a point. Each model identifies different phases of an air parcel that follows the coherent motion: (1) incursion, (1-2) quiescent period, (3-4) warming period, and (4-1) ejection. L_q, L_r and L_f denote the quiescent, warming, and micro-front periods, respectively. A is the ramp amplitude, which is positive and negative for unstable and stable cases, respectively, and τ is the total ramp duration. Scheme 1 neglects L_f, scheme 2 neglects L_q, and scheme 3 takes into account all of the three periods (L_q, L_r, L_f).

In the roughness sublayer, all of the studies have assumed that K_c is dependent on the depth of the roughness sublayer over the measurement height (Cellier and Brunet, 1992; Kaimal and Finnigan, 1994; Graefe, 2004). As a consequence, there is not yet a general methodology to apply Eq. 8.2 because, depending on the surface and weather conditions, it may require different inputs and numerical procedures (Castellví *et al*., 2012). Likely, the most general methodology to apply Eq. 8.2 in the roughness sublayer, which is valid over tall, homogeneous and moderately heterogeneous canopies, was derived by Castellví and Snyder (2009c), hereafter referred as the *CS09* method, which is briefly described in Appendix A.

This study was motivated by the need for a SR method to estimate the flux of a scalar that does not involve the eddy diffusivity. As a consequence, it is shown that the method proposed may operate either in

the roughness or inertial sublayers by taking measurements of the scalar at three heights. Equation 8.2 can be applied with measurements taken at one height, but it requires measurements of the wind speed, canopy parameters and the use of semi-empirical relationships as inputs. Therefore, in the roughness sublayer, Eq. 8.2 may require calibration. It is of interest to mention that the proposed method can be derived by combining the flux-gradient relationship and Eq. 8.2. However, according to our knowledge, there is a lack of research on the latter method, maybe because, in the traditional SR framework, scalar flux estimates have been performed from measurements taken at one height above the canopy. This study focuses on sensible heat flux estimation in the roughness sublayer.

8.1 Theory

8.1.1 Background

Above the canopy, two conditions are assumed. First, the smallest-scale eddies that are superimposed on the coherent motion are statistically independent. When steady conditions are met over a period, $t - t_0$, where t is time and the subscript 0 denotes the initial time, A and τ can be determined using structure functions (Van Atta, 1977; Chen *et al*., 1997a). Second, the coherent motion is responsible for the entire flux of the scalar. Therefore, the changes in the local gradient made by small eddies are neglected (Castellví, 2004) and, to estimate the mean flux of the scalar, the actual time series over $(t - t_0)$ is statistically equivalent to a series showing a regular sequence of identical ramps (Van Atta, 1977; Paw U *et al*., 1995; Chen *et al*., 1997a).

These assumptions allow a consideration of three relationships.

First, the mean concentration $\left(\overline{C}\right)$ over $\left(t-t_0\right)$ observed at Z can be decomposed as (Castellví and Snyder, 2010a; Castellví, 2012):

$$\overline{C}=\overline{C_s}+\overline{C_b} \tag{8.3}$$

where subscripts s and b refer to a coherent structure and a base-line concentration, respectively. Specifically, $\overline{C_b}$ is the concentration observed during the quiescent period. Consequently, $\overline{C_b}$ is neither dependent on time nor on Z because $\frac{\partial C_{(Z,t_0)}}{\partial Z}=0$, where the quiescent period starts at t_0 (Gao *et al*., 1989), which implies $\overline{C_b}=C_{(Z,t_0)}$.

Second, after ramp analysis, $t-t_0=N\tau$, where N is a natural integer. This relationship implies that steady conditions are statistically significant for $\Delta t=\tau$ and mean quantities can be estimated over τ. According to the ramp model shown in scheme 3 of Fig. 8.1, which is considered the most realistic, the mean concentration can be expressed as:

$$\overline{C}=\frac{A}{2}\frac{\left(\tau-L_q\right)}{\tau}+\overline{C_b} \tag{8.4}$$

Since $\overline{C}$ does not depend on L_f, Eq. 8.4 is also valid for scheme 1. For scheme 2, because L_q is neglected, $\overline{C}$ does not depend on ramp time phases. Since any ramp model can be used to identify the mean coherent structure, estimation of the actual $\overline{C}$ from Eq. 8.4 should not be compromised by the model selected. It is important to note that the ramp dimensions determined by each scheme are different (Chen *et al*., 1997a [Table 1]). For instance, L_q is approximately $0.25\,\tau$ (Qiu *et al*., 1995; Chen *et al*., 1997a) and the ratio of A determined by using scheme 1 and A determined by scheme 2 is approximately 1.23, which is the average of the

ratios from bare soil, straw mulch and a Douglas-fir forest. Thus, by using these ratios, $\overline{C}$ can simply be determined as $\overline{C} = \frac{A}{2} + \overline{C_b}$, which corresponds to scheme 2 of Fig. 8.1. By denoting the vertical extent of the coherent motion as Z_b, $\overline{C_b} = \overline{C_{(Z_b)}}$ because $A_{(Z \geq Z_b)} = 0$.

Third, in the ejection phase (during the micro-front), the renewed air parcel injects scalar into the bulk of the flow and that changes the local vertical gradient up to the top of the coherent structure. Therefore, it should be possible to estimate the local gradient from measurements taken at a point and, consequently, the flux of the scalar (Castellví *et al*., 2002; Castellví, 2004; Castellví and Snyder, 2009c). Further details are given on this issue in the next section using known parameterisations of the eddy's diffusivity. It is shown that F can be estimated without determining the eddy's diffusivity regardless of the measurement height above the canopy.

8.1.2 The role of the coherent motion in changing the local gradient of a scalar above the canopy and flux estimations

In this section, derivations are made for air temperature (T) and the details to account for other scalars are also given. Assuming that no work is done in a volume, the one dimensional diffusion equation links the history of the air temperature with its vertical gradient (Priestley, 1959):

$$\frac{\partial T_{(z,t)}}{\partial t} = \frac{\partial}{\partial z}\left(K_{h_{(z,t)}} \frac{\partial T_{(z,t)}}{\partial z} \right) \tag{8.5}$$

where z is the measurement height above the zero-plane displacement (d) and $K_{h_{(z,t)}}$ is the turbulent eddy diffusivity for heat.

Based on MOST, eddy diffusivity over a period (p) of time, such as 30 minutes, $K_h = \overline{K_{h_{(z,t)}}}$ in the inertial sublayer is expressed as $K_{h,i_{(z)}} = kzu_*\phi_h^{-1}(z/L)$, where k is the Von Kármán's constant, u_* is the friction velocity, L is the Obukhov length and $\phi_h(z/L)$ is the stability function for heat transfer (Stull, 1988; Kaimal and Finnigan, 1994). In the roughness sublayer, K_h is expressed as $K_{h,r_{(z)}} = \varepsilon K_{h,i_{(z)}}$, where ε is the enhancement factor, which can be estimated as $\varepsilon = \frac{z^*}{z}$, where z^* is the roughness sublayer's depth above d (Cellier and Brunet, 1992; Mölder *et al*., 1999; Graefe, 2004). Assuming that wind shear dominates the generation of turbulence, while in the roughness sublayer K_h is constant and in the inertial sublayer, $K_h = az$, where $a = ku_*$ is constant over p. Hereafter, T in Eq. 8.5 will refer to a mean value over a period (Π) not longer than p, such as 10 or 15 minutes.

In relation to the ramps observed in the time series taken at Z, Eq. 8.4 can be used to determine T because the maximum order of ramp periods observed over natural surfaces is in the order of a minute (Chen *et al*., 1997a), thus ramp dimensions can be obtained from series of Π minutes. By virtue of Eq. 8.4, since the ramp periods observed above the canopy are not dependent on z (Chen *et al*., 1997b; Paw U *et al*., 2005) and because T_b is constant with height and time (i.e., it is the base line), Eq. 8.5 can be rewritten as follows:

$$\frac{\partial A_{(z,t)}}{\partial t} = \frac{\partial}{\partial z}\left(K_{h_{(z,t)}} \frac{\partial A_{(z,t)}}{\partial z} \right) \tag{8.6}$$

With the initial, neutral conditions of t_0 (Gao *et al*., 1989) and the boundary conditions equal to $A_{(z\geq zb,t)}=0$, Eq. 8.6 allows a determination of how the local gradient changes with time.

The roughness sublayer. Since K_h is a constant, the gradient can be determined from equation (Wang and Brass, 1998; Castellví, 2004):

$$\frac{\partial A_{(z,t)}}{\partial z}=\frac{2}{\sqrt{\pi K_h}}\int_{t_0}^{t}\frac{\partial A_{(z,s)}}{\partial s}\,d\left(\sqrt{(t-s)}\right) \tag{8.7}$$

where *s* is the variable of integration.

Inertial sublayer. Since $K_h=az$, the gradient can be calculated from (Fitzmaurice *et al*., 2004):

$$\frac{\partial A_{(z,t)}}{\partial z}=-\frac{1}{z}\frac{d}{dt}\left[\int_{t_o}^{t}A_{(z,s)}\frac{2}{\pi^2}I(0,1;x)ds\right] \tag{8.8}$$

where $x=\int_{s}^{t}\frac{a_{(s)}ds}{4z}$ and $I(0,1;x)=\int_{0}^{\infty}\frac{e^{-xu^2}}{\left(J_{0_{(u)}}^2+Y_{0_{(u)}}^2\right)}\frac{du}{u}$ is a class of Jaeger integral from the Kernel function and where J_0 and Y_0 are the zero-order Bessel functions of the first and second type, respectively. In Eq. 8.8, x is small because using the mean-value theorem to solve x from t_0 to $t=t_0+\Pi$ leads to $x=\frac{\bar{a}\tau}{4z}$, where $\bar{a}$ must be in the order of $\bar{a}\approx ku_*$, and in the inertial sublayer instrumentation is deployed at considerable height. The latter allows the approximation $I(0,1;x\to 0)\approx\frac{\pi^2}{4}\frac{1}{\sqrt{\pi x}}$ (Phillips and Mahon, 2011). Thus, Eq. 8.8 approximates Eq. 8.7.

Estimating the gradient of the scalar at the surface layer. Using the mean-value theorem to solve Eq. 8.7 from t_0 to $t=t_0+\Pi$ leads to:

$$\frac{\partial A_{(z,t)}}{\partial z} = -\frac{2}{\sqrt{\pi K_h}} f \frac{A_{(z,t)}}{\sqrt{\tau}} \tag{8.9}$$

where f is the weight resulting from the mean-value theorem that, in principle, may depend on z, i.e. the integration is in respect to time. From Eqs. 8.4 and 8.9, the temperature gradient is determined as:

$$\frac{\partial T_{(z,t)}}{\partial z} = -\omega \frac{A_{(z,t)}}{\sqrt{\tau \pi K_h}} \tag{8.10}$$

where $\omega = f\frac{\tau - L_q}{\tau}$. Half-hourly gradients can be estimated as $\frac{\partial \overline{T}}{\partial z} = -\omega \frac{A}{\sqrt{\tau \pi K_h}}$ by using the mean ramp dimensions obtained from the half-hourly time series. The flux gradient relationship combined with Eq. 8.10 allows F to be estimated as:

$$F = \omega \sqrt{\frac{K_h}{\tau \pi}} A \tag{8.11}$$

Discussion of weights of f and ω. The performance of Eq. 8.11 under non-neutral conditions. It may be of interest to mention that comparisons of the weight (ω) from different ramp models must be accompanied by their ratio in determining $\frac{A}{\sqrt{\tau}}$. For example, because $L_q \approx 0.25\tau$, in schemes 1 and 2 $\omega = 0.75f$ and $\omega = f$, respectively. The averaged $\frac{A}{\sqrt{\tau}}$ using scheme 1 over bare soil, straw mulch and a Douglas-fir forest is 0.75 times the averaged $\frac{A}{\sqrt{\tau}}$ determined using scheme 2 (Chen *et al*., 1997a [Table 1]). Consequently, from Eq. 8.10, the weight (f) is independent of the ramp model used and, therefore, the flux.

By using Eqs. 8.2 and 8.11 in scheme 2, the following relationship holds: $f_c\sqrt{K_c} = f\sqrt{K_h}$. Different experiments support that, by setting $K_c = K_h$ and $f_c = 1$ in Eq. 8.2, F_{SR} is close to F_{EC} and, therefore, $f = 1$. However, agreement between F_{SR} and F_{EC} holds for a wide range of stability conditions with measurements taken at different heights. Therefore, in practice, by using MOST to estimate K_h, the unknown weight f in Eq. 8.11 can be set to one regardless of the stability conditions or the measurement height.

Considerations necessary to account for density corrections. As previously demonstrated, Eq. 8.5 assumes that no work is performed within the volume and, therefore, under adiabatic conditions, the enthalpy of an air parcel at z remains constant and T does not change with time. Since turbulent fluctuations of the vapour pressure usually are much higher than those of the air pressure, the air pressure remains constant in relation to vapour pressure fluctuation at a given z. Therefore, ascended air parcels that were moistened while in contact with the surface had to perform work under constant pressure. That is, an air parcel enriched with water vapour has to expand to decrease its density against a nearly constant pressure. This work must be accounted for in Eq. 8.5. For an adiabatic process, the first law of the thermodynamics allows for the determination of the air temperature fluctuations to be derived from the work performed due to density changes of a moistened parcel (Webb *et al*., 1980). Accordingly, Paw U *et al*. (2000) showed that the work performed per unit area and time (W) can be estimated as $W = 0.076\ LE$ and the buoyant sensible heat flux (H_v) is approximately ($W + H$). Specifically, the latter implies that Eq. 8.5 must be solved using the virtual air temperature (T_v) as a scalar and H_v as the energy flux; i.e., H_v is approximately the enthalpy per unit time and

area. Regardless, derivation of Eq. 8.10 is not compromised and a comparison of F_{SR} versus F_{EC} $\omega \approx 1$ has proven to hold for T_v both in the roughness and the inertial sublayer (Castellví and Snyder, 2010a, 2010b).

8.1.3 Scalar flux estimation above the canopy

The kinematic flux, $F = -K_c \frac{\partial \overline{C}}{\partial z}$, combined with a generalised form of Eq. 8.10 and the use of scheme 2 for simplicity, i.e. $\omega = 1$, allows for the estimate of F as:

$$F = \frac{A^2}{\pi\tau}\left(\frac{d\overline{C}}{dz}\right)^{-1} \tag{8.12}$$

Sensible heat and buoyant heat fluxes. Equation 8.12 allows for the estimation of the buoyant heat flux (H_b):

$$H_b = \rho C_p \frac{A_{T_v}^2}{\pi\tau_{T_v}}\left(\frac{d\overline{T_v}}{dz}\right)^{-1} \tag{8.13}$$

where ρ and C_p are the air density and specific heat at a constant pressure, respectively. The work of expansion originates from the fluctuations in the air temperature of those eddies that are close to the sources, which suggests using Eq. 8.13 when measurements are taken close to the canopy. In this case, determination of the sensible heat flux requires application of the procedure described by Scothanus *et al*. (1983). When the gradient of the virtual temperature is close to the air temperature, i.e. A is related to a gradient as in Eq. 8.4, the sensible heat flux can be estimated from Eq. 8.13 by using the air temperature.

Latent heat and carbon dioxide fluxes. The procedure described in Webb *et al*. (1980) (WPL) was applied to correct the latent and carbon dioxide fluxes, as determined in Eq. 8.2, to study the resolution of the

surface energy balance over a rangeland grass area (Castellví *et al*., 2008). Since the closure achieved was excellent, the WPL density correction appears suitable for Eq. 8.12.

8.2 Materials and Methods

8.2.1 Half-hourly sensible heat flux estimates

The trial was carried out from March 1st to August 31st 2011. The H estimates were determined using time series of 30 minutes to estimate the mean ramp dimensions A_{30} and τ_{30} as described by Castellví *et al*. (2012) and the half-hourly gradient $\left(\frac{d\overline{T_{30}}}{dz}\right)$ was calculated after determining $\overline{T_{30_{(z)}}}$ as the average of the three 10 min air temperatures at z:

$$H = \rho C_p \frac{A_{30}^2}{\pi \tau_{30}} \left(\frac{d\overline{T_{30}}}{dz}\right)^{-1} \tag{8.14}$$

The CS09 method. In the same canopy, performance of *CS09* was studied in the year 2010, as described in the previous chapter (Castellví *et al*., 2012). The ramp dimensions, the turbulent standard deviation of the horizontal wind speed (σ_u) and the mean horizontal wind speed required as input were determined at Z=4m. The LAI was set equal to 4.25 m^2 m^{-2} and the zero plane displacement was estimated as $d = 0.7h$, where h is the canopy height. The c_d values obtained were $c_d = 0.075$ for $z/L > 0$ and $c_d = 0.2$ for $z/L \leq 0$. The discontinuity in c_d can be considered apparent. That is, in Eq. A2, the deviations in the scales of d/h and $u*/\sigma_u$ from their actual half-hourly values are embodied in c_d (Castellví *et al*., 2012).

8.2.2 Datasets and performance evaluation

After excluding rainy days, the dataset used for comparison included samples that passed the Foken's quality control test up to level 7 (flag#7) (Mauder and Foken, 2004). The test checks the assumptions of steady flow and developed turbulence invoked in the EC method. Therefore, the test ranks the variances and covariances by levels of reliability. Up to flag#7, i.e. from 1 to 7, the dataset includes high quality flux measurements recommended for research purposes up to flag#3 and measurements that can be considered useful for routine applications and gap filling from flag#4 to flag#7. Because the radiation shields were not aspirated, only samples with natural ventilation were used. The MET-21 radiation shield performed similar to Stevenson screens. Therefore, the minimum recommended threshold is u=2.5m/s (World Meteorological Organization, 2008). Two datasets were used to test Eq. 8.14. One set excluded samples where the half-hourly mean horizontal wind speed (u_{8m}) measured with a sonic anemometer at Z=8m was $u_{8m} < 3$ m/s. Because the probes were used to determine the local gradient at Z=6.5m and Z=9.5m, part of the error due to heating may have been balanced. Therefore, a second dataset was formed for samples with 2 m/s $\leq u_{8m} \leq$ 3 m/s.

The roughness sublayer depth above the ground ($Z^* = (z^*+d)$) may oscillate around the measurement heights of Z=6.5m and Z=9.5m. However, Eq. 8.12 assumes that the instrumentation is deployed in the roughness or the inertial sublayers. Therefore, Z^* was estimated half-hourly using Eq. A2. Accordingly, the samples were split into three sublayers. One sublayer had samples collected when all of the three measurement heights fell in the inertial sublayer (ISL), i.e. $Z^* < 6.5$ m; another sublayer had samples taken in the roughness sublayer (RSL), or $Z^* > 9.5$ m. In the

third sublayer, Z^* falls within the measurement heights, 6.5 m $\leq Z^* \leq$ 9.5 m, and the instrumentation was deployed in the transition sublayer (TSL).

Linear regression analysis with a slope and intercept, coefficient of determination (R^2) and the root mean square error (RMSE) were used to compare estimates versus the measured H at z=8m (H_{EC}). Since regression analysis assumes that H_{EC} is free of errors, the coefficient $D\left(=\sum H / \sum H_{EC}\right)$ was also determined as an integrated evaluation by averaging out random errors in the half-hourly estimates; i.e., the bias is $(D-1)$ times the average of H_{EC}.

8.3 Results

Since light winds were required to gather samples in the ISL, the samples fell in the TSL and RSL sublayers. Within the TSL, samples were gathered for unstable and stable cases. However, all the stable cases corresponded with samples gathered during daylight hours, i.e., under the influence of regional advection of sensible heat flux in general starting approximately two hours after noon. In the RSL, the samples were gathered under unstable conditions.

For each case (i.e., each combination of sublayer, stability conditions and u_{8m} threshold), Table 8.1 shows the number of samples (N) available for each sublayer, the results of the linear fitting (R^2), the RMSE and the D, which compares the H estimates from Eq. 8.14 ($H_{Eq.8.14}$) versus H_{EC}. The performance of Eq. 8.14 and the CS09 method is shown for all of the data.

Table 8.1. Sensible heat flux estimates: Eq. 8.14 versus H_{EC} determined in the roughness (RSL) and transition (TSL) sublayers. For all of the data the comparison is shown for Eq. 8.14 and for the CS09 method.

	N	Int.	Slope	R^2	RMSE	D
Case (U_{8m})			*RSL Unstable*			
>3	734	-17	1.16	0.82	52	1.08
[2,3]	434	11	0.95	0.82	45	1.01
≥2	1168	-5	1.08	0.81	49	1.05
Case (U_{8m})			*TSL Unstable*			
>3	348	-21	1.23	0.85	51	1.09
[2,3]	43	-1	0.99	0.82	28	0.97
≥2	391	-18	1.21	0.86	49	1.08
Case (U_{8m})			*TSL Stable*			
>3	60	3	1.57	0.82	38	1.51
[2,3]	138	-3	1.55	0.58	38	1.61
≥2	198	-2	1.54	0.68	38	1.58
Case			*All of the data*			
Eq. 8.14	1757	-13	1.13	0.89	48	1.04
CS09	1757	10	0.97	0.94	28	1.06

U_{8m} is the mean wind speed in m s^{-1} measured at 8 m, N is the number of samples, the slope and the intercept (*Int.*, in W m^{-2}) are determined from a linear regression analysis. R^2 is the coefficient of determination, *RMSE* is the root mean square error in W m^{-2}, and D is the integrated H estimates over the integrated H_{EC}.

The RSL. Regardless of u_{8m}, Table 8.1 shows that, in general, the slopes were close to one, the intercepts were negligible, the coefficients of determination were approximately R^2=0.8, and the RMSE were approximately 50 Wm^{-2}. Coefficients of D were close to one (D-1 was within 8%), thus the bias was negligible at 11 W m^{-2} for all of the data. The good performance is shown in Fig. 8.2a, which compares $H_{Eq.8.14}$ versus H_{EC} for all the samples, i.e., for $u_{8m} \geq 2$ m/s. The different agreement obtained for datasets $u_{8m} > 3$ m/s and 2 m/s $\leq u_{8m} \leq 3$ m/s may be attributed to the weight f. However, using different thresholds for u_{8m}, such as $u_{8m} \geq 2$ m/s, $u_{8m} \geq 3$ m/s, $u_{8m} \geq 4$ m/s and $u_{8m} \geq 5$ m/s, gave the averaged weights of f $\left(\overline{f} = 1/D\right)$ of 0.95, 0.93, 0.95 and 0.94, respectively. For the latter two datasets, i.e. $u_{8m} \geq 4$ m/s and $u_{8m} \geq 5$ m/s (not shown in Table 8.1) agreement between $H_{Eq.8.14}$ and H_{EC} was excellent. A plot comparing the

weight f versus z/L did not show a pattern (not shown). Therefore, it was found that f cannot be refined by the wind speed and stability conditions. Regardless, in general, by setting $f = 1$, the H estimates were close to the EC method, which is in agreement with previous experiments comparing Eq. 8.2 and F_{EC}.

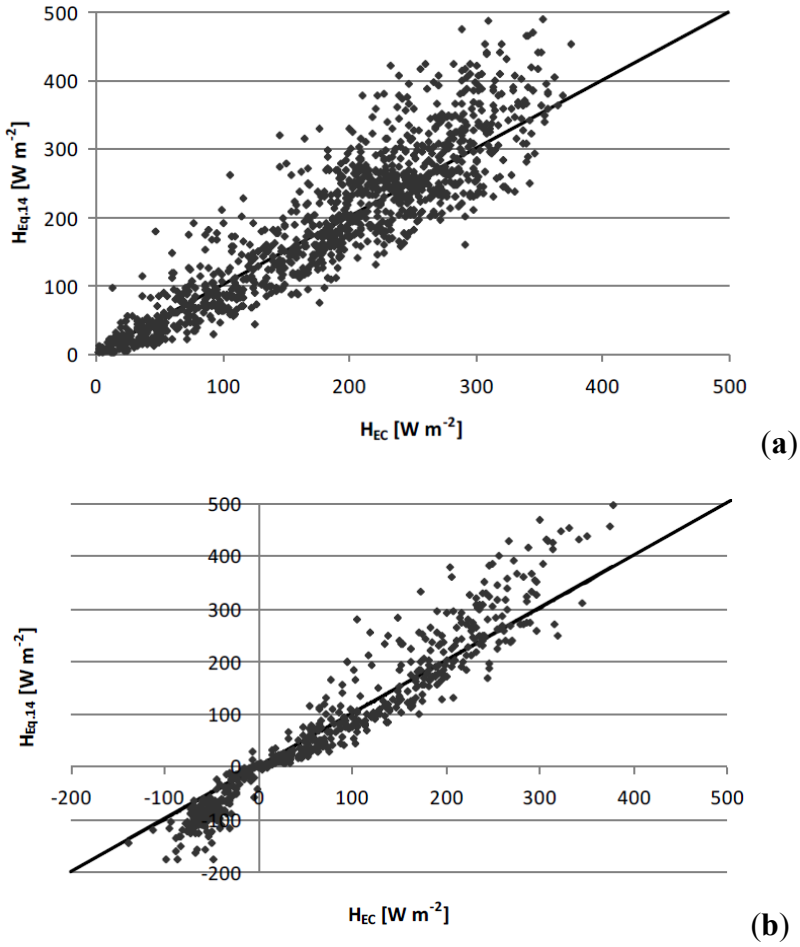

Figure 8.2. ***(a)*** *Sensible heat flux estimated using Eq. 8.14 ($H_{Eq.8.14}$) versus the flux measured with the Eddy Covariance technique (H_{EC}) for all of the samples where $u_{8m} \geq 2$ m/s in the roughness sublayer (RSL);* ***(b)*** *Sensible heat flux estimated using Eq. 8.14 ($H_{Eq.8.14}$) versus the one measured by Eddy Covariance technique (H_{EC}) for all of the samples, including the stable and unstable cases, in the transition sublayer (TSL).*

The TSL. Figure 8.2b shows $H_{Eq.8.14}$ versus H_{EC} for all of the samples shown in Table 8.1. For the unstable cases, $H_{Eq.8.14}$ performed similarly in the RSL. That is, despite the fact that $H_{Eq.8.14}$ and H_{EC} were close, agreement for the dataset of 2 m/s $\leq u_{8m} \leq$ 3 m/s was excellent.

For stable cases, however, $H_{Eq.8.14}$ was biased with respect to H_{EC}. The bias for all of the data was 21 W m^{-2}. The RMSE was moderate, with a RMSE = 38 W m^{-2}, but it was larger than the measurement error, which was approximately 20-25 W m^{-2} (Foken, 2008a). The correlation for the threshold of $u_{8m} > 3$ m/s was $R^2 = 0.82$, which was higher than for the dataset for 2 m/s $\leq u_{8m} \leq$ 3 m/s, which was $R^2 = 0.58$. For the latter dataset, the half-hourly H estimates calculated by averaging Eq. 8.12 for periods of 10 minutes slightly improved the statistics, with R^2=0.65, RMSE=30Wm^{-2} and D = 1.42, but not the slope, which was 1.5, or the intercept, which was 5 W m^{-2}.

Therefore, while accounting for the 10-minute variability in mean ramp dimensions and gradients may slightly improve the performance for this case, other contributions that were not relevant for unstable cases played a role. The integration of three sources of error may explain the bias. First, under the influence of regional advection, evapotranspiration rates are large; second, half-hourly EC fluxes may underestimate the actual fluxes around noon under clear skies due to poor sampling of convective motions (Sakai *et al*., 2001; Finnigan *et al*., 2003). Obviously, Eq. 8.14 does not account for the contribution of such large eddies; however, it is likely that the error in the *H* estimates is not the same as that in H_{EC} because the input requirements and the numerical procedure used are different. Regardless, the RMSE and D shown in Table 8.1 could be considered too large in relation to the actual *H* because part of the EC flux is missed. Third, Eq.

8.2 has proven to perform excellently under the influence of regional advection. However, the latter does not necessarily mean that the weight f can be expected to be close to one because Eq. 8.2 requires measurements taken at one height. Thus, Eq. 8.2 operates either in the RSL or in the ISL. Subsequently, further research, likely involving the surface energy balance, is required to evaluate the performance of Eq. 8.12 in the TSL.

All cases (RSL and TSL). Regardless of the u_{8m} threshold (not shown in Table 8.1), $H_{Eq.8.14}$ and H_{EC} were highly correlated with $0.87 \leq R^2 \leq 0.90$, the RMSE were moderate at 42 W m^{-2} $\leq$ RMSE $\leq$ 52 W m^{-2} and deviation of D with respect to one was within 7%. The latter is inferred from Fig. 8.2 (a) and (b) and the results are shown in Table 8.1 for all the data. Therefore, in practice, $\overline{f}$ can be set to one.

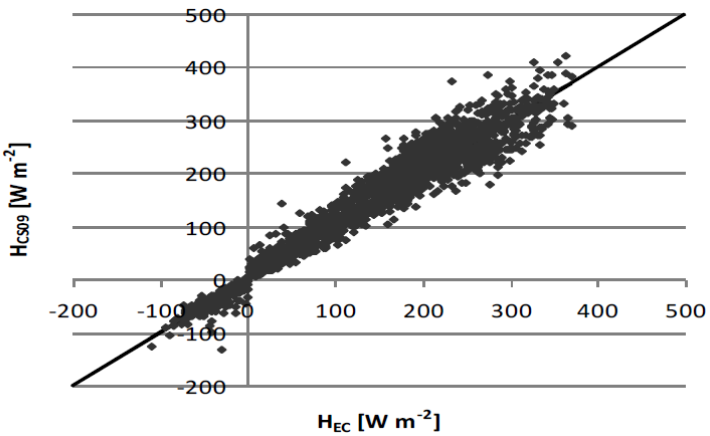

Figure 8.3. Sensible heat flux estimated using the CS09 method versus the flux measured by the Eddy Covariance technique (H_{EC}) for all of the data, including the stable and unstable cases, in the three sublayers (RSL, TSL, ISL).

Figure 8.3 shows the performance of the *CS09* method versus H_{EC} for all of the data. Table 8.1 shows that the *CS09* method's performance was excellent. It was closer to the EC method than Eq. 8.14, which indicates

that the c_d calibration performed one year before against H_{EC} still applied. This issue corroborates that the *CS09* method is robust (Castellví *et al*., 2012). A crucial difference between Eq. 8.14 and the *CS09* method is that Eq. 8.14 is free from calibration because, in principle, c_d is site, i.e. climate, and canopy specific, i.e. it depends on the Reynolds number and the type of leaves (Brutsaert, 1988). Thus, in practice, for a given canopy c_d must be determined in fitting the H estimates against H_{EC}.

8.4 Concluding remarks

On the basis that the one-dimensional diffusion equation holds above the canopy and that coherent structures are responsible for most of the turbulent scalar exchange, a method for estimating the flux of a scalar that does not require measurements of the wind speed and knowledge of canopy parameters as input was derived. For H, the input required can be calculated from measurements of air temperature taken at three heights, but the intermediate level must record the data at high frequency. For other scalars, the flux requires a density correction. Since gas analysers are expensive, the main advantages are for estimating H. Regardless, the method avoids shortcomings and corrections related to coordinate rotation, sensor separation, frequency response, alignment problems, and interference from tower or instrument-mounting structures that are inherent in the EC method. Additionally, there is no need to measure and/or estimate the canopy parameters or the empirical relationships or coefficients that are inherent in other methods based on MOST and SR. Finally, because the mean flux of the scalar can be estimated for periods shorter than a half hour, steady conditions are less compromised than they are when using the EC method.

The measurements taken have shown that for unstable conditions with $u_{8m} \geq 2$ m/s, the H estimates and H_{EC} were close. Since the method was biased for stable cases under the influence of regional advection of sensible heat flux, further studies are required to check the performance of Eq. 8.14 for stable cases. Regardless, integrated H estimates closely matched the integrated H_{EC}.

For unstable cases, this study concludes that to estimate sensible heat flux by taking measurements at approximately two times the canopy height, the proposed method is an alternative to other methods because it is reliable, affordable, simple to apply and exempt from calibration.

Appendix A. *The CS09 method for estimating the flux of a scalar from measurements taken at one level in the roughness sublayer.*

The *CS09* method combines the original SR equation, $F = (\alpha Z)\dfrac{A}{\tau}$, for scalar flux estimation (Paw U *et al*., 1995) with the following expression to estimate α (Castellví, 2004):

$$\alpha = \left[\frac{k}{\pi}\frac{z^*}{z^2}\pi u_* \phi_h^{-1}(z/L)\right]^{1/2} \tag{A1}$$

where Z and z denote the measurement heights above the ground and above the zero plane displacement (d), respectively. The variable z^* is the roughness sublayer depth above d, u_* is the friction velocity and $\phi_h(z/L)$ is the stability function for heat transfer. Over tall, homogeneous and moderately heterogeneous canopies, half-hourly z^* estimates can be determined as (Castellví and Snyder, 2009b):

$$z^* = h + \frac{(h-h_*)^2}{(h-d)}\frac{I_u^2}{(c_d LAI)} \tag{A2}$$

where h_* is the height from the ground to the bottom of the canopy, c_d is the leaf drag coefficient, *LAI* is the leaf area index, and $I_u = \frac{\sigma_u}{u}$ is the turbulent intensity measured at the canopy's top. The variables σ_u and u are the turbulent standard deviation and the mean of the horizontal wind speed, respectively. Provided that all of the canopy parameters are known, Eq. A2 can be determined from measurements taken by a bi-dimensional sonic anemometer deployed at the canopy top, because d can be estimated as a portion of the canopy height, $\phi_h(z/L)$ is well defined and the relationship $u_* \approx 0.5\sigma_u$ holds at the canopy's top (Kaimal and Finnigan, 1994). F can be iterated by starting at neutral conditions until convergence is achieved.

9 Corrected surface energy balance to measure and model evapotranspiration

Analyses carried out on water use in the Mediterranean region have shown that on average 72% of available water is used for irrigation purposes (Hamdy, 1999) and about 99% of water uptake from the soil by plants is lost as evapotranspiration (ET). Therefore, accurately estimating ET rates is crucial in water resource management in arid and semi-arid environments where irrigation is necessary and water is quite scarce and expensive.

At present, different methods are available for determining ET. Some methods are more suitable than others because of their accuracy or cost, or because they are particularly suitable for the given space and time scales. Often it is necessary to predict ET, so it must be modelled. Among the indirect methods of measuring ET rates, the most accurate techniques are the micrometeorological ones (i.e. Bowen ratio, Eddy covariance, aerodynamic methods, radiation temperature methods, etc…) (Heilman *et al*., 1996; Villalobos *et al*., 2000; Wullschleger *et al*., 2000), and thus, from an energy point of view, ET may be considered as equivalent to the energy used to transport water from the inner cells of the leaves and plant organs and from the soil to the atmosphere. In this case, it is 'latent heat' (λE, with λ latent heat of vaporization equal to $2.45 \cdot 10^6$ J kg^{-1} at 20°C) and expressed as energy flux density (W m^{-2}). When ET is considered as latent heat flux density, it is worth considering all the energy components acting above a vegetated surface, i.e. the energy balance may be written as:

$$R_N = H + \lambda E + G \tag{9.1}$$

where all the terms are in W m^{-2}, R_N and G are directly measurable, while H can be directly measured and/or estimated by micrometerological techniques. R_N-G is commonly termed available energy and the surface heat storage at daily or longer time scales is negligible. The energy available at the land surface used for photosynthesis (typically less than 1% of net radiation) can be neglected. The fluxes may be considered conservative, i.e. when they are only vertical and expected to remain constant, independent of their height, over a horizontal homogeneous surface.

Since the mid-1990s, the Fluxnet network has provided long-term high quality observations of heat and mass exchanges between the land surface and atmosphere, for a wide range of ecosystems. The methods which measure land surface-atmosphere exchanges of heat and mass are numerous and have been summarised in a number of publications (Twine *et al*., 2000; Baldocchi, 2003; Finnigan, 2004). Eddy Covariance (EC) is the most widely used technique at flux-tower sites worldwide. However, an analysis by Wilson *et al*. (2002) of surface flux measurements at 27 EC sites distributed across North America and Western Europe, showed that energy budget closure (Eq. 9.1) evaluations were absent for all the investigated sites. Aubinet *et al*. (2000) reported a similar finding based on analyses of EC data collected at European sites where, typically, annual energy closure ranges between 5% and 30% (Guo *et al*., 2009a). Many studies have provided explanations for energy imbalance (Twine *et al*., 2000; Oncley *et al*., 2007), including suggestions that are: (i) sampling errors associated with different measurement source areas for the energy components, (ii) systematic bias caused by calibration, inherent time response and the mounted structures of instruments, (iii) neglected energy

sinks, (iv) the loss of low and/or high frequency contributions to turbulent flux, and (v) neglected advection of scalars. Consequently, the sensible heat and latent heat associated with turbulent movement are systematically underestimated. The current inability of EC data to close the energy budget is a well-known issue, which has led several authors to emphasize the necessity of finding a way to deal with it (Mahrt, 1998; Wilson *et al*., 2002; Baldocchi, 2003; Liu *et al*., 2006). In order to improve the usefulness of eddy covariance measurements, Twine *et al*. (2000) suggested adjusting sensible and latent heat to force the energy equilibrium. However, some researchers have pointed out the difficulty of applying and evaluating ecosystem models using flux measurements which lack energy closure (Kustas *et al*., 1999; El Maayar *et al*., 2008) and the imperative need for resolving observed energy budget imbalances in measured data prior to their use in test models. Despite all these recommendations, researchers are still testing land surface models in which the energy budget is assumed to be closed, using EC data which do not generally satisfy the conservation of energy (Zhang *et al*., 2005; Ju *et al*., 2006; Kucharik *et al*., 2006).

Therefore, micrometeorological approaches are often difficult to apply, both from theoretical and technical points of view. They also require large flat fields and constant technical assistance. Nevertheless, micrometeorological methods are currently indispensable for the calibration of other methods.

A variety of methods are available to measure, or estimate, plant water use in the field. Sap flow, for example, is a suitable and relatively simple method for measuring plant transpiration (Cohen *et al*., 1993; Trambouze *et al*., 1998; Rana *et al*., 2005; Motisi *et al*., 2012). Sap flow measurements

can be taken both in herbaceous and woody plants and in any conductive organ, including roots. Depending on the method, measurements are taken in the part of the conductive organ where the sensors are located, or in the whole perimeter of the conductive organ. Some methods are suitable for stems of small diameters, while others can be used in large trees. Calibration is convenient in all cases, being compulsory for the invasive methods, since the insertion of the probes alters the xylem characteristics.

The heat-pulse velocity (HPV) system developed by Green (1998) is based on the compensation heat-pulse (CHP) method (Swanson and Whitfield, 1981). The method allows to monitor tree transpiration and explore the short-term water-use dynamics of trees (Green *et al*., 1989; Moreno *et al*., 1996).

However, since sap flow is measured at the branch or trunk scale, transpiration measurements should be scaled up to the whole stand (Zhang *et al*., 1997). Scaling-up procedures may vary according to the characteristics of the stand (Smith and Allen, 1996).

The crop coefficient (K_c) approach of estimating evapotranspiration in well-watered conditions is the most practical and recommended method (Allen *et al*., 1998). The concept of K_c was introduced by Jensen (1968) and further developed by the other researchers (Doorenbos and Pruitt, 1975, 1977; Burman *et al*., 1980; Allen *et al*., 1998). The crop coefficient is the ratio of the actual crop evapotranspiration (ET_c) to reference crop evapotranspiration (ET_0) and it integrates the effects of characteristics that distinguish field crops from grass, like ground cover, canopy properties and aerodynamic resistance. For irrigation scheduling purposes, daily values of crop ET_c can be estimated from crop coefficient curves, which reflect the changing rates of crop water use over the growing season, if the

values of daily ET_0 are available. FAO paper 56 (Allen *et al*., 1998) presents a procedure to calculate ET_c using three K_c values that are appropriate for four general growth stages (in days) for a large number of crops.

To make the use of K_c operational, research and experiments have been carried out worldwide, and they have led to determination of the average value that K_c may take in the course of the season over the years. It is worth highlighting that the K_c is affected by all the factors that influence soil water status, for instance, the irrigation method and frequency (Doorenbos and Pruitt, 1977; Wright, 1982; Consoli *et al*., 2006b), the weather factors, the soil characteristics and the agronomic techniques that affect crop growth (Stanghellini *et al*., 1990). Consequently, the crop coefficient values reported in the literature can vary even significantly from the actual ones if growing conditions differ from those where the mentioned coefficients were experimentally obtained (Tarantino and Onofrii, 1991).

Therefore, the general objective of this study was to identify a useful procedure for correcting the energy budget measurements of sensible and latent heat fluxes to measure and model the evapotranspiration of irrigated orange orchards in semi-arid Mediterranean conditions. The key points may be outlined as follows:

- the evaluation of the Bowen Ratio (BR) correction method to solve the unclosed surface energy balance at the study site;
- the evaluation of the performance of the sap flow method (T_{SF}) to measure actual evapotranspiration by comparison with the micrometeorological method (corrected eddy covariance data);

- the development of a model of orange orchard evapotranspiration applying a Penman-Monteith approach, using standard meteorological variables as input to determine canopy resistance;
- the evaluation of the crop coefficient method (K_c) effectiveness to determine the water requirements of the orange orchard and to verify the suitability of the K_c value proposed for a generic citrus crop.

9.1 Materials and Methods

Continuous energy balance measurements from January 2010 to December 2011 were analyzed. The freely distributed TK2 package (Mauder and Foken, 2004) was used to determine the first and second order statistical moments and fluxes on a half-hourly basis following the protocol used as a comparison reference described in Mauder *et al*. (2007). This software corrects for the errors in the wind speed vertical components, sensor separation and path-length averaging and eliminates spurious flux values.

The micrometeorological dataset used for comparison included samples (of high and low frequency data) that passed the Foken's quality control test up to level 7 (Mauder and Foken, 2004). The test checks the assumptions of steady flow and developed turbulence invoked in the EC method. Then, variances and covariances are discriminated in levels of reliability. Up to level 7 (i.e. from 1 to 7), the dataset includes high quality flux measurements recommended for research purposes (up to level 3) and measurements that can be considered useful for routinely applications and gap filling (from 4 to 7). The range -20 $Wm^{-2} \leq H_{EC} \leq 20$ Wm^{-2} was excluded [taken as the EC measurement error (Foken, 2008a)].

9.1.1 Energy closure at the orange orchard and correction of measured sensible and latent heat fluxes

The EC method applied at the study site, allows for estimates of H and λE by directly measuring fluctuations in the vertical wind velocity and scalar concentration (Arya, 1988; Campbell and Norman, 1998). By contrast with the Bowen ratio (BR) method, EC does not force the energy budget to close though, beneficially, it offers separate estimates of H and λE.

At this point, the problem, of course, is how best to close the energy balance for the EC method. As reported by Twine *et al*. (2000), there are two approaches. The first assumes that measurements of H are accurate so that λE can be calculated merely by subtracting G and H from R_N (Eq. 9.1); this approach is known in literature as the residual method. However, since no compelling evidence exists to confirm that the EC method only underestimates λE (Katul *et al*., 1999; Twine *et al*., 2000), a second approach uses the Bowen ratio to close the energy budget.

The BR approach assumes that for relatively homogeneous vegetated surfaces, R_N-G measurements may be considered reliable and representative of the EC flux footprint. That is, any errors in R_N-G measurements are necessarily much smaller than the energy imbalance determined from simultaneous EC measurements.

The BR approach then assumes that the EC technique provides correct estimates of the Bowen ratio (β=H/λE) even though it underestimates H and λE, as some studies tend to confirm (Barr *et al*., 1994; Blanken *et al*., 1997; El Maayar *et al*., 2008). Thus, rearrangement of Eq. 9.1 yields the following:

$$\lambda E = \frac{R_N - G}{1 + \beta} \tag{9.2}$$

Then corrected estimates of λE are assumed to be given by Eq. 9.2, after which H can also be inferred from:

$$H = R_N - \lambda E - G \tag{9.3}$$

Equations 9.2 and 9.3 effectively redistribute the imbalance to H and λE according to their relative measured proportions.

In the following, the corrected latent and sensible heat fluxes refer to λE_{corr} and H_{corr} as calculated from data using Eqs. 9.2 and 9.3.

Crop evapotranspiration ($ET_{c,corr}$) was calculated by transforming λE_{corr} into millimetres of water. Calculating $ET_{c,corr}$ on a daily time scale was performed by adding hourly values for 24-hour periods.

9.1.2 Sap flow and soil evaporation measurements

Measurements of water consumption at tree level were performed by using the HPV (Heat Pulse Velocity) technique. For HPV measurements, two 4-cm sap flow probes with 4 embedded thermocouples (Tranzflo NZ Ltd, Palmerston North, NZ) were inserted into the trunks of three trees. The probes were positioned at the North and South sides of the trunk at 50cm from the ground and wired to a data-logger (CR1000, Campbell Sci.) for heat pulse control and measurement; the sampling interval was 30 min. Data from the two probes were processed according to Green *et al*. (2003) to integrate sap flow velocity over sapwood area and calculate transpiration. So, the sapwood fraction of water was determined both on sample trees during the experiment and directly on the trees with the sap flow probes, at the end of the observation period. Wound-effect correction (Green *et al*., 2003) was done on a per tree basis.

Scaling up the sap flow from a single tree to the field scale requires analysing plant size variability, to determine the mean of those monitored. This was obtained by analysing the spatial variability of plant leaf area (Jara *et al*., 1998). Thus, scaling was performed only on the basis of the ratio between orchard LAI and tree leaf area.

During each irrigation season, daily soil evaporation was observed over a 7-day period in spring/summer (June-July), summer (August-September) and autumn (October) with microlysimeter measurements for a total of 42 observations. Small undisturbed soil samples were located in rings of limited height which were closed at the bottom, weighed and reinstalled in the field. Measurements of soil evaporation E_s were obtained using sets of four microlysimeters replicated three times for a total of 12. Microlysimeters, made from 3-mm-thick aluminium pipe, were 12.5 cm long with a diameter of 11.5 cm. A portable electronic balance was used to weigh the microlysimeters daily between 07:30 and 09:30 a.m. solar time (Han and Felker, 1997). Two microlysimeters were placed in dry soil and two in the saturated zone near the wet spots of the emitters.

9.1.3 Modelling crop evapotranspiration

Orange orchard crop evapotranspiration ($ET_{c,mod}$) was analysed using the Penman-Monteith model. $ET_{c,mod}$ was calculated hourly using:

$$\lambda E = \frac{\Delta A + \left(\rho C_p D / r_a\right)}{\Delta + \gamma\left(1 + r_c / r_a\right)} \tag{9.4}$$

where $A=R_N-G$ (W m^{-2}), ρ is the air density in kg m^{-3}, Δ is the slope of the saturation pressure deficit versus temperature function in kPa °C^{-1}, γ is the psychrometric constant in kPa °C^{-1}, C_p is the specific heat of moist air in

J kg^{-1} $°C^{-1}$, D is the vapour pressure deficit of the air in kPa, r_c is the bulk canopy resistance in s m^{-1} and r_a is the aerodynamic resistance in s m^{-1}.

As highlighted by Rana *et al*. (2005), r_c is not constant for irrigated crops, but varies depending on the available energy and vapour pressure deficit. Katerji and Perrier (1983) proposed calculating r_c as:

$$\frac{r_c}{r_a} = a\frac{r^*}{r_a} + b \tag{9.5}$$

where a and b are empirical calibration coefficients that require experimental determination; r^* (s m^{-1}) is given as (Monteith, 1965):

$$r^* = \frac{\Delta + \gamma}{\Delta\gamma} \cdot \frac{\rho C_p D}{A} \tag{9.6}$$

In our study, the canopy resistance was calculated with Eq. 9.4, by introducing the λE_{corr} values calculated with Eq. 9.2, together with the measured values of D and A, and the estimated values of r_a:

$$r_a = \frac{\ln(z-d)/(h_c-d)}{ku^*} \tag{9.7}$$

where z is the reference point above the canopy, d (m), the zero plane displacement, is estimated as a portion of the canopy height where an intermediate scaling is d=0.75 h_c (Brutsaert, 1988), h_c is the mean height of the orchard (3.75 m), k=0.4 is the von Karman constant and u^* is the friction velocity (m s^{-1}) measured by the EC method.

The obtained values of r_c were combined with Eq. 9.5 to estimate parameters a and b.

This model is particularly suited to canopy crops covering orchard soils, as suggested by Villalobos *et al*. (2000), Wullschleger *et al*. (2000) and Rana *et al*. (2005).

The model was calibrated using 3 months of data (June-August) during the 2010 irrigation season. The results are shown in Fig. 9.1, where the r_c/r_a ratio is related to the r^*/r_a ratio. A linear curve fit resulted in a=0.364 and b=0.0422 (coefficient of determination R^2=0.6287).

The final expression of the model on a hourly time scale is:

$$\lambda E_{\mathrm{mod}} = \frac{\Delta A + \left(\rho C_p D / r_a\right)}{\Delta + \gamma\left(1.0422 + 0.364\left(r^* / r_a\right)\right)} \tag{9.8}$$

The calculation of the orange orchard $ET_{c,mod}$ on a daily time scale was obtained by adding hourly values of λE_{mod} (from Eq. 9.8), after dividing by λ.

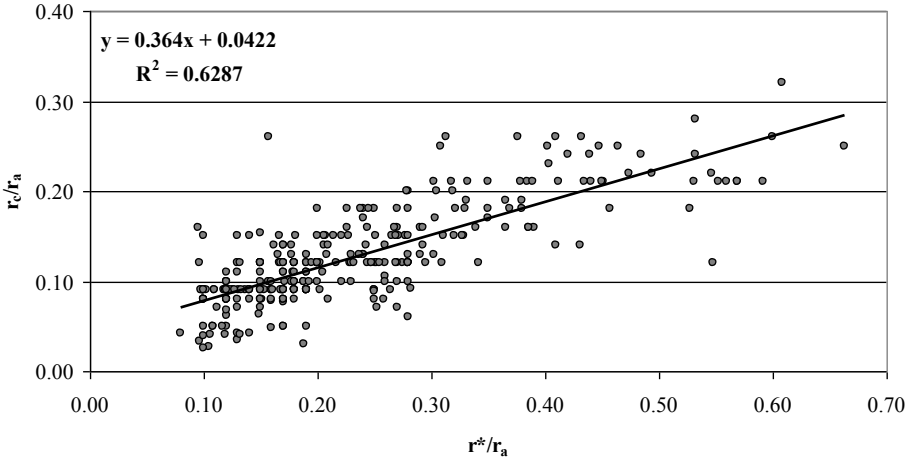

Figure 9.1. Linear relation between r_c/r_a and r^*/r_a during June-August 2010; r_c, r_a and r^* are canopy, aerodynamic and climatic resistance, respectively.

9.1.4 Determining the crop coefficient K_c

Crop evapotranspiration ($ET_{c,mod}$) on a daily time scale was calculated with Eq. 9.8. Generally, crop coefficients are determined by calculating the ratio K_c=$ET_{c,mod}/ET_0$, where $ET_{c,mod}$ is the evapotranspiration of a well-

watered crop and ET_0 is the reference evapotranspiration calculated by the Penman-Montetih method (Allen *et al*., 1998). The variables used for ET_0 determination were measured in an agrometeorological station of the Sicilian Agrometerological Service (SIAS) located 3.0 km away from the experimental field. The station was equipped with instruments for measuring standard meteorological variables (solar radiation, wind speed and direction, air temperature, relative humidity).

9.2 Results and Discussion

9.2.1 Weather conditions

Figure 9.2 shows the daily weather variables during the two study periods. Air temperature (T_a) reached a maximum in July, approximately 30°C, while the minimum value occurred during February (about 5°C).

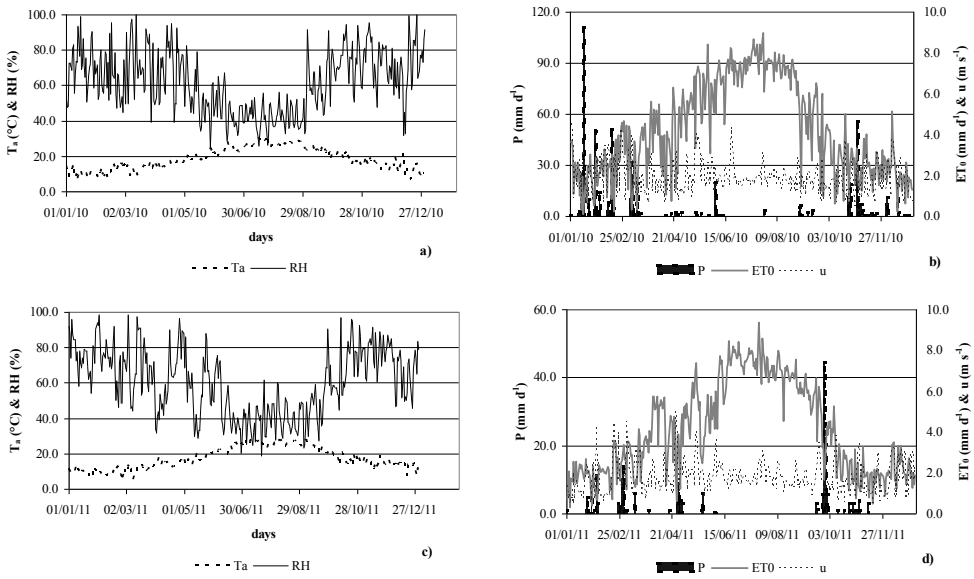

*Figure 9.2. Daily values of weather variables during the study periods in 2010 (**a**, **b**) and 2011 (**c**, **d**). T_a is the mean air temperature (°C), RH the mean relative humidity (%), P the precipitation (mm d^{-1}), u the mean wind speed (m s^{-1}), ET_0 the reference evapotranspiration (mm d^{-1}).*

The relative humidity (*RH*) presented the inverse behaviour. The maximum wind speed (*u*) at 2m above a standardized grass field was about 4.5 m s^{-1} during January-June and October-November. Most precipitation (*P*) was during January-February and October-November; the irrigation seasons (May-September) were almost dry. The accumulated rainfall during 2010 was 588mm, whereas for 2011 it was only 300mm. Reference evapotranspiration (ET_0) followed the oscillation of solar radiation (data not shown) with a maximum of about 9mm d^{-1} during July, and a mean value of about 4.2 mm d^{-1}.

9.2.2 BR-correction of measured sensible and latent heat fluxes

The lack of closure in the energy budget is commonly quantified by the relative difference between (R_N-G) and (H+λE), expressed as a percentage: 100×[((R_N-G)/(H+λE))-1].

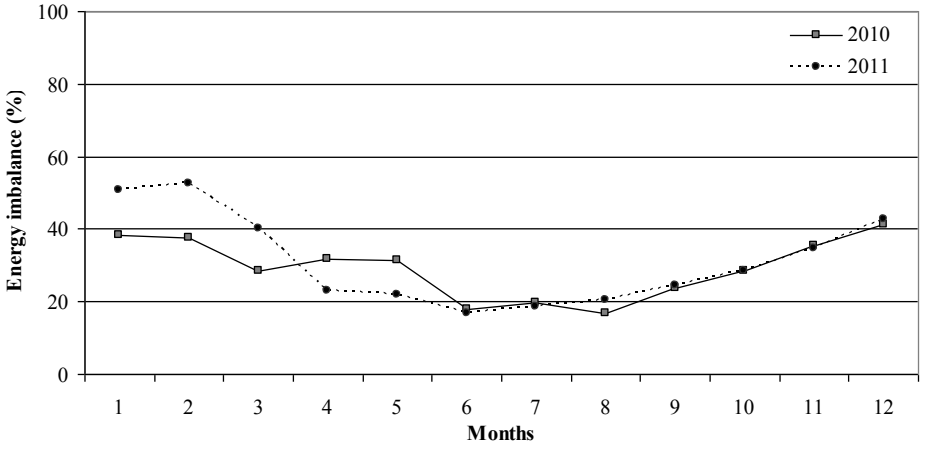

Figure 9.3. Average monthly energy imbalance in measured data during 2010 and 2011.

Figure 9.3 shows the average variation of monthly observed energy imbalance at the selected site. Assuming that R_N and G measurements are rather accurate (Twine *et al*., 2000; Wilson *et al*., 2002), during both monitored years ($H+\lambda E$) is underestimated at the site. This may arise from an underestimation of H or λE, or both. The mean annual energy imbalance is 29.3% during 2010 and 31.1% in 2011, showing peaks during winter and a variation of about 30%.

Despite Eddy Covariance being among the most advanced in situ measurement techniques which directly provides λE, the lack of closure of the EC-based energy balance is widely known (Wilson *et al*., 2002; Testi *et al*., 2006; de Teixeira *et al*., 2008). The λE data quality from the orange orchard was verified by studying the energy balance closure; fluxes ($H+\lambda E$) and available energy (R_N-G) were compared for the entire period (years 2010 and 2011) of measurement on a hourly time scale. The energy balance ratio, i.e. the ratio of turbulent energy fluxes to available energy, was 0.89 in 2010 and 0.86 in 2011. The RMSE (root mean square error) for 1 h values of turbulent fluxes was 0.13 and 0.12 MJ m^{-2} h^{-1}, during 2010 and 2011 highlighting how good the dataset was.

The diurnal flux trend of individual components of the energy balance for the orange orchard showed that the latent heat flux (λE) was always in excess of the sensible heat flux (H) during daylight hours and the H was higher than the soil heat flux (G). At night, the Eddy Covariance results showed H and λE approaching zero.

Daily averages of energy balance fluxes are given in Table 9.1. Unstable atmospheric conditions predominated above the orchard, with the sensible heat flux (H) accounting for about 30% of R_N during both the monitoring periods.

Table 9.1. Daily average of the energy balance components for orange orchard during the 2010-2011 monitoring period; net radiation (R_N), soil heat flux (G), latent heat flux (λE), sensible heat flux (H) and evaporative fraction (E_F).

Month/year	R_n (MJ m^{-2} d^{-1})	G (MJ m^{-2} d^{-1})	λE (MJ m^{-2} d^{-1})	H (MJ m^{-2} d^{-1})	E_F (-)
Jan/2010	4.83	-0.04	3.39	0.27	0.70
Feb/2010	5.61	0.02	4.93	1.10	0.88
Mar/2010	8.86	-0.11	5.10	3.29	0.57
Apr/2010	9.64	0.06	4.99	4.19	0.52
May/2010	13.67	0.27	7.76	5.59	0.58
June/2010	15.65	0.25	9.23	6.19	0.60
July/2010	17.01	0.43	10.1	6.44	0.61
Aug/2010	15.01	0.26	9.98	5.67	0.68
Sept/2010	9.58	-0.25	8.27	2.18	0.84
Oct/2010	6.14	-0.38	5.59	0.89	0.86
Nov/2010	4.07	-0.43	4.28	0.69	0.95
Dec/2010	3.25	-0.56	2.37	0.34	0.61
Mean	*9.45*	*-0.04*	*6.33*	*3.07*	*0.70*
Jan/2011	3.24	-0.38	1.49	1.43	0.41
Feb/2011	5.79	-0.33	2.51	1.79	0.41
Mar/2011	8.42	0.06	1.48	3.48	0.33
Apr/2011	10.87	0.12	5.22	5.76	0.49
May/2011	13.27	0.13	7.39	6.08	0.56
June/2011	17.15	0.26	9.29	7.66	0.55
July/2011	16.96	0.48	9.86	7.21	0.60
Aug/2011	15.35	0.43	8.84	6.16	0.59
Sept/2011	10.98	0.00	7.89	3.57	0.72
Oct/2011	6.47	-0.37	5.24	1.58	0.77
Nov/2011	3.83	-0.41	2.89	0.77	0.68
Dec/2011	1.67	-0.55	2.16	-0.41	0.97
Mean	*9.50*	*-0.05*	*5.46*	*3.43*	*0.60*

The significant leaf area index (*LAI*) of the orange crop (LAI of about 4-4.7 m^2 m^{-2}) caused little solar radiation to penetrate the canopy. As a

consequence, the soil heat flux (G) on a daily scale was small and negative, with daily average values less than 1% of R_N. Negative values for G could be the result of both large LAI and frequent drip irrigation which keeps the soil thermal conductivity high. The largest part of R_N was used as latent heat flux (λE), representing on average 67% of R_N during 2010 and 57% of R_N during 2011. The corresponding evaporative fractions ($E_F=\lambda E/(R_N-G)$) were 0.70 and 0.60.

Monthly data show (Fig. 9.4) that, after forcing (the BR approach) the measured energy balance data to close, the discrepancy between the available energy (R_N-G) and turbulent fluxes ($H_{corr}+\lambda E_{corr}$) tends to be neglected. In particular, H_{corr} increased by 8.6% and 10%, in 2010 and 2011 with respect to EC measurements of H; λE tends to increase by 2% and 3.7% in 2010 and 2011.

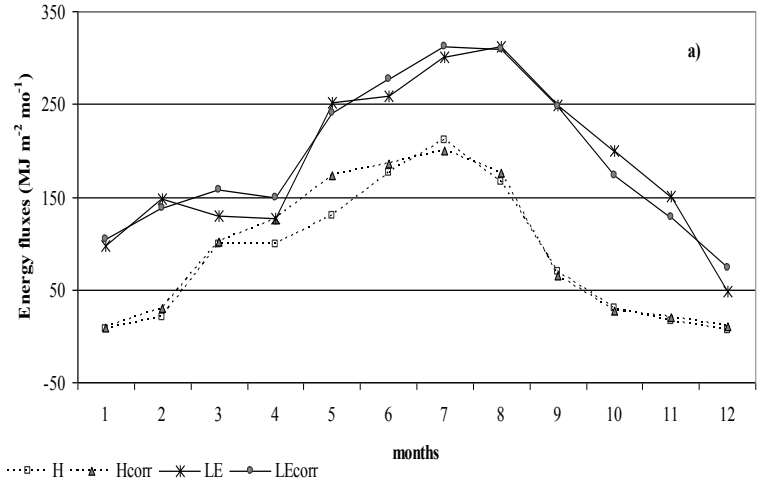

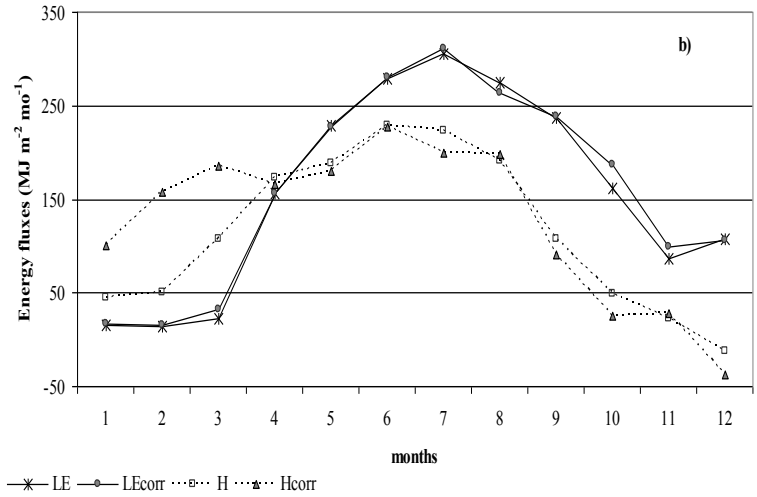

*Figure 9.4. BR-corrected and uncorrected measurements from EC of monthly total sensible heat flux (H) and latent heat flux (λE) during 2010 (**a**) and 2011 (**b**) monitoring periods.*

9.2.3 Comparison between BR-corrected eddy covariance and sap flow measurements of evapotranspiration

Scatter plots of T_{SF} versus $ET_{c,corr}$ hourly values showed general dependence with a saturation-type response, a good degree of linearity at low $ET_{c,corr}$ values and a lack of increase in T_{SF} at high $ET_{c,corr}$ flux values (Fig. 9.5). For orange trees, fairly good linearity was observed both in the morning and afternoon values, whereas the midday values showed a weak relationship, with a small slope value, denoting lower xylem flux (SF values) in comparison with canopy transpiration as estimated by BR-corrected EC.

Analysis of the daily variation of average $ET_{c,corr}$ and T_{SF} fluxes (Fig. 9.6) shows that T_{SF} divergence from $ET_{c,corr}$ begins at about 09:00 a.m. local time. Midday T_{SF} fluxes were almost steady for most of the period while $ET_{c,corr}$ ones followed the daily trend of atmospheric evapotranspiration demand. Midday differences between T_{SF} and $ET_{c,corr}$

denote a depletion of plant water content in relation to the imbalance between tree crown water loss by transpiration, as estimated by EC, and water transport from the tree's root mass as estimated by SF. This imbalance is recovered in the afternoon and nocturnal hours, with higher T_{SF} than $ET_{c,corr}$ fluxes.

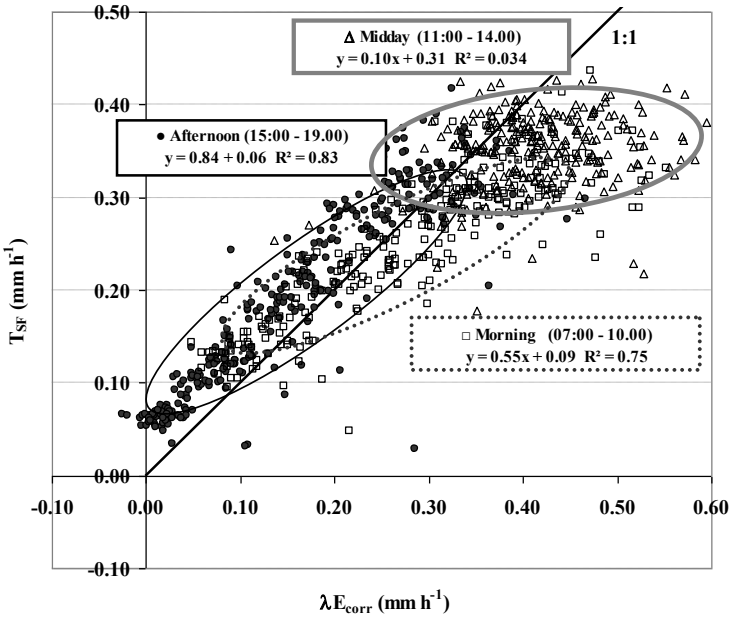

Figure 9.5. Scatter plots of hourly values of daytime upscaled trunk SF versus BR-corrected EC measurements of ET. Observation period was July-August 2010.

Most of the differences here in water-use dynamics could be interpreted by tree capacitance. The imbalance between canopy transpiration and tree water uptake is revealed by a large hysteresis (data not shown), with higher afternoon SF values. It is interesting to note that the hysteresis loop appears specularly reflected, with a larger hysteresis in the morning-midday hours (Motisi *et al*., 2012).

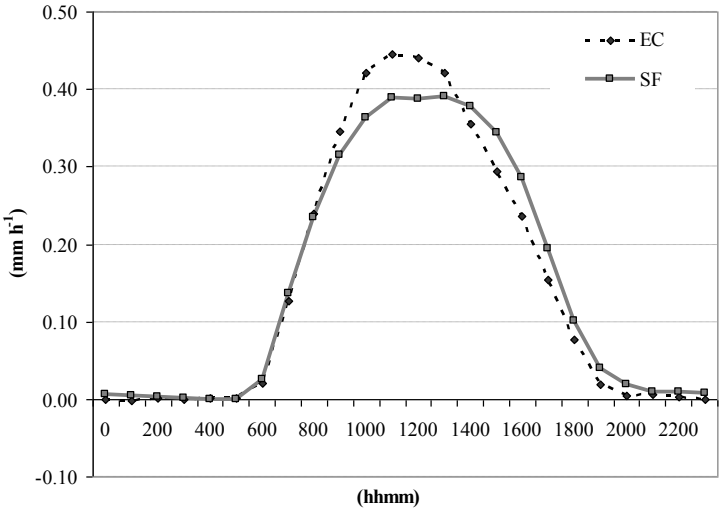

Figure 9.6. Diurnal changes of upscaled SF. Each data point represents the average of all the values in the observation period (July-August 2010).

Furthermore, as orchards in general are well coupled to the atmosphere, their transpiration is mainly regulated by the resistance that water vapour encounters in its movement from inside the leaf to the atmosphere (Villalobos *et al*., 2000). Canopy conductance (g_c) is, therefore, an essential parameter for understanding the mechanisms of plant evaporation in orchards, but it is very difficult to measure at the correct scale.

Villalobos *et al*. (2009), analysing the canopy conductance of mandarin, found that it always peaked in the morning, followed by a lower plateau, and (sometimes) another small peak in the afternoon. This pattern of g_c, with an early maximum later depressed in the hotter midday, is typical for water-stressed plants. A similar diurnal course of g_c was also found in unstressed olives, another Mediterranean sclerophyllous tree crop, both at orchard (Villalobos *et al*., 2000) and leaf level (Moriana *et al*., 2002). Leaves, which reach low water potential during hot dry afternoons, accumulate water during the night. In the morning, the guard cells of the

stomata are turgid and can open quickly. Later, when vapour pressure deficit (VPD) increases, the transpiration rate surpasses uptake. The leaf water potential drops and the stomata close, thus reducing g_c and transpiration. This process goes on until water uptake can sustain the transpiration rate again and a new dynamic equilibrium is reached. This feedback system increases transpiration efficiency because the stomata are well open only during the coolest hours of the day (when the evaporative demand of the atmosphere is lower) and carbon can be assimilated at a lower cost in terms of water. The sensitivity of the feedback indicates adaptation to dry climates.

In this study, the difference between total values of T_{SF} and $ET_{c,corr}$ during 2010 and 2011 was about 10% which may be attributed to soil evaporation and which is not taken into account by the sap flow method.

The distribution of the evapotranspiration rate between soil evaporation (E_s) and transpiration is difficult to compare to other studies, because of the small number of E_s measurements available in our study and the difficulties of extrapolating them from different ground cover fractions. In this experiment, evaporation from the soil was 11% and 12% of the total $ET_{c,corr}$ in 2010 and 2011. From the data of Moreshet *et al*. (1983), obtained in an orange orchard with the same percentage of ground cover by vegetation (about 80%) as in this study, it is possible to calculate that their E_s varied between 0.24 and 0.61 mm d^{-1}. The lower values of E_s are related to the lower energy available to evaporate water at the soil level due to the high canopy ground cover.

9.2.4 Crop evapotranspiration by a Penman-Monteith-type model

The comparison between daily crop evapotranspiration ($ET_{c,mod}$) simulated by the model in Eq. 9.8 and T_{SF} measured by the sap flow method is shown in Fig. 9.7. In particular, the empirical calibration coefficients of Eq. 9.5 were used to model ET_c in 2011, too.

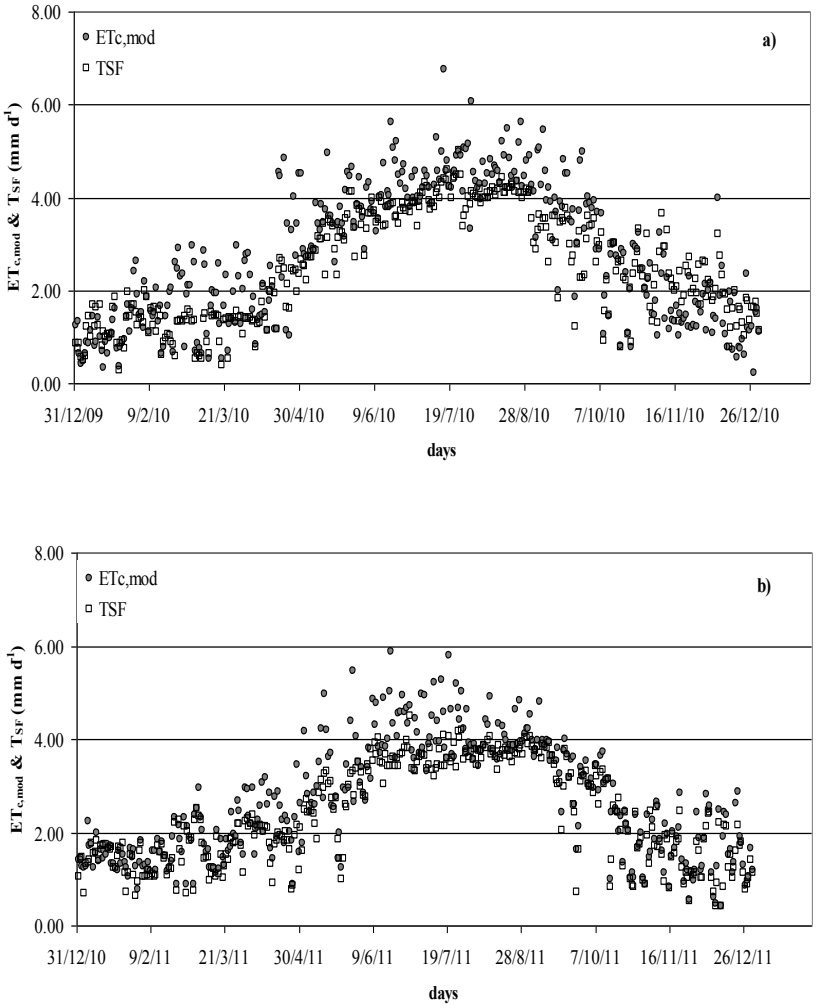

*Figure 9.7. Comparison between the transpiration values measured by the sap flow method (T_{SF}) and evapotranspiration rates calculated by the model of Eq. 8.8 ($Et_{c,mod}$) during 2010 (**a**) and 2011 (**b**).*

For the available data set, the daily values of T measured by sap flow and modelled ET are fairly close during the crop cycle. The total values of the entire experimental periods are 913 mm and 883 mm for the sap flow measurements of transpiration during 2010 and 2011, and 1,008 mm and 984 mm for the modelled ET_c during the two years with small differences, no higher than 3%. The average daily values of $ET_{c,mod}$ and T_{SF} are 3.9 and 3.4 mm d^{-1} during May-October 2010 and 3.7 and 3.2 mm d^{-1} in 2011.

The values of $ET_{c,mod}$ followed atmospheric demand in both growing seasons, being higher during May-October (from flowering to fruit maturation), with peaks of 6.7 and 6.0 mm d^{-1} during 2010 and 2011. The minimum values were around 1.2 mm d^{-1}.

With regard to similar studies found in the literature, which used a calibrated heat pulse method, Cohen (1991) found average transpiration of about 3.0 mm d^{-1} in a high-density grapefruit orchard. Consoli *et al*. (2006b) and Snyder and O'Connell (2007) reported daily ET peaks near 6.0 mm d^{-1} for clean-cultivated mature orange orchards in California using energy balance techniques. Rana *et al*. (2005) using EC measurement systems in citrus (Clementine) orchard in Mediterranean conditions (Southern Italy) found ET rates ranging from 2.0 to 7.0 mm d^{-1}. Paco *et al*. (2006), using the same method in a peach orchard in Portugal, found ET values ranging from 1.4 to 4.0 mm d^{-1}. de Teixeira *et al*. (2008), evaluating ET rates using micrometeorological measurements, showed average daily values of mango orchard ET ranging from 1 to 6.3 mm d^{-1}. Sammis *et al*. (2004) used EC measurements to determine ET rates of flood-irrigated pecans in the USA; they found an average total ET of about 1,100 mm $year^{-1}$.

Therefore, the methodology proposed in this work may be valid for characterizing the evapotranspiration process on a field scale.

9.2.5 Analysis of crop coefficient values

Figure 9.8 compares the crop coefficient calculated daily with the K_c value given by Allen *et al*. (1998) for a generic citrus crop. These authors report a constant value of the crop coefficient between 0.45 and 0.65 (it is 0.65 in our experimental conditions), depending on the percentage of crop cover throughout the growth cycle. In this study, K_c varies between 0.20 and 1.10, with a mean value of 0.68.

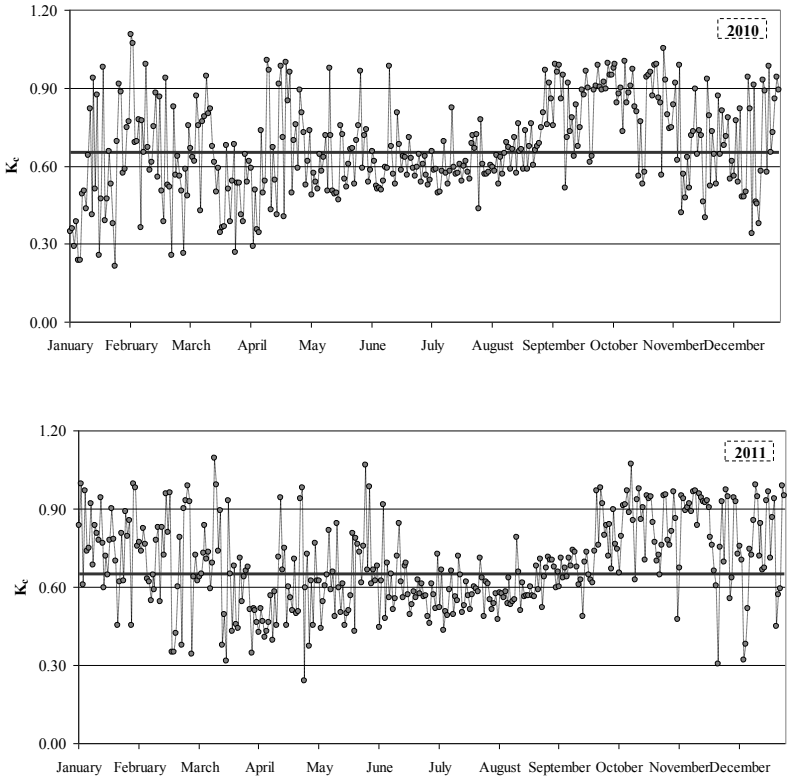

Figure 9.8. Comparison between the calculated daily crop coefficient (K_c) and the value (constant) given by FAO 56 for the whole experimental period.

During rainy periods, mainly at the start of the year, $ET_{c,mod}$ rates exceeded ET_0, producing daily K_c values exceeding 1. As reported by Rana *et al*. (2005), the higher values of K_c in the period January-June could be due to the following reasons: (i) the period coincides with phenological stages, the 'flowering' and 'swelling of buds' of active growth, when stomatal conductance is usually high (Bethenod *et al*., 2000); (ii) the period corresponds to days with high wind speed (Fig. 9.2) and vapour pressure deficit, which can cause high tree ET rates that are much greater than ET_0.

Similar results were reported by Azevedo *et al*. (2003), who find higher K_c values for mango orchard with peaks around 0.71 during the crop stages.

Many studies highlight greater accuracy when the crop coefficient curves are plotted with variables more closely related to crop development: LAI, canopy percentage shading the ground or thermal-based variables. This approach is considered an improvement over the FAO guidelines which suggest estimating K_c values as a function of the length of the four phenological stages into which crop development is divided.

Linear relationships are reported between K_c and LAI values for green bean and melon (Orgaz *et al*., 2006), grapevine (Williams *et al*., 2003), young olive orchard (Testi *et al*., 2004), and orange orchard (Consoli *et al*., 2006b). In particular, Testi *et al*. (2004) found that the K_c values determined in late autumn, winter and spring are usually high, variable and relatively independent of LAI or ground cover; during summer soil evaporation decreases and K_c is lower, far less variable and LAI-dependent. These K_c values are linearly correlated to LAI or ground cover: the authors proposed a linear model to predict it. This model has shown

great robustness despite its empirical nature. Ayars *et al*. (2003) found that K_c was a linear function of the amount of light intercepted by peach (*Prunus persica* L.) trees. Consoli *et al*. (2006b) found nearly linear relationships between the normalized ratio for orange trees (K_c over peak K_c) and LAI, ground cover percentage (C_g) and PAR light interception (LI). For comparable C_g values of 20, 50 and 70%, the observed K_c values were 27, 31 and 43% higher in the experiment than the K_c values reported in FAO 56 (Allen *et al*., 1998).

9.3 Concluding remarks

Accurate knowledge of the partitioning of available energy between sensible and latent heat is needed to develop reliable tools for the study of short-term or long-term processes within agricultural crop ecosystems, which are particularly fragile when water availability is limited. This accurate knowledge requires the best possible data measurement and requires that the problem of closing measured energy budgets is resolved using rigorous procedures which respect the principle of energy conservation.

In our study, a long-term energy balance monitoring programme, integrated with sap flow measurements and biophysical ancillary data, was used to obtain reliable evapotranspiration estimates of irrigated orange orchards. In the implemented procedure, the Bowen ratio method was used to correct the Eddy Covariance measurements of sensible and latent heat fluxes for energy closure proving efficacious for orange orchards. In particular, after forcing the measured energy balance data to close, sensible heat flux increased by an average of about 9% with respect to EC

measurements of *H*; latent heat flux tends to increase by about 3% during the monitoring period.

The BR-corrected crop evapotranspiration (ET_c) rates were compared with upscaled transpirational data by sap flow heat pulse (T_{SF}) method, showing a saturation-type response, with a good degree of linearity at low $ET_{c,corr}$ values and a lack of increases of T_{SF} at high $ET_{c,corr}$ flux values. The difference between total values of T_{SF} and $ET_{c,corr}$ during the monitoring period was about 10% which may be attributed to soil evaporation and which is not taken into account by the sap flow method.

By using the BR-corrected latent heat flux values, crop evapotranspiration rates ($ET_{c,mod}$) were analysed and modelled, starting from a simple formulation based on the Penman-Monteith model, where canopy resistance was determined as a function of standard microclimatic variables. The calibration coefficients of the proposed model depend only on the crop and are valid for the study site. Modelled ET_c helped calculate the crop coefficient (K_c) of orange orchards during the growing seasons; this was compared with the FAO 56 approach based on a constant K_c over the different growth stages.

Modelled ET_c values were compared with daily transpiration (T_{SF}) data measured by the sap flow method, with fairly good results. Simultaneous use of $ET_{c,mod}$ and T_{SF} measurements provides an interesting experimental insight into the biophysical behaviour of tree crops.

10 Summary and Conclusions

During the PhD course, I've had the opportunity to carry out micrometeorological studies in deep. The subject of my study concerned the analysis of mass and energy exchange processes within one of the most relevant crop (i.e. orange orchards) of the agricultural Sicilian context. The analysis and studies carried out were focused on the comprehension of the water transfer (and/or energy transfer) complex mechanisms in these crop systems.

The PhD course was also a good opportunity to establish an international cooperation on the topic of my research; a great support to my study derives from the research I've joined with the University of Lleida (Spain) and professor Francesc Castellví Sentis. This collaboration, in fact, allowed me to develop and consolidate the use of alternative Surface Renewal (SR) analyses (with respect to the most traditional theory on SR) able to estimate reliable sensible heat flux (H) values within the plant-atmosphere system. The results of these alternative SR methods (based on the α-calibration parameter and the profile of a scalar) may contribute to enhance the existing literature on the technique.

My PhD study was conceived as a long monitoring program of micrometeorological features of the study orange orchard at different spatial scales (plant, orchard, farm). Micrometeorological observations at orchard level were integrated with physiological and microclimatic data obtained at plant level (i.e. sap flow data for transpiration, surface crop resistance, leaf area index, etc.). These different observations were normalized to the same spatial scale (through an up-scaling process) and compared and integrated to examine the complex processes of mass and

energy exchange within the investigated agricultural system. The comparison between micrometeorological evapotranspiration fluxes and sap flow transpiration values has highlighted the role of the plant capacitance and stomatal control in the water transfer towards the atmosphere.

The analysis of the derived actual crop evapotranspiration fluxes, by means of the resolution of the energy balance equation opportunely corrected for closure, and crop coefficient values may contribute to improve irrigation water management within the studied agricultural context. The crop coefficient values obtained from the study were compared with those suggested and reported by the well known FAO56 paper, highlighting several differences depending on the adopted irrigation method and the way to estimate the reference evapotranspiration rate.

Finally, still numerous could be the studies and the investigations to carry out starting from the long micrometeorological program, numerous are the data not yet published or not yet examined in deep and this could be a good opportunity to continue my research on these topics in the future.

The PhD was really an opportunity for me to enhance my background on hydrological processes and I greatly hope to have contributed with a little “brick” to readers micromet knowledge.

References

Allen R. G., Pereira L. S., Raes D., Smith M., 1998. Crop evapotranspiration. Guidelines for computing crop water requirements. Irrigation and Drainage Paper No. 56, FAO, Rome, 300 pp.

Allen R. G., Pruitt W. O., Wright J. L., Howell T. A., Ventura F., Snyder R., Itenfisu D., Steduto P., Berengena J., Yrisarry J. B., 2006. A recommendation on standardized surface resistance for hourly calculation of reference ET_0 by the FAO56 Penman-Monteith method. Agr. Water Manage., 81 (1-2), 1-22.

Amiro B. D., 1990. Drag coefficients and turbulence spectra within three boreal forest canopies. Bound.-Layer Meteorol., 52, 227–246.

Anandakumar K., 1999. Sensible heat flux over a wheat canopy: optical scintillometer measurements and surface renewal analysis estimations. Agric. Forest Meteorol., 96, 145–156.

Anderson F. E., Snyder R. L., Miller R., Drexler J., 2003. A micrometeorological investigation of a restored California wetland ecosystem. Bull. Am. Meteorol. Soc., 84(9), 1170–1172.

Arya S. P., 2005. Micrometeorology and Atmospheric Boundary Layer. Pure appl. geophys. 162, 1721-1745.

Arya S. P., 1988. Introduction to Micrometeorology. Academic Press, San Diego, 307 pp.

Aubinet M., Grelle A., Ibrom A., Rannik U., Moncrieff J., Foken T., Kowalski A. S., Martin P. H., Berbigier P., Bernhofer C., Clement R., Elbers J., Granier A., Grunwald T., Morgenstern K., Pilegaard K., Rebmann C., Snijders W., Valentini R., Vesala T., 2000. Estimates of the annual net carbon and water exchange of European forests: the EUROFLUX methodology. Adv. Ecol. Res., 30, 114-175.

Ayars J. E., Johnson R. S., Phene C. J., Trout T. J., Clark D. A., Mead R. M., 2003. Water use by drip-irrigated late-season peaches. Irrig. Sci., 22, 187-194.

Azevedo P. V., Silva B. B., da Silva V. P. R., 2003. Water requirements of irrigated mango orchards in northeast Brazil. Agric. Water Manage., 58, 241-254.

Baldocchi D. D., 2003. Assessing ecosystem carbon balance: problems and prospects of the Eddy covariance technique. Glob. Chang. Biol., 9, 479-492.

Barr A. G., King K. M., Gillespie T. J., denHartog G., Neumann H. H., 1994. A comparison of Bowen ratio and eddy correlation sensible and latent heat flux measurements above deciduous forest. Bound.-Layer Meteorol., 71, 21-41.

Bastiaanssen W. G. M., Menenti M., Feddes R. A., Holtslang A. A. M., 1998. A remote sensing surface energy balance algorithm for land (SEBAL): 1 Formulation. J. Hydrol., 212-213, 198-212.

Becker P., Edwards W. R. N., 1999. Corrected heat capacity of wood for sap flow calculations. Tree Physiol., 19, 767-768.

Bethenod O., Katerji N., Goujet R., Bertolini J. M., Rana G., 2000. Determination and validation of corn crop transpiration by sap flow measurement under field conditions. Theor. Appl. Climatol., 67, 153-160.

Blaney H. F., Criddle W. D., 1950. Determining water requirements in irrigated areas from climatological and irrigation data. U.S.D.A. Soil Conservation Service Tech. Paper 96, 48 pp.

Blanken P. D., Black T. A., Yang P. C., Newmann H. H., Nesic Z., Staebler R., denHartog G., Novak M. D., Lee X., 1997. Energy balance and canopy conductance of a boreal aspen forest: partitioning overstory and understory components. J. Geophys. Res., 102 (D24), 28915-28928.

Braaten D. A., Shaw R. H., Paw U K. T., 1993., Boundary-layer flow structures associated with particle reentrainment. Bound.-Layer Meteorol., 65, 255-272.

Brotzge J. A., Crawford K. C., 2003. Examination of the Surface Energy Budget: A Comparison of Eddy Correlation and Bowen Ratio Measurement Systems. J. Hydrometeorol., 4, 160-178.

Brutsaert W., 1988. Evaporation into the Atmosphere – Theory, History, and Applications. D. Reidel P.C., Dordrecht, Holland, 299 pp.

Burman R. D., Wright J. L., Nixon P. R., Hill R. W., 1980. Irrigation management-water requirements and water balance, In: Irrigation, Challenges of the 80's, Proc. of the Second National Irrigation Symposium, Am. Soc. Agric. Eng., St. Joseph, MI, 141–153.

Campbell G. S., Norman J. M., 1998. An introduction to environmental biophysics, 2nd edn., Springer, New York, 286 pp.

Castellví F., 2012. Fetch requirements using surface renewal analysis for estimating scalar surface fluxes from measurements in the inertial sublayer. Agric. Forest Meteorol., 152, 233-239.

Castellví F., 2010. Estimation of scalar surface fluxes using surface renewal analysis. Overview and case study over natural grassland. In: Horizons in Earth Science Research. Nova Science Publishers Inc., New York (NY, USA) (Chapter 7).

Castellví F., 2004. Combining surface renewal analysis and similarity theory: a new approach for estimating sensible heat flux. Water Resour. Res. 40, W05201, doi:10.1029/2003WR0026770.

Castellví F., Martinez-Cob A., 2005. Estimating sensible heat flux using surface renewal analysis and the variance method. A study case over olive trees at Sastago (NE, Spain). Water Resour. Res. 41, W09422, doi:10.1029/2005WR004035.

Castellví F., Snyder R. L., 2010a. A comparison between latent heat fluxes over grass using a weighing lysimeter and surface renewal analysis. J. Hydrol., 381, 213-220.

Castellví F., Snyder R. L., 2010b. A new procedure to estimate sensible heat flux using surface renewal analysis. A case study over grapevines. J. Hydrometeorol., 11(2), 496-508.

Castellví F., Snyder R. L., 2009a. Combining the dissipation method and surface renewal analysis to estimate scalar fluxes from the time traces over rangeland grass near Ione (California). Hydrol. Process., 23, 842–857.

Castellví F., Snyder R. L., 2009b. On the performance of surface renewal analysis to estimate sensible heat flux over two growing rice fields under the influence of regional advection. J. Hydrol., 375, 546–553.

Castellví F., Snyder R. L., 2009c. Sensible heat flux estimates using surface renewal analysis. A study case aver a peach orchard. Agric. Forest Meteorol., 149, 1397–1402.

Castellví F., Consoli S., Papa R., 2012. Sensible heat flux estimates using two different methods based on Surface renewal analysis. A study case over an orange orchard in Sicily. Agric. Forest Meteorol., 152, 58-64.

Castellví F., Snyder R. L., Baldocchi D. D., 2008. Surface energy-balance closure over rangeland grass using the eddy covariance method and surface renewal analysis. Agric. Forest Meteorol., 148, 1147-1160.

Castellví F., Snyder R. L., Baldocchi D. D., Martinez-Cob A., 2006. A comparison of new and existing equations for estimating sensible heat flux using surface renewal and similarity concepts. Water Resour. Res., 42, W08406, doi:10.1029/2005WR004642.

Castellví F., Perez P. J., Ibañez M., 2002. A method based on high temperature frequency measurements to estimate the sensible heat flux avoiding the height dependence. Water Resour. Res., 38, 1-9.

Cellier P., Brunet Y., 1992. Flux-gradient relationships above tall plant canopies. Agric. Forest Meteorol., 58, 93–117.

Chen W., Novak M. D., Black T. A., Lee X., 1997a. Coherent eddies and temperature structure functions for three contrasting surfaces. Part I: ramp model with finite microfront time. Bound.-Layer Meteorol., 84, 99-123.

Chen W., Novak M. D., Black T. A., Lee X., 1997b. Coherent eddies and temperature structure functions for three contrasting surfaces. Part II: renewal model for sensible heat flux. Bound.-Layer Meteorol., 84, 125-147.

Choundhury B. J., Ahmed N. U., Idso S. B., Reginato R. J., Daughtry C. S., 1994. Relations between evaporation coefficients and vegetation indices studied by model simulations. Remote Sens. Environ., 50, 1-17.

Coelho M. B., Villalobos F. J., Mateos L., 2003. Modeling root growth and the soil–plant–atmosphere continuum of cotton crops. Agric. Water Manage., 60, 99-118.

Cohen Y., 1991. Determination of orchard water requirement by a combined trunk sap flow and meteorological approach. Irrig. Sci., 12(2), 93-98.

Cohen M., Girona J., Valancogne C., Ameglio T., Cruizat P., Archer P., 1993. Water consumption and optimisation of the irrigation in orchards. Acta Hort., 335, 349-358.

Cohen Y., Fuchs M., Green G. C., 1981. Improvement of the heat-pulse method for determining sap flow in trees. Plant Cell Environ., 4, 391-397.

Consoli S., Cirelli G. L., Toscano A., 2006a. Monitoring crop coefficient of orange orchards using energy balance and the remote sensed NDVI. Proceedings of Conference on Remote Sensing for Agriculture, Ecosystems, and Hydrology, Stockholm, Sweden.

Consoli S., O'Connell N. V., Snyder R. L., 2006b. Estimation of evapotranspiration of different orange sized orchard canopies using energy balance. J. Irr. Drain. Eng. ASCE, 32(1), 2-8.

de Teixeira A. H. C., Bastiaanssen W. G. M., Moura M. S. B., Soares J. M., Ahmad M. D., Bos M. G., 2008. Energy and water balance measurements for water productivity analysis in irrigated mango trees, Northeast Brazil. Agric. Forest Meteorol., 148, 1524-1537.

Dias N. L., Hong J., Leclerc M. Y., Black T. A., Nesic Z., Krishnan P., 2009. An aerodynamic-variance method for scalar flux gap-filling over forests. Bound.-Layer Meteorol., 132, 401–414.

Doorenbos J., Pruitt W. O., 1977. Guidelines for predicting crop water requirements. FAO – ONU, Rome, Irrigation and Drainage Paper No. 24 (rev.), 144 pp.

Doorenbos J., Pruitt W. O., 1975. Guidelines for predicting crop water requirements. Irrigation and Drainage Paper No. 24, FAO – ONU, Rome, Italy, 193 pp.

Drexler J. Z., Anderson F. E., Snyder R. L., 2008. Evapotranspiration rates and crop coefficients for a restored marsh in the Sacramento-San Joaquin Delta, California, USA. Hydrol. Process., 22(6), 725–735.

Drexler J. Z., Snyder R. L., Spano D., Paw U K. T., 2004. A review of models and micrometeorological methods used to estimate wetland evapotranspiration. Hydrol. Process., 18, 2071-2101.

Duce P., Spano D., Snyder R. L., Paw U K. T., 1997. Surface renewal estimates of evapotranspiration. Short canopies. Acta Hort., 449, vol. 1, 57-62.

Duchemin B., Hadria R., Er-Raki S., Boulet G., Maisongrande P., Chehbouni A., Escadafal R., Ezzahar J., Hoedjes J. C. B., Kharrou M. H., Khabba S., Mougenot B., Olioso A., Rodriguez J. C., Simmoneaux V., 2006. Monitoring wheat phenology and irrigation in central Morocco: on the use of relationships between evapotranspiration, crop coefficients, leaf

area index and remotely-sensed vegetation indices. Agric. Water Manage., 79, 1-27.

El Maayar M., Chen J. M., Price D. T., 2008. On the use of field measurements of energy fluxes to evaluate land surface models. Ecol. Model., 214, 293-304.

Er-Raki S., Chehbouni A., Boulet G., Williams D. G., 2010. Using the dual approach of FAO-56 for partitioning ET into soil and plant components for olive orchards in a semi-arid region. Agric. Water Manage., 97, 1769-1778.

Er-Raki S., Chehbouni A., Guemouria N., Duchemin B., Ezzahar J., Hadria R., 2007. Combining FAO-56 model and ground-based remote sensing to estimate water consumptions of wheat crops in a semi-arid region. Agric. Water Manage., 87, 41-54.

Fernandez J. E., Palomo M. J., Diaz-Espejo A., Clothier B. E., Green S. R., Giron I. F., Moreno J., 2001. Heat-pulse measurements of sap flow in olives for automating irrigation: test, root flow and diagnostic water stress. Agric. Water Manage., 51(2), 99-123.

Figuerola P. I., Berliner P. R., 2005. Evapotranspiration under advective conditions. Int. J. Biometeorol., 49, 403-416.

Finnigan J. J., 2004. A revaluation of long-term flux measurement techniques. Part II: Coordinate systems. Bound.-Layer Meteorol., 113, 1-41.

Finnigan J. J., Clement R., Malhi Y., Leuning R., Cleugh H. A., 2003. A re-evaluation of long-term flux measurement techniques. Part I: averaging and coordinate rotation. Bound.-Layer Meteorol., 107, 1-48.

Fitzmaurice J., Wang J., Brass R. L., 2004. Sensible heat flux estimated from one-level air temperature near the land surface. Geophys. Res. Lett., 31, L07102, doi:10.1029/2003GL018452.

Foken T., 2008a. Micrometeorology. Springer-Verlag, Berlin Heidelberg, 306 pp.

Foken T., 2008b. The energy balance closure problem: an overview. Ecological Applications, 18(6), 1351-1367.

Foken T., 2006. 50 years of the Monin–Obukhov similarity theory. Bound.-Layer Meteorol., 119, 431-447.

Foken T., Wichura B., 1996. Tools for quality assessment of surface-based flux measurements. Agric. Forest Meteorol., 78, 83-105.

Gao W., Shaw R. H., Paw U K. T., 1989. Observation of Organized Structure in Turbulent-Flow within and above a Forest Canopy. Bound.-Layer Meteorol., 47, 349-377.

Garai A., Kleissl J., 2011. Air and surface temperature coupling in the convective atmospheric boundary layer. J. Atmos. Sci., doi: 10.1175/JAS-D-11-057.1.

Göckede M., Rebmann C., Foken T., 2004. A combination of quality assessment tools for eddy covariance measurements with footprint modelling for the characterisation of complex sites. Agric. Forest Meteorol., 127, 175-188.

Graefe J., 2004. Roughness layer corrections with emphasis on SVAT model applications. Agric. Forest Meteorol., 124, 237-251.

Granier A., 1987. Evaluation of a transpiration in a Douglas-fir stand by means of sap flow measurements. Tree Physiol., 3, 309-320.

Green S., 2009. Measurements of Sap Flow by the Heat-Pulse Method. An instruction manual for the HPV system. New Zeland.

Green S. R., Clothier B., Jardine B., 2003. Theory and Practical Application of Heat Pulse to Measure Sap Flow. Agron. J., 95, 1371-1379.

Green S. R., Clothier B., 1988. Water use of kiwifruit vines and apple trees by the heat-pulse technique. J. Exp. Bot., 39, 115-123.

Green S. R., McNaughton K. G., Clothier B. E., 1989. Observations of night-time water use in kiwifruit vines and apple trees. Agric. Forest Meteorol., 48, 251-261.

Guo J. X., Bian L. G., Dai Y. J., 2009a. Multiple time scale evaluation of the energy balance during the maize growing season, and a new reason of energy imbalance. Sci. China Ser. D-Earth Sci., 52, 108-117.

Guo X., Hongsheng Z., Cai X., Kang L., Zhu T., Leclerc M. Y., 2009b. Flux-variance method for latent heat and carbon dioxide fluxes in unstable conditions. Bound.-Layer Meteorol., 131, 363–384.

Hamdy A., 1999. Water Resources in the Mediterranean Region: from Ideas to Action. In: Background Documentation for Thematic Session. Consultation of Experts from MENA Region on: World Water Vision-Water for Food and Rural Development. CIHEAM-IAMB, Valenzano, 27-29 May 1999, pp. 1-23.

Han H., Felker P., 1997. Field validation of water-use efficiency of the CAM plant Opuntia ellisiana in south Texas. J. Arid Environ., 36, 133-148.

Harman I. N., Finnigan J. J., 2007. A simple unified theory for flow in the canopy and roughness sublayer. Bound.-Layer Meteorol., 123, 339–363.

Hargreaves G. H., Samani Z. A., 1985. Reference crop evapotranspiration from temperature. Appl. Eng. Agric., 1(2), 96-99.

Heilman J. L., McInnes K. J., Gesch R. W., Lacano R. J., Savage M. J., 1996. Effects of trellising on the energy balance of a vineyard. Agric. Forest Meteorol., 81, 79-93.

Heilman J. L., McInnes K. J., Savage M. J., Gesch R. W., Lascano R. J., 1994. Soil and canopy energy balances in a West Texas vineyard. Agric. Forest Meteorol., 71, 99-114.

Heilman J. L., Heilman W. E., Moore D. G., 1982. Evaluating the crop coefficient using spectral reflectance. Agron. J., 74, 967-971.

Higbie R., 1935. The rate of absorption of a pure gas into a still liquid during short periods of exposure. Trans. Am. Inst. Chem. Eng., 31, 355–388.

Högström U., 1988. Non-dimensional wind and temperature profiles in the atmospheric surface layer: a re-evaluation. Bound.-Layer Meteorol., 42, 55–78.

Holzer M., Siggia E. D., 1994. Turbulent mixing of a passive scalar. Phys. Fluids, 6, 1820-1837.

Hongyan C., Jiayi C., Hu F., Qingcun Z., 2004. The coherent structure of water vapour transfer in the unstable atmospheric surface layer. Bound.-Layer Meteorol., 111, 534–552.

Horst T. W., 1999. The footprint for estimation of atmosphere-surface exchange fluxes by profile techniques. Bound.-Layer Meteorol., 90, 171-188.

Howell F. J., Mahrt L., 1997. Multiresolution flux decomposition. Bound.-Layer Meteorol., 83, 117–137.

Jara J., Stockle C. O., Kjelgaard J., 1998. Measurement of evapotranspiration and its components in a corn (*Zea mays* L.) field. Agric. Forest Meteorol., 92, 131-145.

Jensen M. E., 1968. Water consumption by agricultural plants, In: Kozlowski, T.T. (Ed.), Water Deficits and Plant Growth, Vol. II. Academic Press, Inc., New York, NY, pp. 1–22.

Jia X., Dukes M. D., Jacobs J. M., Irmak S., 2006. Weighing lysimeters for evapotranspiration research in a humid environment. T. ASABE, 49(2), 1-12.

Johnson L., Roczen D., Youkhana S., Neemani R. R., Bosch D. F., 2003. Mapping vineyard leaf area with multispectral satellite imagery. Comput. Electron. Agric., 38, 33-44.

Johnson T., Odin H., 1978. Measurements of evapotranspiration using a dynamic lysimeter. Swedish University of Agricultural Sciences, College of Forestry, Studia Forestalia Suecica, Uppsala, Sweden, vol. 146, 29 pp.

Ju W., Chen J. M., Black T. A., Barr A. G., Liu J., Chen B., 2006. Modelling multi-year coupled carbon and water fluxes in a boreal aspen forest. Agric. Forest Meteorol., 140, 136-151.

Kaimal J. C., Finnigan J. J., 1994. Atmospheric Boundary Layer Flows: Their Structure and Measurement. Oxford Univ. press., 302 pp.

Kanda M., Inagaki A., Letzel M. O., Raasch S., Watanabe T., 2004. LES study of the energy imbalance problem with eddy covariance fluxes. Bound.-Layer Meteorol., 110, 381-404.

Katerji N., Perrier A., 1983. Modélisation de l'évapotranspiration réelle ETR d'une parcelle de luzerne: rŏle d'un coefficient cultural. Agronomie, 3(6), 513-521.

Katerji N., Rana G., 2008. Crop evapotranspiration measurements and estimation in the Mediterranean region. CRA-SCA, Bari, 173 pp.

Katul G., Hsieh C.-I., Bowling D., Clark K., Shurpali N., Turnipseed A., Albertson J., Tu K., Hollinger D., Evans B., Offerle B., Anderson D., Ellsworth D., Vogel C., Oren R., 1999. Spatial variability of turbulent fluxes in the roughness sublayer of an even-aged pine forest. Bound.-Layer Meteorol., 93, 1-28.

Katul G. G., Hsieh C., Sigmon J., 1997. Energy–inertial scale interaction for velocity and temperature in the unstable atmospheric surface layer. Bound.-Layer Meteorol., 82, 49-80.

Katul G. G., Hsieh C., Oren R., Ellsworth D., Philips N., 1996. Latent and sensible heat flux predictions from a uniform pine forest using surface renewal and flux variance methods. Bound.-Layer Meteorol., 80, 249–282.

Kidston J., Brümmer C., Black T. A., Morgenstern K., Nesic Z.,·McCaughey J. H., Barr A. G., 2010. Energy Balance Closure Using

Eddy Covariance Above Two Different Land Surfaces and Implications for CO_2 Flux Measurements. Bound.-Layer Meteorol., 136, 193-218.

Kluitenberg G. J., Ham J. M., 2004. Improved theory for calculating sap flow with the heat pulse method. Agric. Forest Meteorol., 126, 169-173.

Kovasznay L. S. G., Kibens V., Blackwelder F., 1970. Large scale motion in the intermittent region of a turbulent boundary layer. J. Fluid Mech., 41, 1-283.

Kramer P. J., 1974. Fifty Years of Progress in Water Relations Research. Plant Physiol., 54, 463-471.

Kramm G., Dlugi R., Lenschow D. H., 1995. A Re-Evaluation of the Webb Correction Using Density-Weighted Averages. J. Hydrol., 166, 283–292.

Kucharik C., Barford C., El Maayar M., Wofsy S. C., Monson R. K., Baldocchi D. D., 2006. Evaluation of a dynamic global vegetation model (DGVM) at the forest stand-level: vegetation structure, phenology, and seasonal and inter-annual CO_2 and H_2O vapor exchange at three AmeriFlux study sites. Ecol. Model., 196, 1-31.

Kustas W. P., Prueger J. R., Humes K. S., Starks P. J., 1999. Estimation of surface heat fluxes at field scale using surface layer versus mixed layer atmospheric variables with radiometric temperature observations. J. Appl. Meteorol., 38, 224-238.

Lascano R. J., Baumhardt R. L., Lipe W. N., 1992. Measurement of water flow in young grapevines using the stem heat balance method. Am. J. Enol. Viticult., 43, 159-165.

Lee X., 1998. On Micrometeorological Observations of Surface-Air Exchange over Tall Vegetation. Agric. Forest Meteorol., 91, 39–50.

Liu H. J., Cohen S., Tanny J., Lemcoff J. H., Huang G., 2008. Transpiration estimation of banana (*Musa* sp.) plants with the thermal dissipation method. Plant Soil, 308, 227-238.

Liu H., Randerson J. T., Lindfors J., Massman W., Foken T., 2006. Consequences of incomplete surface energy balance closure for CO_2 fluxes from open-path CO_2/H_2O infrared gas analyzers. Bound.-Layer Meteorol., 120, 65-85.

Lu P., Urban L., Zhao P., 2004. Granier's thermal dissipation probe (TDP) method for measuring sap flow in trees: theory and practice. Acta Bot. Sinica, 46, 631-646.

Mahrt L., 1998. Flux sampling errors for aircraft and towers. J. Atmos. Oceanic Technol., 15, 416-429.

Marshall D.C., 1958. Measurement of sap flow in conifers by heat transport. Plant Physiol., 33, 385-396.

Mauder M., Foken T., 2004. Documentation and instruction manual of the eddy covariance software package TK2. Universität Bayreuth, Abt.Mikrometeorologie, Arbeitsergebnisse, pp. 26–44. http://www.geo.unibayreuth.de/mikrometeorologie/ARBERG.

Mauder M., Desjardins R. L., Pattey E., Worth D., 2010. An Attempt to Close the Daytime Surface Energy Balance Using Spatially-Averaged Flux Measurements. Bound.-Layer Meteorol., 136, 175-191.

Mauder M., Oncley S. P., Vogt R., Weidinger T., Ribeiro L., Bernhofer C., Foken T., Kosiek W., De Bruin H. A. R., Liu H., 2007. The energy balance experiment EBEX-2000. Part II. Intercomparison of eddy-covariance sensors and post-field data processing methods. Bound.-Layer Meteorol., 123, doi:10.1007/s10546-006-9139-4.

Meijninger W. M. L., de Bruin H. A. R., 2000. The sensible heat fluxes over irrigated areas in western Turkey determined with a large aperture scintillometer. J. Hydrol., 229, 42-49.

Mengistu M. G., Savage M. J., 2010. Open water evaporation estimation for a small shallow reservoir in winter using surface renewal. J. Hydrol., 380, 27–35.

Meyers T. P., Hall M. E., Lindberg S. E., Kim K., 1996. Use of the modified Bowen-ratio technique to measure fluxes of trace gases. Atmos. Environ., 30(19), 3321-3329.

Mohan M., Tiwari M. K., 2004. Study of momentum transfers within a vegetation canopy. Proc. Indian Acad. Sci. (Earth Planet Sci.), 113(1), 67-72.

Monteith J. L., 1965. Evaporation and environment. In: Fogg GE (ed) The State and Movement of Water in Living Organism. Proceedings of the XIX Symposium on Society for Experimental Biology. Academic Press, New York, 205-234.

Moreno F., Fernandez J. E., Clothier B. E., Green S. R., 1996. Transpiration and root water uptake by olive trees. Plant and Soil, 184, 85-96.

Moreshet S., Cohen Y., Fuchs M., 1983. Response of mature "Shamouti" orange trees to irrigation of different soil volumes at similar levels of available water. Irri. Sci., 3, 223-236.

Moriana A., Villalobos F. J., Fereres E., 2002. Stomatal and photosynthetic responses of olive (*Olea europaea* L.) leaves to water deficits. Plant Cell Environ., 25(3), 395-405.

Motisi A., Consoli S., Rossi F., Minacapilli M., Cammalleri C., Papa R., Rallo G., D'urso G., 2012. Eddy covariance and sap flow measurement of energy and mass exchange of woody crops in a Mediterranean environment. 8th International workshop on sap flow. Volterra (Italy), May 8-12.

Mölder M., Grelle A., Lindroth A., Halldin S., 1999. Flux-profile relationships over a boreal forest-roughness sublayer corrections. Agric. Forest Meteorol., 99, 645-658.

Mugnai S., 2004. Elementi di ecofisiologia vegetale, in: ARSIA, Uso razionale delle risorse nel florovivaismo: l'acqua, Quaderno 5/2004, Firenze, 35-47.

Norman J. M., Kustas W. P., Humes K. S., 1995. A two-source approach for estimating soil and vegetation energy fluxes from observations of directional radiometric surface temperature. Agric. Forest Meteorol., 80, 87-109.

Oncley S. P., Foken T., Vogt R. *et al*., 2007. The energy balance experiment EBEX-2000. Part I: Overview and energy balance. Bound.-Layer Meteorol., 123, 1-28.

Orgaz F., Testi L., Villalobos F. J., Fereres E., 2006. Water requirements of olive orchards. II. Determination of crop coefficients for irrigation scheduling. Irrig. Sci., 24(2), 77-84.

Paco T. A., Ferreira M. I., Conceicao N., 2006. Peach orchard evapotranspiration in a sandy soil: comparison between eddy covariance measurements and estimates by the FAO56 approach. Agric. Water Manage., 85(3), 305-313.

Panin G. N., Bernhofer Ch., 2008. Parametrization of Turbulent Fluxes over Inhomogeneous Landscapes. Atmospheric and Oceanic Physics, 44 (6), 701–716.

Paw U K. T., Brunet Y., 1991. A surface renewal measure of sensible heat flux density. Proc. of the 20th Conference on Agriculture and Forest Meteorology, Salt Lake City, 52-53.

Paw U K. T., Snyder R. L., Spano D., Su H. B., 2005. Surface renewal estimates of scalar exchanges. In: Micrometeorology in Agricultural Systems, Agronomy Monograph No. 47, edited by J. L. Hatfield and J. M. Baker, pp. 455-483.

Paw U K. T., Baldocchi D. D., Meyers T. P., Wilson K. B., 2000. Correction of Eddy-Covariance measurements incorporating both advective effects and density fluxes. Bound.-Layer Meteorol., 97, 487-511.

Paw U K. T., Qiu J., Su H.-B., Watanabe T., Brunet Y., 1995. Surface renewal analysis: a new method to obtain scalar fluxes. Agric. Forest Meteorol., 74, 119-137.

Paw U K. T., Brunet Y., Colineau S., Shaw R. H., Maitani T., Qiu J., Hipps L., 1992. On coherent structures in turbulence within and above agricultural plant canopies. Agric. Forest Meteorol., 61, 55-68.

Penman H. L., 1956. Estimating evaporation. Trans. Amer. Geoph. Union, 37, 43-50.

Perez P. J., Castellví F., Martinéz-Cob A., 2008. A simple model for estimating the Bowen ratio from climatic factors for determining latent and sensible heat flux. Agric. Forest Meteorol., 148, 25-37.

Phillips W. R. C., Mahon J., 2011. On approximations to a class of Jaeger integrals. Proc. R. Soc. A, 467, 3570-3589.

Pingtong Z., Takahashi H., 2000. A first-order closure model for the wind flow within and above vegetation canopies. Agric. Forest Meteorol., 103, 301–313.

Priestley C. H. B., 1959. Turbulent Transfer in the Lower Atmosphere.Univ. of Chicago Press, Chicago, 130 pp.

Prueger J. H., Hipps L. E., Cooper D. I., 1996. Evaporation and the development of the local boundary layer over an irrigated surface in an arid region. Agric. Forest Meteorol., 78, 223-237.

Prueger J. H., Kustas W. P., Hipps L. E., Hatfield J. L., 2004. Aerodynamic parameters and sensible heat flux estimates for a semi-arid ecosystem. Journal of Arid Environments, 57, 87–100.

Qiu J., Paw U K. T., Shaw R. H., 1995. Pseudo-Wavelet analysis of turbulence patterns in three vegetations layers. Bound.-Layer Meteorol., 72, 177–204.

Rana G., Katerji N., 2000. Measurement and estimation of actual evapotranspiration in the field under Mediterranean climate: a review. Eur. J. Agron., 13, 125-153.

Rana G., Katerji N., de Lorenzi F., 2005. Measurement and modelling of evapotranspiration of irrigated citrus orchard under Mediterranean conditions. Agric. Forest Meteorol., 128, 199-209.

Raupach M. R., Thom A. S., 1981. Turbulence in and above plant canopies. Annu. Rev. Fluid Mech., 13, 97-129.

Raupach M. R., Finnigan J. J., Brunet Y., 1996. Coherent eddies in vegetation canopies: the mixing-layer analogy. Bound.-Layer Meteorol., 78, 351-382.

Raupach M. R., Antonia R. A., Rajagopalan S., 1991. Rough-wall Turbulent Boundary Layers. Appl. Mech. Rev., 44, 1-25.

Reyes J. F., Jara J., Jeldres R., 2007. Design parameters evaluation of a sap flow meter for small trees. IDESIA, 25(1), 53-62.

Sakai K. R., Fitzjarrald D. R., Moore K. E., 2001. Importance of Low-Frequency Contributions to Eddy Fluxes Observed over Rough Surfaces. J. Appl. Meteorol., 40, 2178-2192.

Sammis T. W., Mexal J. G., Miller D., 2004. Evapotranspiration of flood-irrigated pecans. Agric. Water Manage., 69, 179-190.

Schotanus P., Nieuwstadt F. T. M., DeBruin H. A. R., 1983. Temperature measurement with a sonic anemometer and its application to heat and moisture fluctuations. Bound.-Layer Meteorol., 26, 81-93.

Simmons L. J., Wang J., Sammis T. W., Miller D. R., 2007. An evaluation of two inexpensive energy-balance techniques for measuring water use in flood-irrigated pecans (*Carya illinoinensis*). Agric. Water Manage., 88, 181-191.

Smith D. M., Allen S. J., 1996. Measurement of sap flow in plant stems. J. Exp. Bot., 47 (305), 1833-1844.

Smith M., Allen R. G., Monteith J. L., Perrier A., Pereira L. S., Segeren A., 1991. Report on the expert consultation on revision of FAO methodologies

for crop water requirements. FAO Land and Water Development Division, FAO, Rome, 129 pp.

Snyder R. L., O'Connell N. V., 2007. Crop coefficients for microsprinkler-irrigated, clean-cultivated, mature citrus in an arid climate J. Irrig. Drain. Eng., 133(1), 43-52.

Snyder R. L., Orang M., Matyac S., Grismer M. E., 2005. Simplified estimation of reference evapotranspiration from pan evaporation data in California. J. Irrig. Drain. Eng., 131(3), 249-253.

Snyder R. L., Paw U K. T., Spano D., Duce P., 1997. Surface renewal estimates of evapotranspiration. Theory. Acta Hort., 449, vol. 1, 49-55.

Snyder R. L., Spano D., Paw U K. T., 1996. Surface renewal analysis for sensible and latent heat flux density. Bound.-Layer Meteorol., 77, 249-266.

Spank U., Bernhofer C., 2008. Another Simple Method of Spectral Correction to Obtain Robust Eddy-Covariance Results. Bound.-Layer Meteorol., 128, 403-422.

Spano D., Duce P., Snyder R. L., Paw U K. T., 1997a. Surface renewal estimates of evapotranspiration. Tall canopies. Acta Hort., 449, vol. 1, 63-68.

Spano D., Snyder R. L., Duce P., Paw U K. T., 1997b. Surface renewal analysis for sensible heat flux density using structure functions. Agric. Forest Meteorol., 86, 259–271.

Sparrow E. M., Husar R. B., Goldstein R. J., 1970. Observation and other characteristics of thermals. J. Fluid Mech., 41, 793-800.

Stanghellini C., Bosma A. H., Gabriels P. C. J., Werkoven C., 1990. The water consumption of agricultural crops: how crop coefficient are affected by crop geometry and microclimate, Acta Hort., 278, 509-516.

Stoy P. C., Katul G. G., Siqueira M. B. S., Juang J.-Y., Novick K. A., McCarthy H. R., Oishi A. C., Uebelherr J. M., Kim H.-S., Oren R., 2006. Separating the effects of climate and vegetation on evapotranspiration

along a successional chronosequence in the southeastern US. Global Change Biol., 12, 2115–2135.

Stull R. B., 1988. An Introduction to Boundary Layer Meteorology. Kluwer Academic Publishers, Dordrecht, The Netherlands, 666 pp.

Swanson R.H., 1962. An instrument for detecting sap movement in woody plants. Paper 68. USDA Forest Serv. Rocky Mountain Forest Range Exp. Stn., Fort Collins, CO.

Swanson R.H., Whitfield D.W.A., 1981. A numerical analysis of heat-pulse velocity theory and practice. J. Exp. Bot., 32, 221-239.

Tarantino E., Onofrii M., 1991. Determinazione dei coefficienti colturali mediante lisimetri, Bonifica, 7, 119-136.

Terradellas E., Morales G., Cuxart J., Yagüe C., 2001. Wavelet methods: application to the study of the stable atmospheric boundary layer under non-stationary conditions. Dynam. Atmos. Oceans, 34, 225–244.

Terradellas E., Soler M. R., Ferreres E., Bravo M., 2005. Analysis of oscillations in the stable atmospheric boundary layer using wavelet methods. Bound.-Layer Meteorol., 114, 489–518.

Testi L., Orgaz F., Villalobos F. J., 2006. Variations in bulk canopy conductance of an irrigated olive (*Olea europaea* L.) orchard. Environ. Exp. Bot., 55, 15-28.

Testi L., Villalobos F. J., Orgaz F., 2004. Evapotranspiration of a young irrigated olive orchard in southern Spain. Agric. Forest Meteorol., 121, 1-18.

Thom A. S., 1971. Momentum absorption by vegetation. Quart. J. R. Meteorol. Soc., 97, 414–428.

Todd R. W., Evett S. R., Howell T. A., 2000. The Bowen ratio-energy balance method for estimating latent heat flux of irrigated alfalfa evaluated in a semi-arid, advective environment. Agric. Forest Meteorol., 103, 335-348.

Trambouze W., Voltz M., 2001. Measurement and modelling transpiration of a Mediterranean vineyard. Agric. Forest Meteor., 107, 153-166.

Trambouze W., Bertuzzi P., Voltz M., 1998. Comparison of methods for estimating actual evapotranspiration in a row cropped vineyard. Agric. Forest Meteorol., 91, 193-208.

Twine T. E., Kustas W. P., Norman J. M., Cook D. R., Houser P. R., Meyers T. P., Prueger J. H., Starks P. J., Wesely M. L., 2000. Correcting eddy-covariance flux underestimates over a grassland. Agric. Forest Meteorol., 103, 279-300.

Van Atta C. W., 1977. Effect of coherent structures on structure functions of temperature in the atmospheric boundary layer. Arch. Mech., 29, 161-171.

Ventura F., Spano D., Duce P., Snyder R. L., 1999. An evaluation of common evapotranspiration equations. Irrig. Sci., 18, 163-170.

Vickers D., Mahrt L., 2003. The cospectral gap and turbulent flux calculations. J. Atmos. Ocean. Technol., 20, 660–672.

Villalobos F. J., Orgaz F., Testi L., Fereres E., 2000. Measurement and modeling of evapotranspiration of olive (*Olea europea* L.) orchards. Agric. Forest Meteorol., 13, 155-163.

Villalobos F. J., Testi L., Moreno-Perez M. F., 2009. Evaporation and canopy conductance of citrus orchards. Agric. Water Manage., 96, 565-573.

Wang J., Bras R. L., 1998. A new method for estimation of sensible heat flux from air temperature. Water Resour. Res., 34(9), 2281-2288.

Webb E. K., Pearman G. I., Leuning R., 1980. Correction of Flux Measurements for Density Effects due to Heat and Water Vapour Transfer. Quart. J. Roy. Meteorol. Soc., 106, 85-100.

Wilczak J. M., Oncley S. P., Stage S. A., 2001. Sonic anemometer tilt correction algorithms. Bound.-Layer Mmeteorol., 99, 127-150.

Williams D. G., Cable W., Hultine K., Yepez E. A., Er-Raki S., Hoedjes J. C. B., Boulet G., de Bruin H. A. R., Chehbouni A., Timouk F., 2003. Suivi de la repartition de l'evapotranspiration dans une oliveraie (*Olea europaea* L.) a l'aide des techniques de l'eddy covariance, des flux de seve et des isotopes stables. Vemes Journees de l'Ecologie Fonctionnelle, 12 au 14 Mars 2003 a Nancy.

Wilson K., Goldstein A., Falge E. *et al*., 2002. Energy balance closure at fluxnet sites. Agric. Forest Meteorol., 113, 223-243.

Wilson N. R., Shaw R. H., 1977. A higher order closure model for canopy flow. J. Appl. Meteorol., 16, 1197–1205.

World Meteorological Organization, 2008. Guide to Meteorological Instruments and Methods of Observation. WMO-No. 8, Geneva, Switzerland.

Wright J. L., 1982. New evapotranspiration crop coefficients. J. Irrig. Drain. Div., ASCE, 108, 57-74.

Wullschleger S. D., Wilson K. B., Hanson P. J., 2000. Environmental control of whole-plant transpiration, canopy conductance and estimates of the decoupling coefficient for large red maple trees. Agric. Forest Meteorol., 104, 157-168.

Zapata N., Martínez-Cob A., 2001. Estimation of sensible and latent heat flux from natural sparse vegetation surfaces using surface renewal. J. Hydrol., 254, 215-228.

Zapata N., Martínez-Cob A., 2002. Evaluation of the surface renewal method to estimate wheat evapotranspiration. Agric. Water Manage., 55, 141-157.

Zhang Y., Grant R. F., Flanagan L. B., Wang S., Verseghy D. L., 2005. Modelling CO_2 and energy exchanges in a northern semiarid grassland using the carbon- and nitrogen-coupled Canadian Land Surface Scheme (C-CLASS). Ecol. Model., 181, 591-614.

Zhang S., Qiu C., Zhang W., 2004. Estimating Heat Fluxes by Merging Profile Formulae and the Energy Budget with a Variational Technique. Adv. Atmos. Sci., 21 (4), 627–636.

Zhang H., Simmonds L. P., Morison J. I. L., Payne D., 1997. Estimation of transpiration by single trees: comparison of sap flow with combination equation. Agric. Forest Meteorol., 87, 155-169.